Prepared for:

Rijkswaterstaat RIZA

Voorspelinstrument duurzame vaarweg

Reducing Computation Time

Report

April 2008

Q4357.10

WL | delft hydraulics

Prepared for:

Rijkswaterstaat RIZA

Voorspelinstrument duurzame vaarweg

Reducing Computation Time

Saskia van Vuren, Anke Hauschild, Willem Ottevanger, Johan Crebas and Mohamed Yossef

Report

April 2008

WL | delft hydraulics

Client:	Rijkswaterstaat RIZA
Title:	Voorspelinstrument duurzame vaarweg

Abstract:

WL | Delft Hydraulics worked on the development of an advanced 2-D morphodynamic model that covers, nearly, the entire Rhine system in the Netherlands (see Van Vuren et al. (2006), Yossef et al. (2006) and Mosselman et al. (2007)). The model contains all kinds of innovative, recently developed aspects, amongst which domain decomposition, sediment transport over non-erodible layers and functionality for sediment management to assess dredging and dumping strategies.

The DVR model is a promising tool for assessing the river's navigability, for locating nautical bottlenecks and for evaluating river intervention measures in order to improve the navigability. Unfortunately, numerical simulations with the DVR model are rather time consuming. This makes the model less suitable for engineering practice at the moment.

The objective of the research presented in this report is to reduce the computation time of a numerical simulation with the DVR model. The following activities were carried out:

1. Optimisation of the grid size;
2. Optimisation of the computation time step and the morphological acceleration factor;
3. Application of parallel computation;
4. Application of a more efficient description of flow through the floodplain;
5. Reduction of the physical processes in sub-domains.

References:	RI-4737 "Vervolg Bouw morfologisch model DVR"

Ver	Author	Date	Remarks	Review	Approved by
1.0	dr. Saskia van Vuren	12 September 2007		dr. ir. Bert Jagers	drs. Kees Bons
2.0	dr. Saskia van Vuren	24 January 2008			
3.0	dr. Mohamed Yossef	25 April 2008		dr. ir. Bert Jagers	dr. A.G. Segeren

Project number:	Q4357.10
Keywords:	River morphology, two-dimensional model
Number of pages:	108
Classification:	Confidential until April 2010
Status:	Final

WL | delft hydraulics

Client:	Rijkswaterstaat RIZA
Title:	Voorspelinstrument duurzame vaarweg

Samenvatting::

Het DVR-programma vraagt om een voorspelinstrument om de voorgestelde maatregelen te evalueren. WL | Delft Hydraulics had de opdracht om een geavanceerd 2D morfodynamisch model te ontwikkelen van het systeem van de Rijn in Nederland (Van Vuren e.a., 2006). Het model bevat verscheidene innovatieve, recent ontwikkelde aspecten (Yossef e.a., 2006). We duiden dit model aan als "DVR-model".

Het DVR-model is een veelbelovende model waarmee de bevaarbaarheid van rivieren kan worden getoetst, nautische knelpunten kunnen worden gevonden en maatregelen ten gunste van de bevaarbaarheid kunnen worden geevalueerd. De beperking van het DVR-model is dat de berekeningen redelijk lang duren. Het model is hierdoor minder geschikt voor het berekeningen uit de praktijk.

De doelstelling van het onderzoek van dit rapport is om de rekentijd van numerieke simulatie met het DVR model te verminderen. De rekentijdreductie wordt onderzocht als volgt:

1. Optimalisatie van het rekenrooster;
2. Optimalisatie van de tijdstap en morfologische versnellingsfactor;
3. Toepassen van parallel rekenen;
4. Toepassen van een meer effectieve beschrijving van stroming door de uiterwaarden;
5. Reductie van de fysische processen in deeldomeinen.

References:	RI-4737 "Vervolg Bouw morfologisch model DVR"

Ver	Author		Date	Remarks	Review		Approved by	
1.0	dr. Saskia van Vuren		12 September 2007		dr. ir. Bert Jagers		drs. Kees Bons	
2.0	dr. Saskia van Vuren		24 January 2008					
3.0	dr. Mohamed Yossef		25 April 2008		dr. ir. Bert Jagers		dr. A.G. Segeren	

Project number:	Q4357.10
Keywords:	River morphology, two-dimensional model
Number of pages:	108
Classification:	Confidential until April 2010
Status:	Final

Contents

1 Introduction

1.1 Background

The Rhine is the most navigated inland waterway in Western Europe. Due to its advantageous location in the Rhine delta, the inland waterways in the Netherlands form a natural access to the continent of Europe. As a consequence of climate change and morphological changes in the Rhine system an increasing number of nautical bottlenecks are expected in the coming years. In order to meet the demands for navigation also in the future, Directorate for Public Works and Water Management introduced the programme Duurzame Vaardiepte Rijndelta (DVR) (Sustainable Navigation Depth for the Rhine Delta). Within the DVR programme, river intervention measures will be defined and evaluated to maintain and improve the navigability of the Rhine.

The DVR programme calls for a prediction tool to evaluate the proposed intervention measures. Accordingly, WL | Delft Hydraulics was commissioned the task of developing an advanced 2-D morphodynamic model of the Rhine system in the Netherlands (Van Vuren et al., 2006). The model contains all kinds of innovative, recently developed aspects, amongst which domain decomposition, sediment transport over non-erodible layers and functionality for sediment management to assess dredging and dumping strategies (Yossef et al., 2006). In this report, we refer to this model as “DVR model”.

The advanced DVR model can be used to assess the long-term large-scale evolution of the Rhine system (scale of longitudinal profile evolution of river reaches, e.g. in response to training works). As the model incorporates also complex time-dependent multi-dimensional phenomena, such as curvature-induced bar-pool patterns in bends, assessment is also possible at the intermediate spatial scale (scale of alternate bars and cross-sectional profile evolution). For a detailed description of the model, reference is made to Van Vuren et al. (2006), Yossef et al. (2006), and Mosselman et al. (2007).

However, carrying out simulations using the earlier developed model proved to be rather time consuming which hinders the use of the model as an operational model. This calls for additional effort to speed up simulations carried out with the model. In this report we develop the model further with the aim of reducing the computation such that the model is operational in its entirety.

1.2 Assignment

This project includes four primary tasks:

1- Reducing the computational time (*this report*).
2- Improving the model.
3- Case study of fixed layer and nourishment in the Bovenrijn.
4- Improving the model’s physical concepts

The objective of the research presented in this report is to reduce the computation time of a numerical simulation with the DVR model. To meet this objective, the following activities are carried out:

- Chapter 2: Optimisation of the grid size;
- Chapter 3: Optimisation of the computation time step and the morphological acceleration factor;
- Chapter 4: Application of parallel computation;
- Chapter 5: Application of a more efficient description of flow through the floodplain;
- Chapter 3: Reduction of the physical processes in sub-domains.

For the purpose of illustration, we investigate the above-mentioned possibilities for computation time reduction for the model domain of the river Waal branch only. Generic knowledge on the possibilities to reduce the computation effort will be produced that also holds for the model domains of the other Rhine branches. Application of the new insights to reduce the computation time, to the model domains of the other Rhine branches is not part of this project.

The work has been carried out within the agreement RI-4737 “Vervolg Bouw morfologisch model DVR”, (in English: Continued construction of morphological model for DVR). The project is known in WL | Delft Hydraulics as Q4357.00.

1.3 Organisation

This report is the second in a series of three within this project. The team contributing to the project consisted of: Chris Stolker, Johan Crebas, Anke Hauschild, Sanjay Giri, Willem Ottevanger, Saskia van Vuren, Kees Sloff, Erik Mosselman, Bert Jagers, Frans van der Knaap and Mohamed Yossef. The later was the project leader and the editor of this report. Arjan Sieben managed the project on behalf of Rijkswaterstaat RIZA.

2 Optimisation of the grid size

2.1 Method

The main focus of this activity is to reduce the computation time by optimising the grid size of the model domain of the Waal branch. To that end, a number of grids has been created by coarsening the original, fine grid in transverse and longitudinal direction by different factors (see section 2.2). For each grid, the morphodynamic model set up has been carried out according to the procedure described by Van Vuren et al. (2006).

The different grids are evaluated on the basis of the following computations:

1. four hydrodynamic computations with a constant discharge level of 1187, 2000, 3080 and 4422 m^3/s.
2. a morphodynamic computation with the schematised hydrograph of the Waal that is presented in Table 2.1 and Figure 2.1.

In order to assess the influence of the coarsening, the model results of the computations with the coarsened grids are compared with the model results of the original fine grid, i.e. the latter model serves as a reference model throughout this chapter.

For the impact assessment of grid coarsening, first, the difference in discharge distribution between the main channel and floodplains is analysed for each new generated grid in Section 2.3. Second, the difference in morphodynamic response after a period of 10 years is assessed in Section 2.4. A limit of acceptability of these differences is defined in Section 2.3 and 2.4.

On the basis of the differences in the results from the reference model and the models with the coarsened grids, recommendations are given in Section 2.5 concerning the grid optimization.

Table 2.1 Schematisation of the discharge hydrograph of the Waal.

Time (days)	Schematisation of the discharge hydrograph of the Waal (m^3/s)
30	2000
8	3080
14	4422
8	3080
86	2000
219	1187

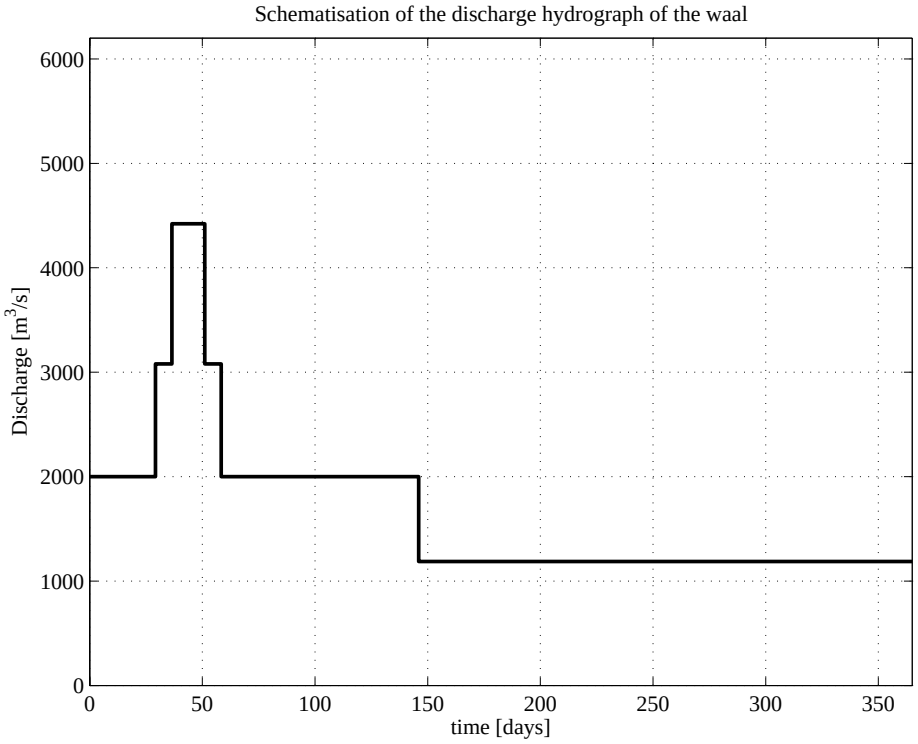

Figure 2.1 Schematisation of the discharge hydrograph of the Waal with four different discharge levels.

2.2 Grid variations

2.2.1 Requirements of the computation grid

A number of grids have been created by coarsening the original, fine grid in transverse and longitudinal direction by different factors. In principle, the extent of grid coarsening is restricted, since the model should still be appropriate for impact assessment studies related to sustainable navigation management. To that end, Mosselman et al. (2005) indicated a number of requirements of the grid covering the main channel. The most important requirements and recommendations are listed below:

- A maximum grid size of 10 m in transverse direction is required to achieve a maximum inaccuracy of 10 m in estimating the position of the navigation channel. This criteria is very restrictive and would yield a very fine model which requires very long time to run, accordingly, it will be relaxed to 20 m.

- A proper reproduction of the cross-section (e.g. representation of amongst others the transverse bed slope and point-bar pool development in the inner- and outer bend) requires a minimum number of 6 grid cells in the main channel;

- A maximum aspect ratio of four is recommended, since the dimension of the grid cells in transverse and longitudinal direction should not differ too much;

- The computational cells should not exceed 20% of the relevant adaptation lengths to obtain a proper representation of spatial lag effects of morphological phenomena of interest. Important adaptation lengths for 2-D morphology are λ_s and λ_w from the theory of Struiksma et al. (1995).

- Groyne head lines, the so-called 'normal lines', enclose the main channel. The groyne head lines are represented by two grid lines, which should smoothly follow the normal lines. This is required to obtain a smooth flow pattern and avoid numerical oscillation yielding disturbances in morphodynamic behaviour.

- The grid should fulfill requirements of smoothness and orthogonality (see Thompson et al. (1985), Wijbenga (1985) and Mosselman (1991)). The smoothness requirement implies that difference between successive grid cell dimensions should be smaller than 10% in the main channel and smaller than 25% in the floodplains. The orthogonality requirement boils down to the fact that a grid cell corner point should not deviate more than 5º from an angle of 90º. The means that the orthogonality parameter, the extent of non-orthogonality, should not exceed sine(5º)=0,087.

Mosselman et al. (2006) indicated the importance of using fixed layer for the grid cells adjacent to the groyne heads. Taking this into account, two additional grid cells are required on top of the 6 grid cell in the main channel required for a proper reproduction of the cross-section. In other words, the main channel should consist of at least of 8 grid cells. The main channel width of the Waal equals approximately 260 m. This implies that the average grid cell width should be at maximum around 32.5 m. Based on the recommended aspect ratio of 4, the length of the grid cells should not exceed 130 m. Since groynes are located at mutual distances of approximately 150-200 m, it is recommended to restrict the grid cell length to 150 m.

It can be concluded that from a theoretical point of view the computation grid in the main channel should fulfil at least the following functional criteria:

1. at least 8 grid cells in transverse direction;
2. at most grid cells of 130 m length in longitudinal direction.

2.2.2 New generated computation grids

Bearing these requirements in mind, six grids have been created by coarsening the original, fine grid in transverse and longitudinal direction by different factors. Different coarsening factors have been applied to the main channel and the floodplains. Note that for all new generated grids the number of grid cells in longitudinal direction in the floodplain should be equal to that of the main channel.

Most of the grids amply fulfil the requirements of the computation grid. However, not all grids perfectly match the functional criteria. Two grids (grid 3 and 4), for instance, do not exactly fulfil the requirement that the outer grid lines enclose the actual location of the groyne heads at either side of the river. One computation grid (grid 2) just satisfies the

requirements and can be considered as the upper limit of grid coarsening. This grid contains the maximum allowed dimensions.

For coarsening of the fine grid a systematic approach was followed. As a first step the grid of the floodplains was coarsened with a factor 4 in transverse direction. This resulted in Grid 1 (see Figure 2.4) and is meant to evaluate to what extent a detailed resolution of the floodplain is required, if one is interested in the evolution of the alluvial part of the river that is restricted to the main channel.

Since Grid 1 features a rather abrupt transition from fine to coarse, another grid was created Grid 1c (see Figure 2.5). In Grid 1c the grid cells of the floodplains were gradually coarsened up to a factor 4. The performance of these two grids is compared order to investigate whether gradual coarsening is required.

Grid 2 presented in Figure 2.6, was developed in an earlier stage of the DVR project. The entire grid was coarsened in Mosselman et al. (2007) by a factor 2. Although grid coarsening in Mosselman et al. (2007) was more or less an arbitrary choice, the grid nicely satisfies the required dimensions and contains the maximum allowed dimensions. The grid is examined in the present study to test the performance of a grid with the maximum allowed dimensions, i.e. the upper limit.

In the next step, in addition to Grid 1, the grid has been coarsened by a factor 1.5 in longitudinal direction along with a coarsening of a factor 1.5 in transverse direction of the grid in the main channel and groyne section: yielding in Grid 3, see Figure 2.7. Grid 4 was coarsened in the same manner, be it that a coarsening factor of 1.75 was used, see Figure 2.8. Note that these coarsening factors result in a worse representation of the position of the groynes, see Figure 2.2.

Since the analysis of model results between Grid 1 and Grid 1c indicated the importance of gradual coarsening in transverse direction, finally Grid 5 (see Figure 2.9) has been constructed containing a gradually coarsened floodplain grid up to a factor 4. Based on the results of Grid 3 and Grid 4, the coarsening of the entire grid in longitudinal direction and the coarsening of the grid in the main channel and groyne section in transverse direction has been restricted to a factor 1.33.

Table 2.2 gives an overview of the coarsening factors in longitudinal and transverse direction of the new generated grids.

Table 2.2 Coarsening factors in transverse and longitudinal direction of the new generated grids.

Gridname ('short name')	**Main channel & groyne section**		**Floodplain**	
	longitudinal	transverse	longitudinal	transverse
grid 1 ('r1')	-	-	-	4
grid 1c ('r1c')	-	-	-	4*
grid 2 ('r2')	2	2	2	2
grid 3 ('r3')	1.5	1.5	1.5	4
grid 4 ('r4')	1.75	1.75	1.75	4
grid 5 ('r5')	1.333	1.333	1.333	4 *

* (gradually, smooth, orthogonal)

The difference in transverse direction between the new generated grids is visualized in Figure 2.2. The green lines indicate the position of the river axis and the groyne heads forming the boundaries of the main channel. The figure illustrates that Grid 3 and Grid 4 do not exactly follow the main channel boundaries. For a comparison with the reference model, respectively a slightly wider and narrower main channel section is used for Grid 3 and Grid 4. The red lines in Figure 2.2 indicate the grid lines that form the boundary of these main channel sections.

Table 2.3 gives an overview of the number of grid cells in the main channel and floodplain section and the grid cell dimensions of new generated grids. The table presents also the ratio between computation time required with the reference model and the new generated model, i.e. the acceleration.

Figure 2.3 to Figure 2.9 show the computational grid of the generated grid in the bend near Nijmegen (km 883-884). The black lines represent the location of the weirs in the model, viz. the schematisation of groynes, summer levees and steep obstacles. The red lines indicate the boundaries of the main channel. The dark blue lines represent the location of the river dikes enclosing the floodplains, the river axis and the position of groynes, derived from topographical maps. The green lines represent the km-locations in the reference grid. Plotting the green lines of the reference grid in the other figures with the new generated grids, gives an indication about the differences with respect to the reference grid.

The location of the weirs differs considerably in the various grids. A comparison of the location of groynes in the model schematisation (black lines) with the actual location of the groynes derived from topographical maps (dark blue lines) indicates to what extent the model schematisation reproduces reality. The best match is achieved by the original grid, Grid 1, Grid 1c and Grid 5.

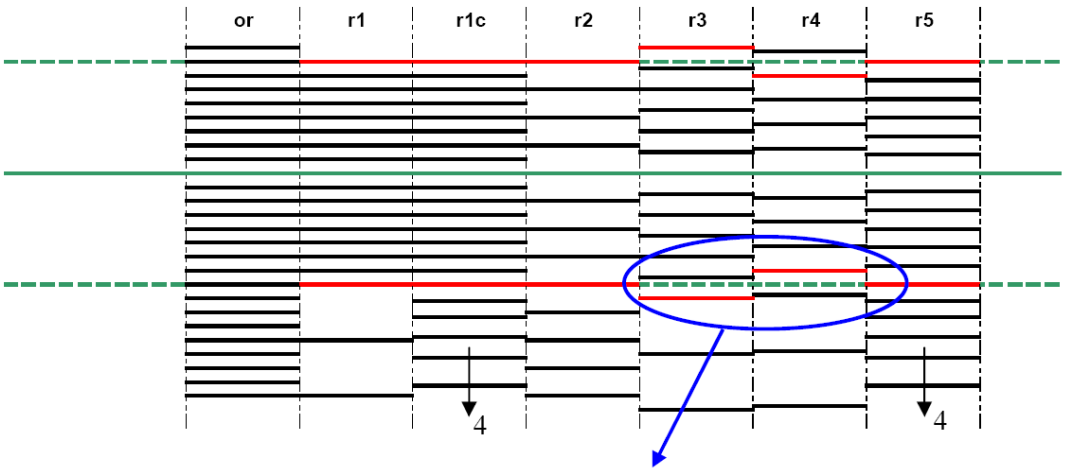

In principle, the red lines indicate the boundaries of the main channel section. The red lines for Grid 3 and 4 show that a slightly wider and narrower main channel section is used for the comparison of Grid 3 and Grid 4 with the reference model. This is because of the fact that the green dotted forming the boundaries of the main channel of the reference grid lines do not correspond with grid lines of Grid 3 and Grid 4.

Figure 2.2 Comparison of grid coarseness in transverse direction (green line: river axis; green dotted line: main channel boundary as defined by the groyne tips; red line: main channel boundary used for the comparison of the discharges through the main channel).

Table 2.3 Characteristics of the grids and computation time compared to the original grid.

Gridname	'or'	'r1'	'r1c'	'r2'	'r3'	'r4'	'r5'
Acceleration w.r.t. reference model (-)	0	1.6	1.2	3.7	3.8	4.1	2.4
number of grid cells	122 x 1401	48 x 1401	54 x 1401	61 x 701	40 x 935	39 x 801	47 x 1051
main channel							
number of grid cells	16	16	16	8	11	9	12
grid cell width (m)	~20	~20	~20	~40	~30	~35	~26
grid cell length (m)	~60	~60	~60	~120	~90	~105	~80
aspect ratio	1:3	1:3	1:3	1:3	1:3	1:3	1:3
floodplains							
number of cells, left	63	19	22	32	18	17	20
number of cells, right	43	13	16	21	12	12	15
grid cell width (m)	15-86	15-326	16-307	34-164	22-326	31-315	16-325
grid cell length (m)	6-123	5-120	6-120	10-240	8-178	12-206	9-156

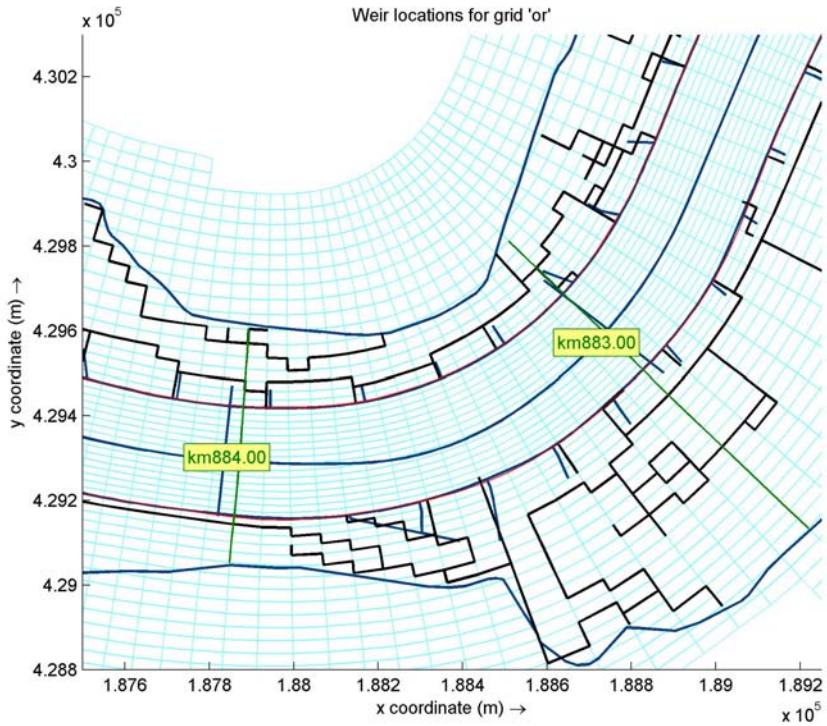

Figure 2.3 Computational grid of the original grid in the bend near Nijmegen (km 883-884) (black lines: model schematisation of the weirs; red lines: the boundaries of the main channel; dark blue lines: actual location of the river dikes enclosing the floodplains, the river axis and the position of groynes; green lines: projections of cross-sections in the reference grid).

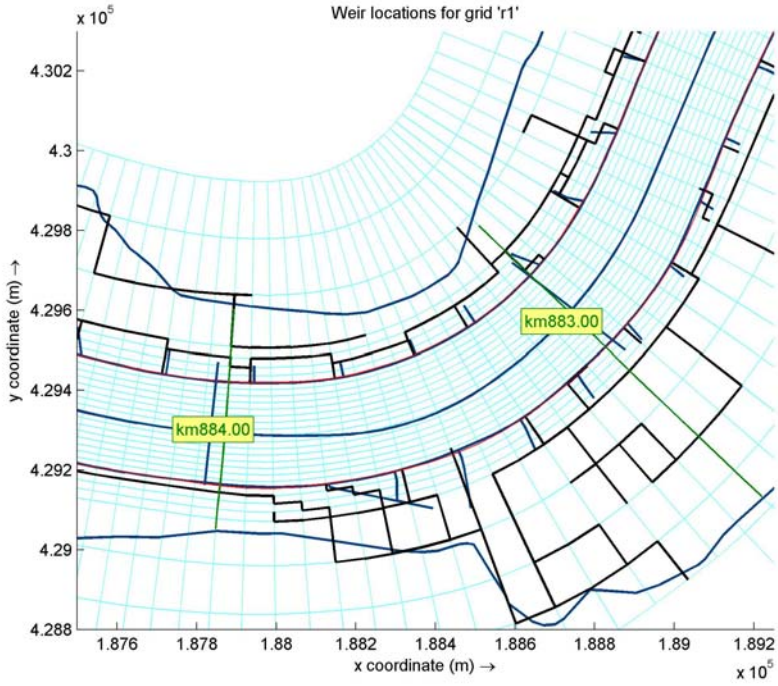

Figure 2.4 Computational grid of Grid 1 in the bend near Nijmegen (km 883-884) (black lines: model schematisation of the weirs; red lines: the boundaries of the main channel; dark blue lines: actual location of the river dikes enclosing the floodplains, the river axis and the position of groynes; green lines: projections of cross-sections in the reference grid).

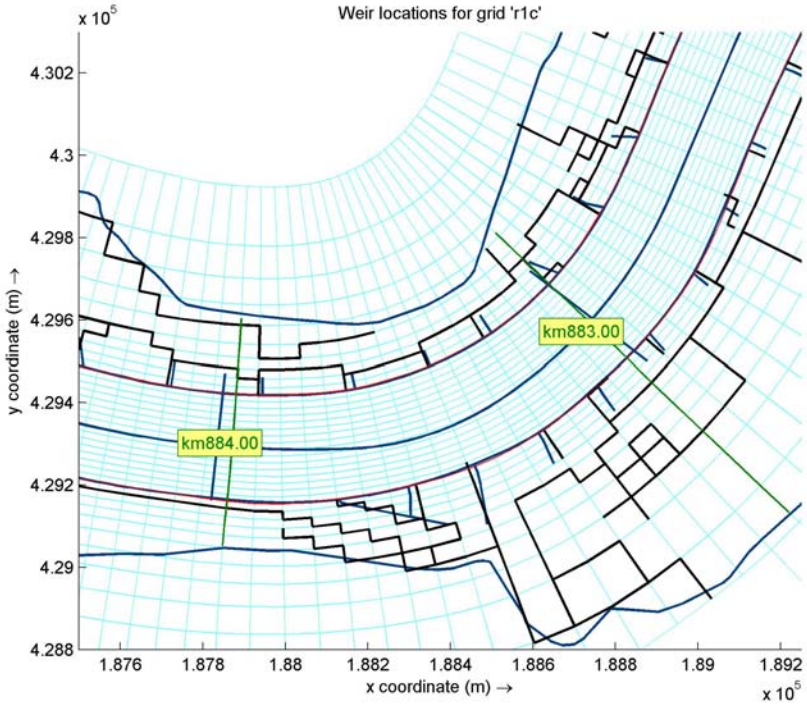

Figure 2.5 Computational grid of Grid 1c in the bend near Nijmegen (km 883-884) (black lines: model schematisation of the weirs; red lines: the boundaries of the main channel; dark blue lines: actual location of the river dikes enclosing the floodplains, the river axis and the position of groynes; green lines: projections of cross-sections in the reference grid).

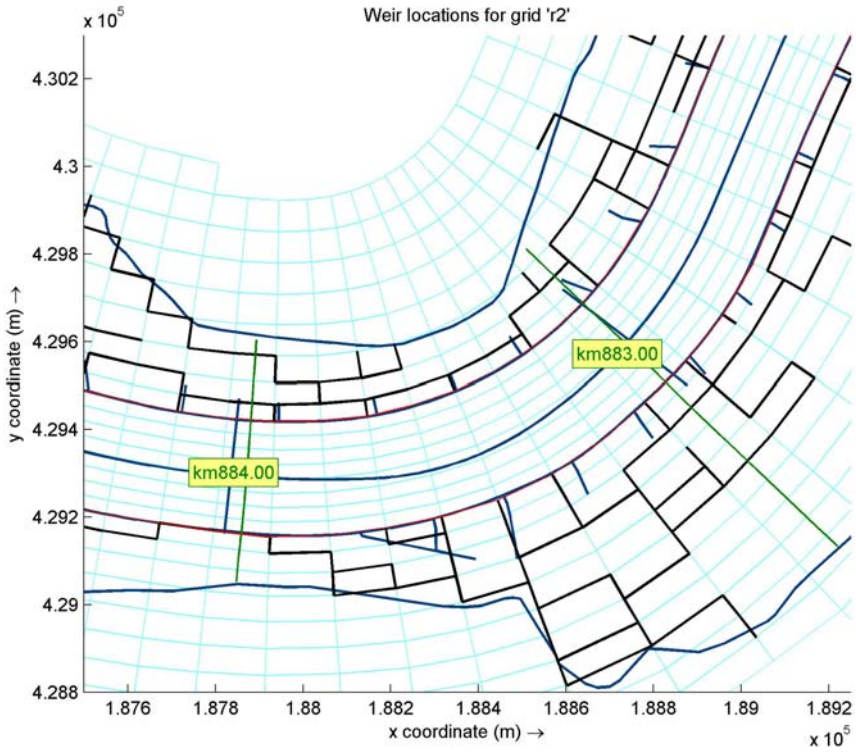

Figure 2.6 Computational grid of Grid 2 in the bend near Nijmegen (km 883-884) (black lines: model schematisation of the weirs; red lines: the boundaries of the main channel; dark blue lines: actual location of the river dikes enclosing the floodplains, the river axis and the position of groynes; green lines: projections of cross-sections in the reference grid).

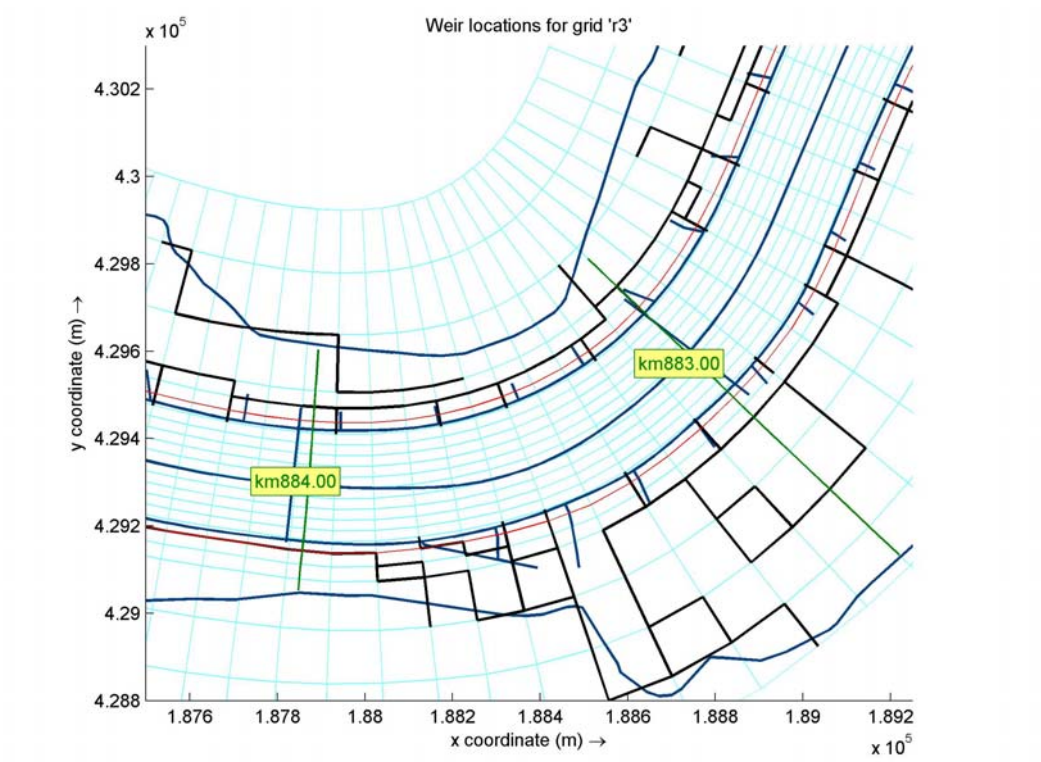

Figure 2.7 Computational grid of Grid 3 in the bend near Nijmegen (km 883-884) (black lines: model schematisation of the weirs; red lines: the boundaries of the main channel; dark blue lines: actual location of the river dikes enclosing the floodplains, the river axis and the position of groynes; green lines: projections of cross-sections in the reference grid).

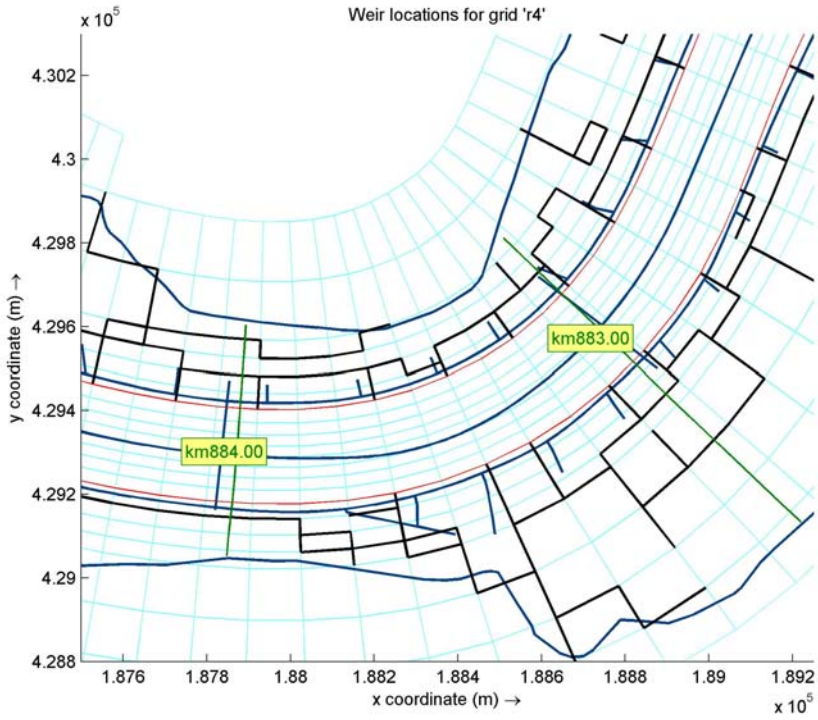

Figure 2.8 Computational grid of Grid 4 in the bend near Nijmegen (km 883-884) (black lines: model schematisation of the weirs; red lines: the boundaries of the main channel; dark blue lines: actual location of the river dikes enclosing the floodplains, the river axis and the position of groynes; green lines: projections of cross-sections in the reference grid).

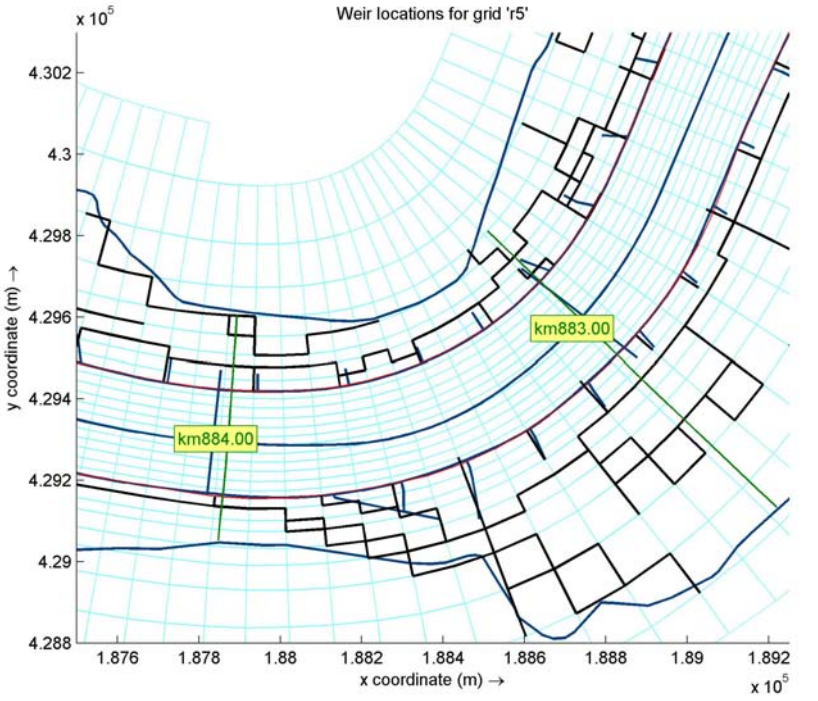

Figure 2.9 Computational grid of Grid 5 in the bend near Nijmegen (km 883-884) (black lines: model schematisation of the weirs; red lines: the boundaries of the main channel; dark blue lines: actual location of the river dikes enclosing the floodplains, the river axis and the position of groynes; green lines: projections of cross-sections in the reference grid).

2.3 Assessment of grid coarsening: difference in discharge distribution between floodplain and main channel

2.3.1 Introduction

The objective of this section is to evaluate the difference in discharge distribution between main channel and floodplains between the reference model and the models of the new generated grids in the previous section. At the end, not the difference between the reference model and the models of the coarsened grid is important, but the difference with respect to the discharge distribution derived from the hydrodynamic WAQUA model (that is officially used in purely hydrodynamic studies related to i.e. Room for the River and design water levels). Because the grid resolution of the reference model is quite high, we presume that the discharge distribution in that model comes close to the discharge distribution in WAQUA. This means that the differences in discharge distribution induced by grid coarsening with respect to the reference model gives a first indication of the differences with respect to the WAQUA model.

How these differences in discharge distribution are calculated is explained in Section 2.3.2. To be able to evaluate the differences, we start by defining a limit of acceptability of the difference in discharge distribution in Section 2.3.3.

Section 2.3.4 presents the differences in discharge distribution. First, the importance of gradually coarsening the grid covering the floodplain is investigated. Second, the impact of an increase in coarsening of the grid in longitudinal direction and in the main channel is addressed. Third, the impact of a grid that has been constructed on the basis of the outcomes of these comparisons is investigated.

River reaches at which the discharge flowing through the main channel differs significantly from that in the reference model, are analysed in more detail in Section 2.3.5. Because at the end all models need to be calibrated on the relevant hydraulics of WAQUA, this section is not meant to identify the optimal grid, but is rather meant to emphasise the need and the importance of a hydraulic calibration involved by (whatever) grid coarsening.

2.3.2 Calculation of the discharge distribution

In order to determine the discharge distribution between main channel and floodplains for all grids and all discharge levels, first the discharge in each grid cell perpendicular to the direction of flow is calculated. The total discharge is derived by adding up the discharges in the direction of flow Q_v of all grid cells in transverse direction:

$$Q_{tot}(n) = \sum_m Q_v(n,m) \qquad (2\text{-}1)$$

The main channel discharge Q_{mc} is calculated analogously but considering only those grid cells that lie between the main channel boundary lines, i.e. the red lines in Figure 2.3 to Figure 2.9. The discharge in the floodplains is the difference between total and main channel discharge.

In Sections 2.3.3 and 2.3.4 the main channel discharges of different grids are compared. Due to coarsening in longitudinal direction, not all grid lines in m-direction of the new generated grids correspond with grid lines of the reference grid. For each grid line in m-direction of the new generated grid i that coincides with a grid line of the reference grid j, the absolute and relative difference in main channel discharge, $dQ_{abs,ij}(m)$ and $dQ_{rel,ij}(m)$ is calculated:

$$dQ_{abs,ij}(n) = Q_{mc,i}(n) - Q_{mc,j}(n) \quad (2\text{-}2)$$

$$dQ_{rel,ij}(n) = 100 \cdot \frac{dQ_{abs,ij}(n)}{Q_{tot}(1)} \quad (2\text{-}3)$$

In other words, since Grid 2 is coarsened by a factor of 2 in longitudinal direction, the main channel discharge at every second m-grid line of the reference grid is compared with the main channel discharge at every m-grid line of Grid 2.

2.3.3 Limit of acceptability of the difference in main channel discharge

A limit of acceptability of the difference in discharge distribution is defined in this section. In absence of observational data, the simulation with the reference model is used as an approximation of the 'true' discharge distribution. Initially, as a limit of acceptability, a maximum difference of 2% between the main channel discharge in the reference model and in the model with coarsened grid was proposed by the client Rijkswaterstaat.

To evaluate whether this limit of acceptability is a realistic requirement, the spatial variation of the discharge flowing through the main channel is quantified for the reference model. Figure 2.10 illustrates that this spatial variation boils down to 3.5% for a discharge of 1187 m^3/s, i.e. this variation exceeds the limit of acceptability of 2 %. A 2-D analysis of the flow pattern showed that the spatial variation in main channel discharge is caused by eddy formation in the groyne fields and lateral in- and out flow into the groyne fields.

The position of the groynes in the model schematisation appears to affect the main channel discharge. Although the location of the groynes in, for instance, the reference grid (Figure 2.3) and Grid 5 (Figure 2.9) both fairly match the actual location of the groynes (indicated by the dark blue lines in the figures), the main channel discharge in Grid 5 appears to deviate up to 5 % from the main channel discharge in the reference model. This becomes evident in Figure 2.11 that presents the main channel discharge of both models for a discharge of 1187 m^3/s.

Considering both aspects, differences up to 3-5% seems justified. Larger deviations are acceptable as long as they can be eliminated or reduced by calibration.

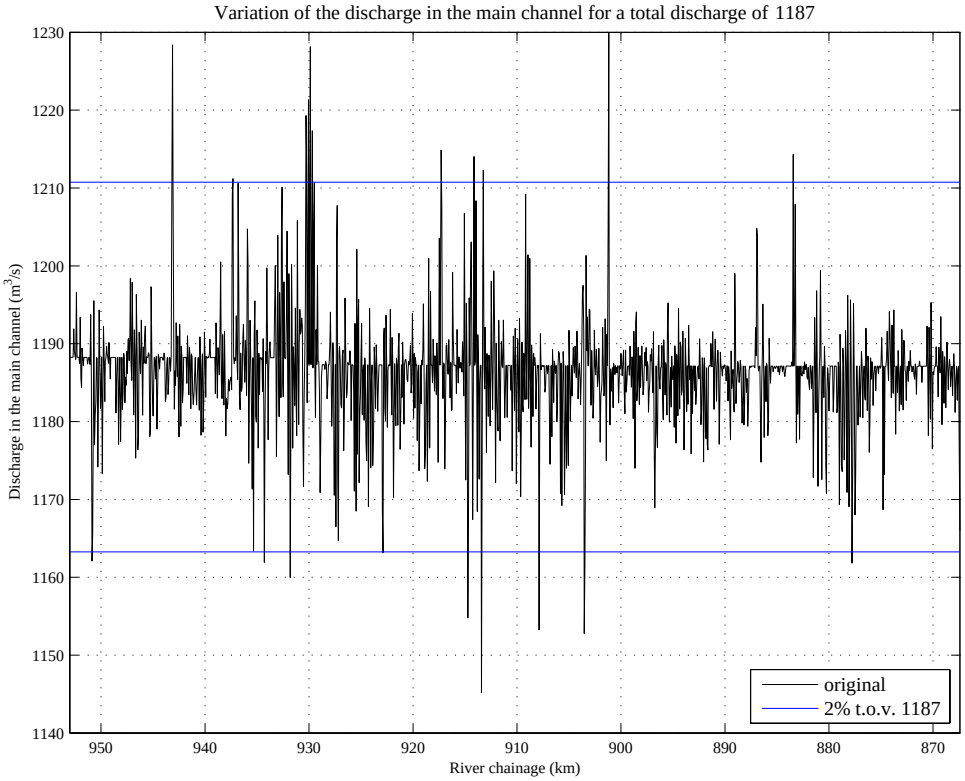

Figure 2.10 Spatial variation of the discharge flowing through the main channel for a discharge of 1187 m^3/s, quantified for the reference model.

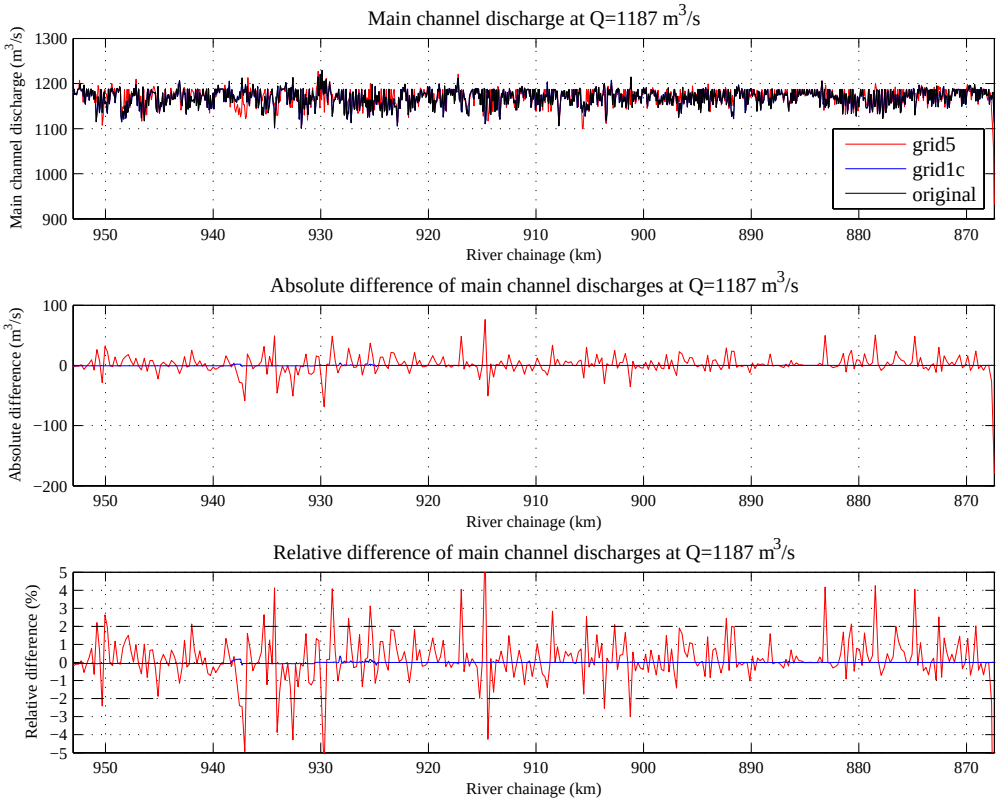

Figure 2.11 Main channel discharge in the reference model and the models of Grid 1c and Grid 5 for a discharge of 1187 m^3/s.

2.3.4 Differences in discharge distribution between floodplain and main channel

Importance of gradually coarsening the grid covering the floodplain

The importance of gradually coarsening the grid covering the floodplain is investigated by comparing the differences in main channel discharge between the reference model and the models of Grid 1 and Grid 1c. In Grid 1, the grid covering the floodplain is coarsened by a factor 4. The transition from fine grid covering the main channel and groyne section to the coarsened floodplain is rather abrupt, see Figure 2.4. In Grid 1c gradually coarsening is applied, see Figure 2.5.

Figure 2.12 presents the differences in absolute values and in terms of percentages. The difference between main channel discharge of Grid 1 and Grid 1c is significant. At a number of locations the coarsening is too abrupt causing a large difference in main channel discharge. The figure clearly indicates the importance of gradually coarsening the grid covering floodplain.

The river reaches between km 907 – km 910 and between km 937 – km 939 at which the discharge flowing through the main channel differs significantly from that in the reference model, are analysed in more detail in Section 2.3.5.

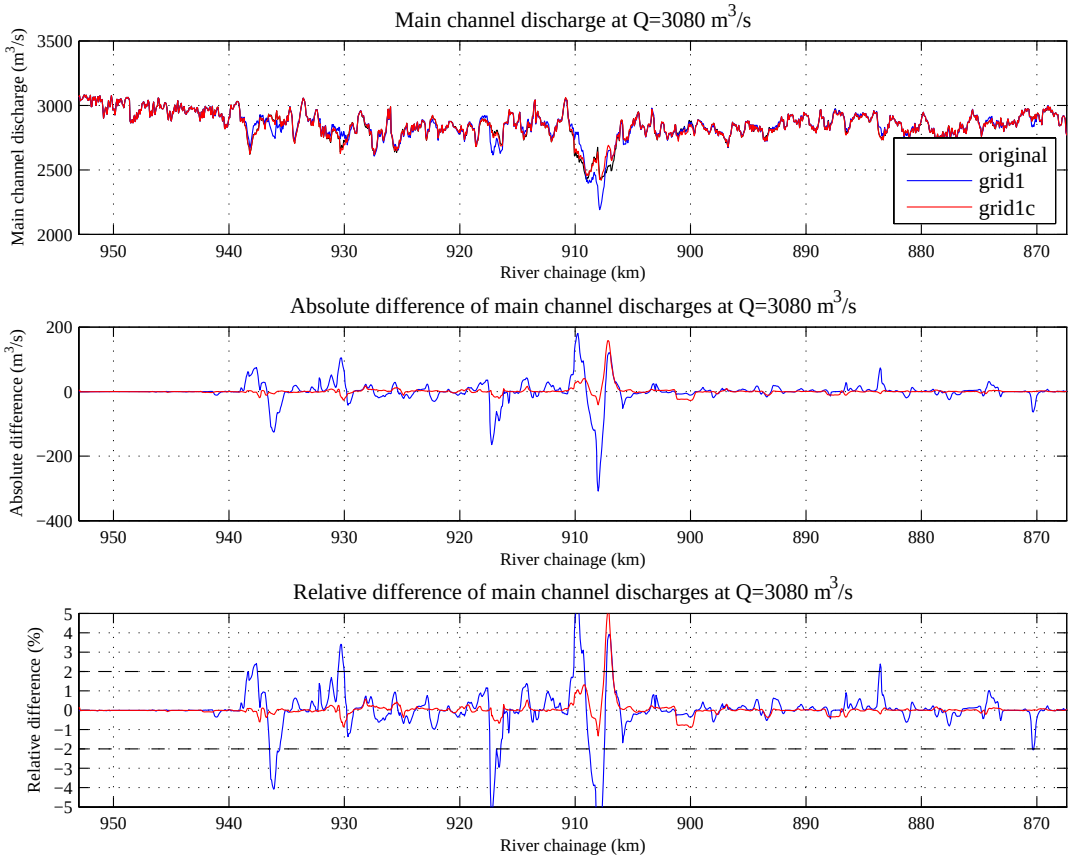

Figure 2.12 Main channel discharge in the reference model and in the models of Grid 1 and Grid 1c for a discharge of 3080 m^3/s.

Grid coarsening in longitudinal and transverse direction

The impact of coarsening of the grid in longitudinal direction and in the main channel is addressed below. For this assessment the model results of Grid 3 and Grid 4 are assessed. This activity took place in parallel with testing the gradually coarsening of the floodplain in transverse direction. Grid 1 with the rather abrupt transition from the fine to coarse grid was used as a base grid. The grid is first coarsened in longitudinal direction by a factor of 1.5 for Grid 3 and by a factor of 1.75 for Grid 4. In addition the same coarsening factors are applied in transverse direction to the grid in the main channel and groyne section. The transverse coarsening of the main channel grid caused a 'shift' of the grid lines bordering the main channel. As indicated in Section 2.2.2, respectively a slightly wider and a slightly narrower main channel section is used for the comparison of Grid 3 and Grid 4 with the reference model.

In Figure 2.13 and Figure 2.14 the main channel discharge of Grids 1, 3 and 4 is compared to that of the reference model for a discharge of 3080 m^3/s. As indicated in the figures the difference in the main channel discharge with respect to the reference model increases, as a result of coarsening the main channel grid in longitudinal and transverse direction. The main channel discharge in Grid 3 deviates more from the reference model than Grid 1. The coarsening in Grid 4 blows up the difference in main channel discharge and often exceeds the limit of acceptability of 3-5%.

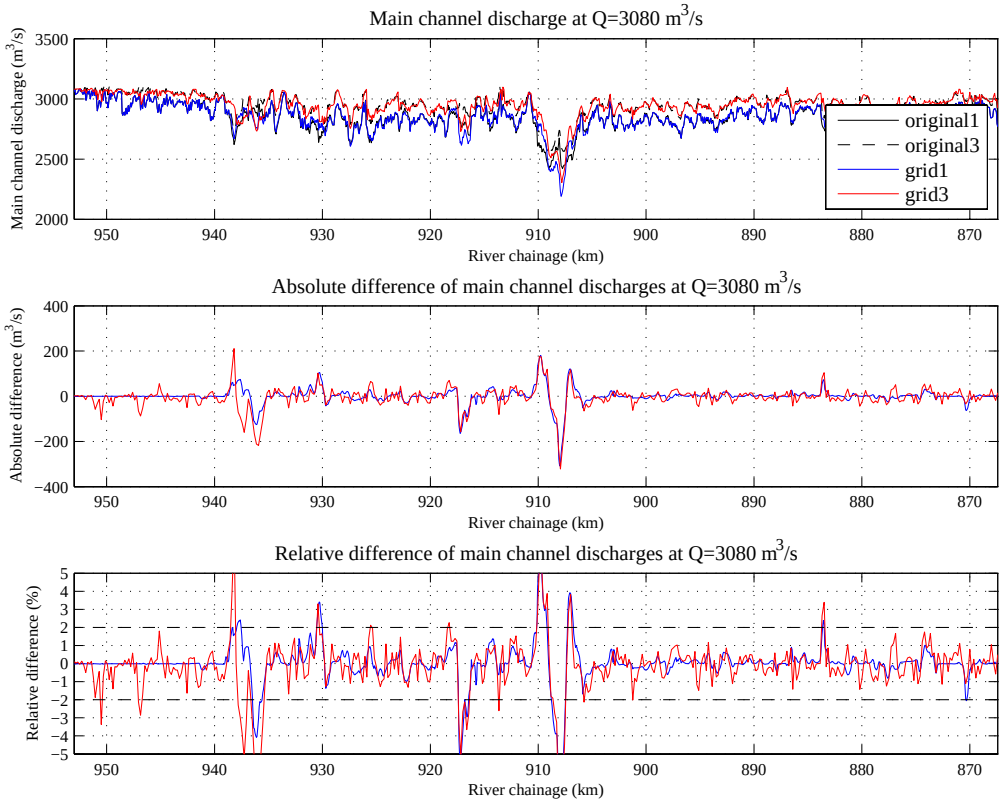

Figure 2.13 Main channel discharge in the reference model and in the models of Grid 1 and Grid 3 for a discharge of 3080 m^3/s.

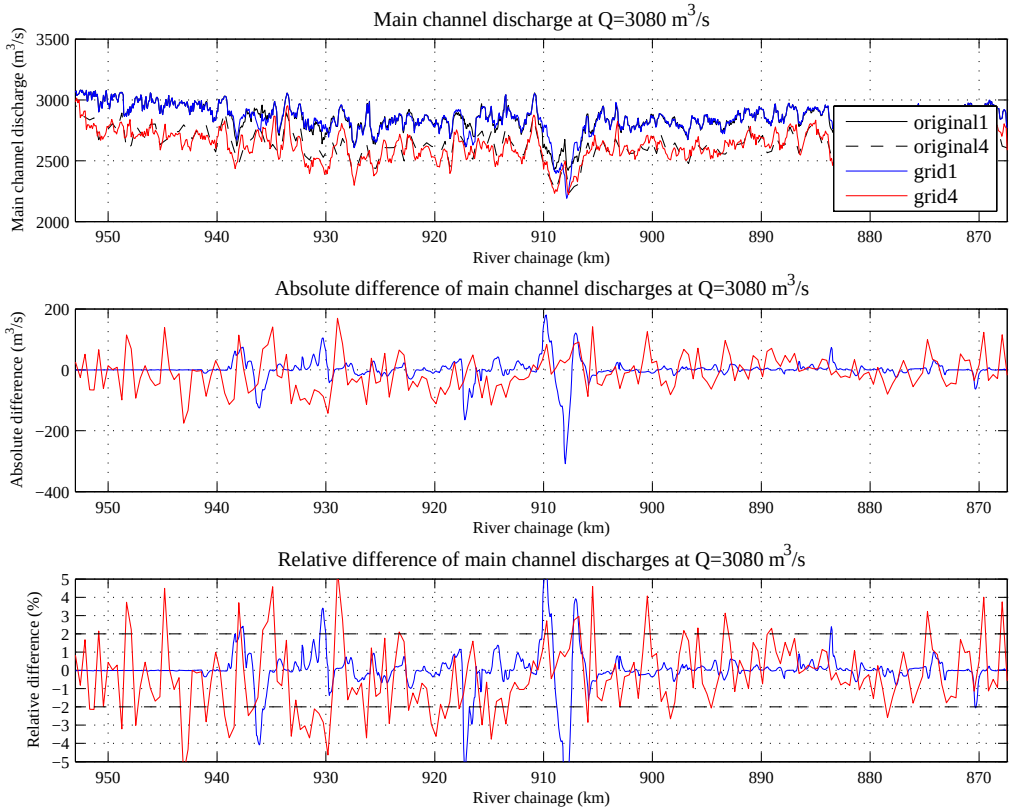

Figure 2.14 Main channel discharge in the reference model and in the models of Grid 4 for a discharge of 3080 m^3/s.

Not only the mutual distance between groynes appears to be relevant, also the extent to which the groynes protrude into the main channel is important. Moreover, in the models a groyne is projected on a discrete number of grid cells, meaning that the height of the groyne in each grid cell resembles the average height in its surrounding distance. In case the grid cells become larger in size, the 'groyne height' is averaged-out over a larger distance. This inevitably affects the flow pattern. Figure 2.8 shows that the groynes in the model schematisation of Grid 4 protrude far into the main channel, contributing to larger deviations in main channel discharge.

In addition to the grid coarsening above, in the preceding DVR project in Mosselman et al. (2006), the grid was coarsened by a factor 2 in longitudinal and transverse direction. This grid resembles more or less the maximum allowed grid. Figure 2.15 shows the performance of this grid for a discharge level of 1187 m^3/s, 2000 m^3/s and 3080 m^3/s. The main channel discharge starts to deviate from the reference model along the entire Waal branch. Deviations become more structural instead of isolated single river locations. Whether these deviations are too large to be removed by a hydraulic calibration depends on the quality of the calibration tool. Reducing the number of grid cells to 8 implies that the average grid cell width is 40 m. Considering the fact that the outer grid cells are fixed in order to avoid large erosion pits near groynes make the alluvial width rather small. We have the impression that the deviations due to this grid are high and would require significant effort to be removed using a calibration tool.

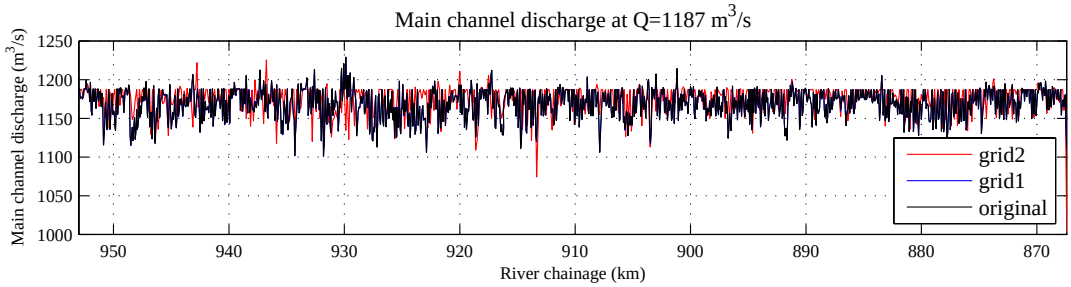
Main channel discharge at Q=1187 m3/s
Main channel discharge (m3/s)
River chainage (km)
grid2
grid1
original

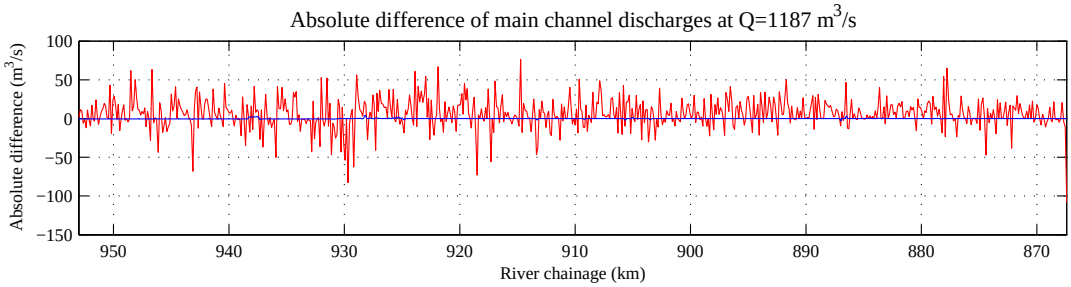
Absolute difference of main channel discharges at Q=1187 m3/s
Absolute difference (m3/s)
River chainage (km)

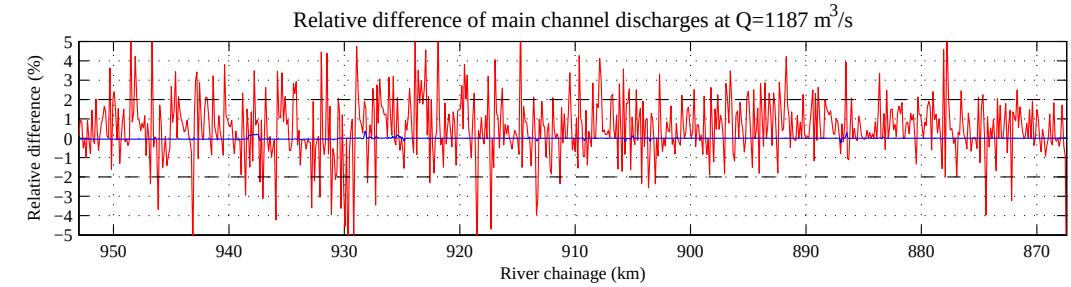
Relative difference of main channel discharges at Q=1187 m3/s
Relative difference (%)
River chainage (km)

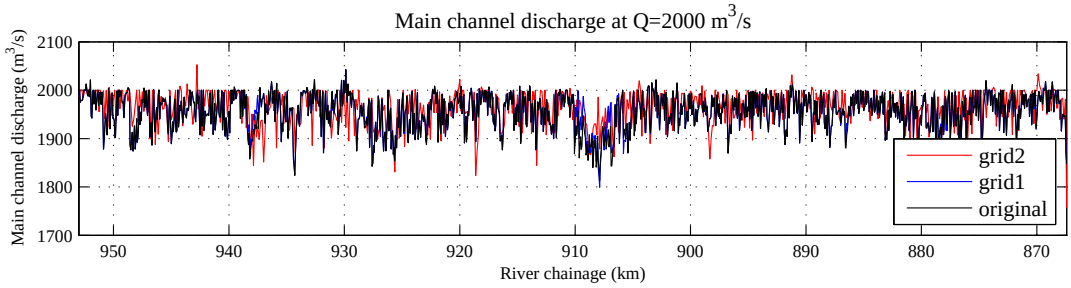
Main channel discharge at Q=2000 m3/s
Main channel discharge (m3/s)
River chainage (km)
grid2
grid1
original

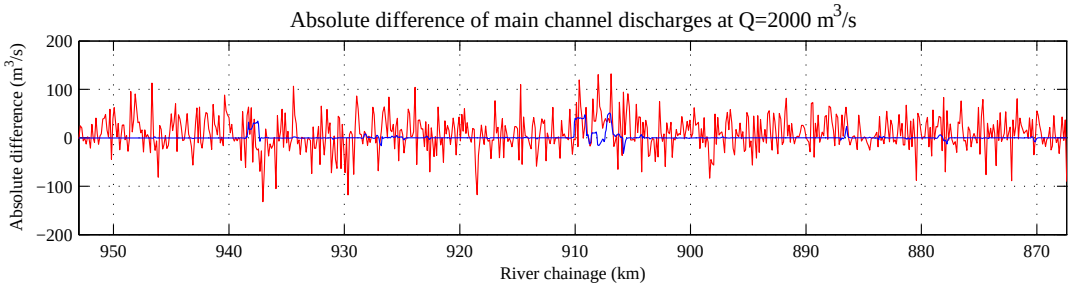
Absolute difference of main channel discharges at Q=2000 m3/s
Absolute difference (m3/s)
River chainage (km)

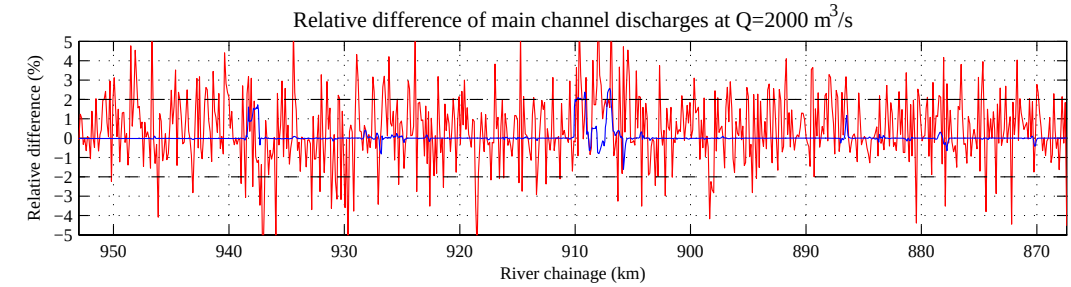
Relative difference of main channel discharges at Q=2000 m3/s
Relative difference (%)
River chainage (km)

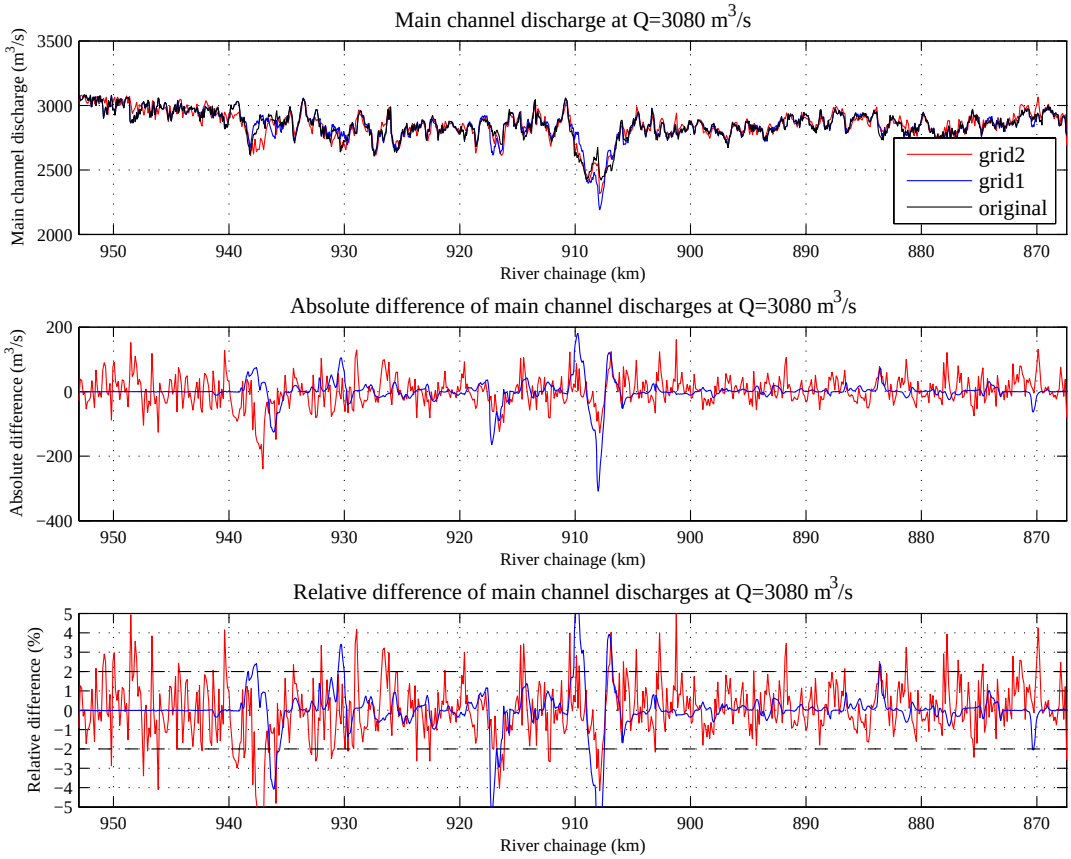

Figure 2.15 Main channel discharge in the reference model and in the models of Grid 2 for a discharge of 1187 m^3/s, 2000 m^3/s and 3080 m^3/s.

Optimisation of the model grid

On the basis of the outcomes of investigating the importance of 1) gradually coarsening the grid covering the floodplain; and 2) grid coarsening in longitudinal and transverse direction, Grid 5 has been constructed. Grid 5 contains a gradually coarsened floodplain grid up to a factor 4. For the coarsening in longitudinal direction of the entire grid and the coarsening in transverse direction of the grid in the main channel and groyne section, a factor 1.33 is used.

Figure 2.16 to Figure 2.19 show the differences in main channel discharge for the reference model and Grid 1c and Grid 5 for a discharge of 1187, 2000, 3080, 4422 m^3/s. The main channel discharge of Grid 5 deviates more from the reference model than Grid 1c. In general, the differences in main channel discharge fulfil reasonably well the limit of acceptability. The differences appear to be larger for the lower discharge of 1187 and 2000 m^3/s than for the higher discharge of 3080 and 4422 m^3/s. Apparently, the main channel discharge is more sensitive to differences in the positions and heights of groynes for lower than for higher discharges.

At a few river reaches, among which the reaches between km 907 – km 910 and km 937 – km 939, the difference in main channel discharge exceeds this limit. The discharge

distribution and flow pattern for these river reaches are analysed in more detail in Section 2.3.5.

The larger deviations are acceptable as long as they can be eliminated or reduced by calibration. Since the larger deviations are not structural, but concerns single river locations, the deviations can be reduced by calibration. It is expected that via imposing inflow and outflow points of discharges, the differences in main channel discharge can be reduced. The tool for imposing lateral discharges which is developed in Section 5.3 could be used for calibration purposes.

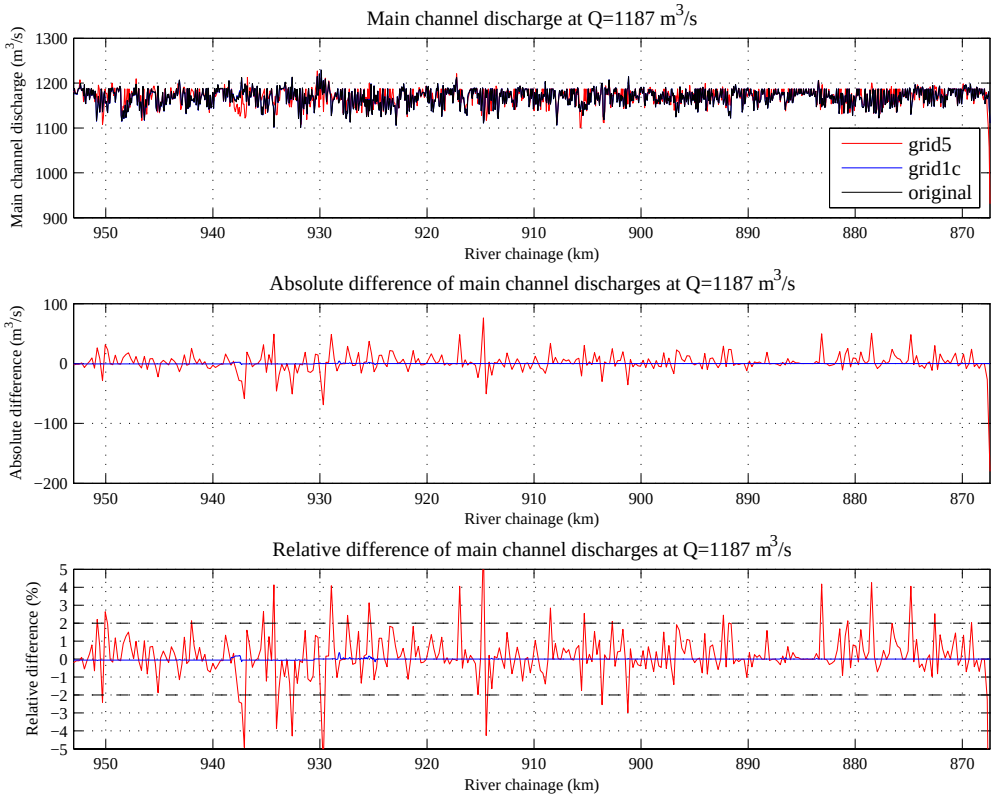

Figure 2.16 Main channel discharge in the reference model and in the models of Grid 5 for a discharge of 1187 m^3/s.

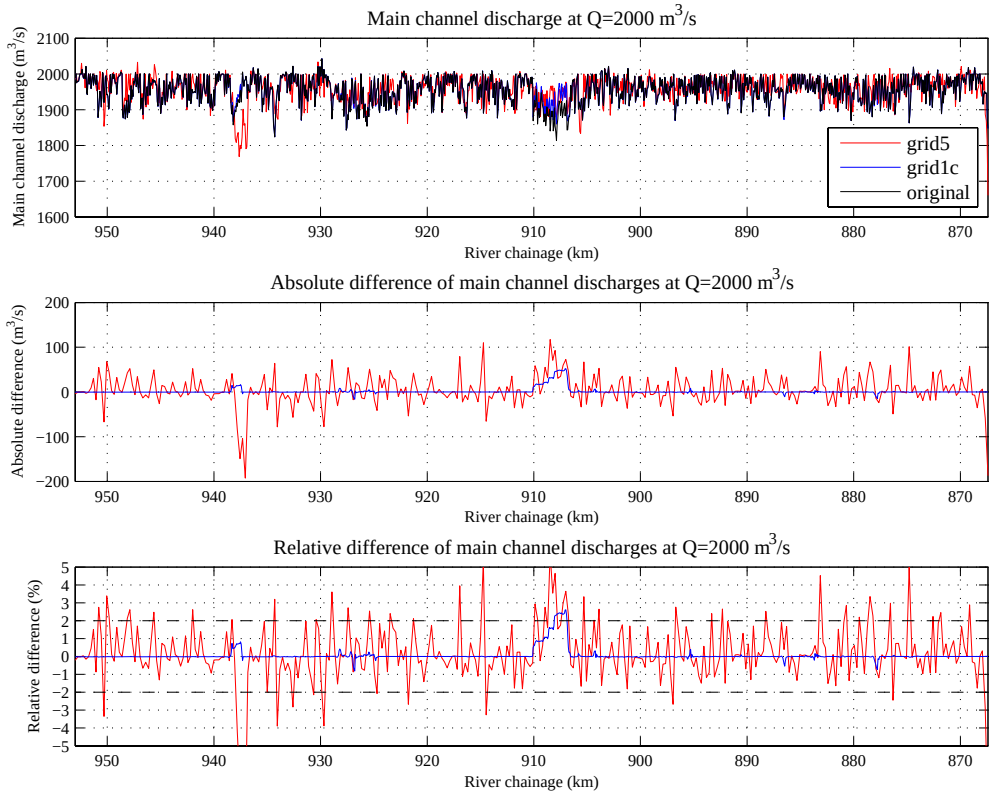

Figure 2.17 Main channel discharge in the reference model and in the models of Grid 5 for a discharge of 2000 m^3/s.

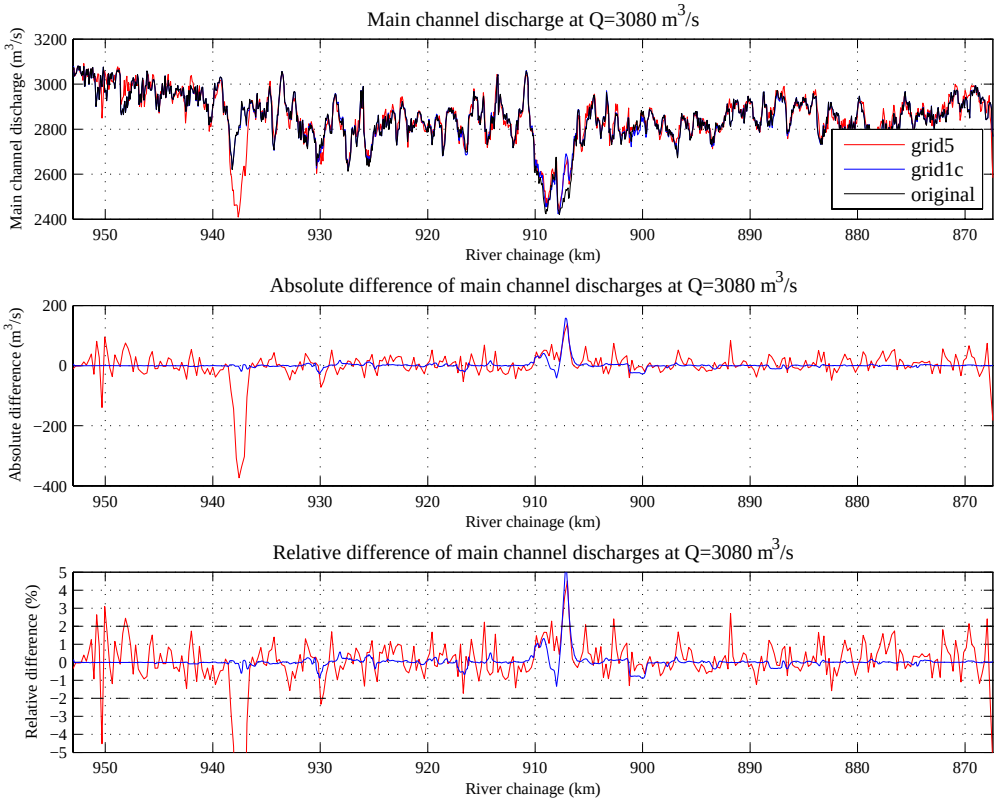

Figure 2.18 Main channel discharge in the reference model and in the models of Grid 5 for a discharge of 3080 m^3/s.

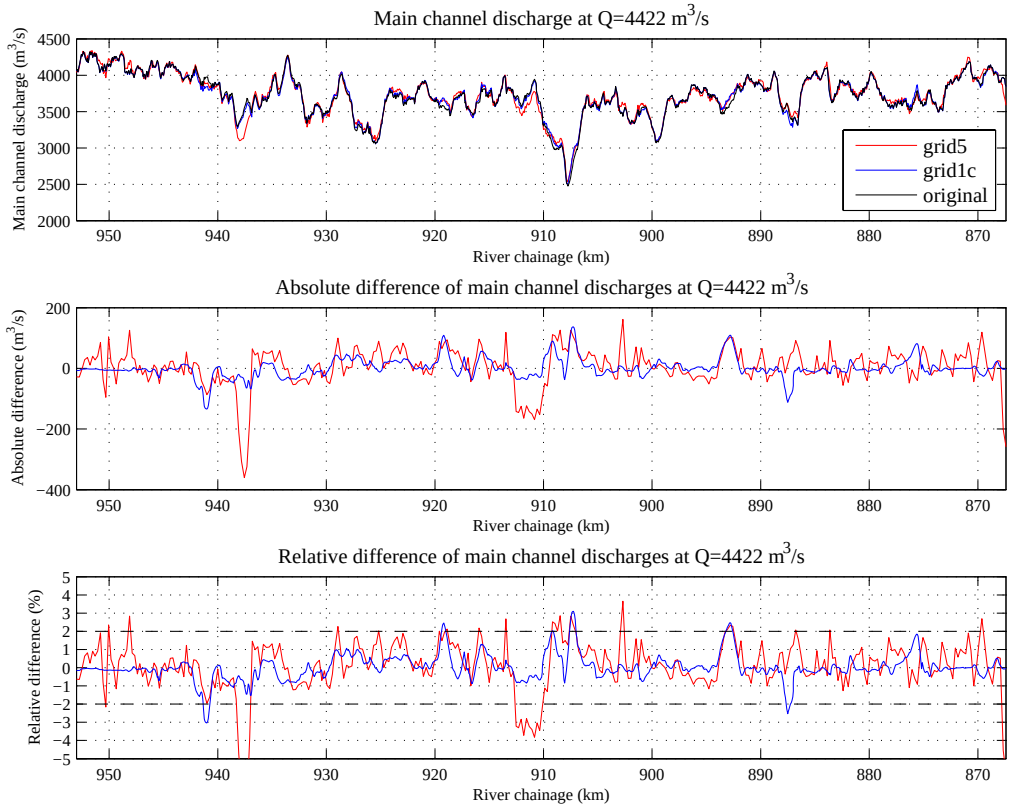

Figure 2.19 Main channel discharge in the reference model and in the models of Grid 5 for a discharge of 4422 m^3/s.

2.3.5 Deviations in discharge distributions and need for a hydraulic calibration tool

River reach near Ochten km 907-910

Figure 2.20 shows an aerial photograph of the bend near Ochten. The photograph illustrates the location of a large open water area between km 906 and km 908 in the floodplain 'Willemspolder', followed by a sudden width-reduction just beyond km 908. The inflow of water into the open water area is partly restricted by longitudinal levees at either sides of the river.

The location Ochten with the large variation in floodplain width in combination with the large ponds appears to be sensitive for grid coarsening. Grid coarsening results in an averaging-out of the geometrical information.

Slightly coarsening the grid already significantly affects the flow pattern. This is clearly indicated in Figure 2.21 to Figure 2.23. The figures show the flow pattern indicating the depth-averaged flow velocity during a discharge of 3080 m^3/s, along with the unit discharge, for the reference model and the models of Grid 1 and Grid 1c. The unit discharge presents the discharge per unit of grid cell width. To focus on what enters and leaves the main channel the unit discharge is curtailed at 1 $m^3/s/m$. The black lines in the figure represent the

weirs. It becomes evident that different flow patterns develop in the models of the various grids. The differences are more pronounced at the left side than at the right side.

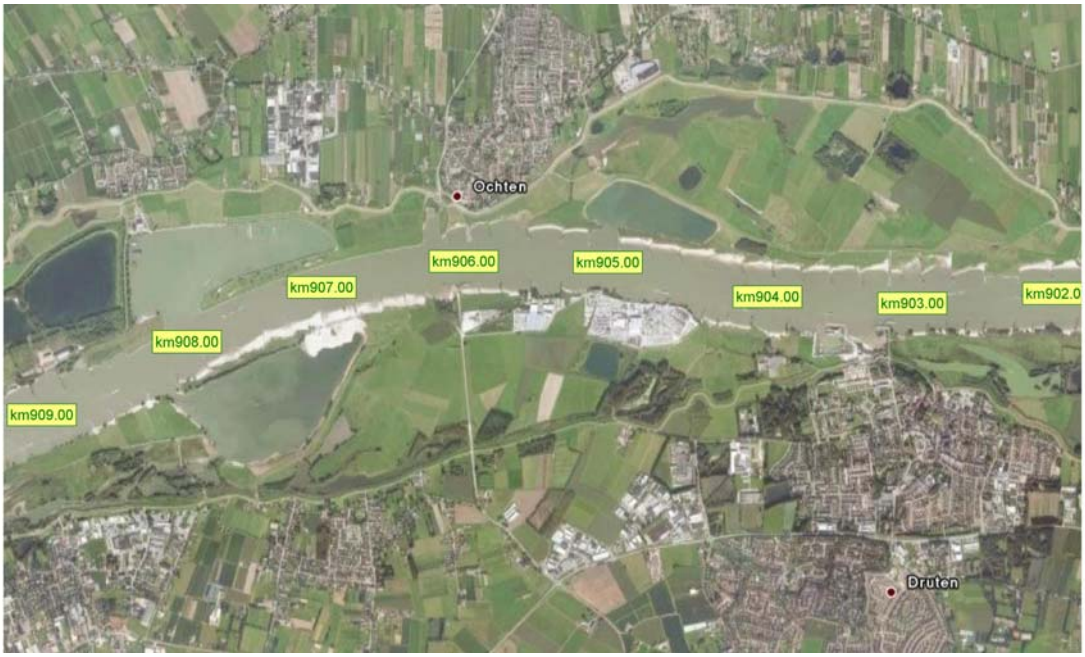

Figure 2.20 Aerial photograph of the bend near Ochten with river chainage (source: Google Earth).

An explanation for the differences in flow pattern and main channel discharge can be found in a combination of the following factors:

1. In the reference grid there is a gap between two levees in the floodplain at the left side at km 907, whereas these levees are connected in Grid 1 and Grid 1c. The difference in model schematisation is indicated by the red circles in Figure 2.21, Figure 2.22 and Figure 2.23. The closure of the weirs in Grid 1 and Grid 1c prevents water flowing into the pond from upstream direction at discharges above bankfull. As a consequence, in comparison to the reference model a local increase in main channel discharges is predicted at km 907, see Figure 2.12. It has not been verified whether the gap or the closure is correct. It is known that some of these gaps have been errors in Baseline in the past. In this study, we presume the Baseline projection of the reference model is correct.

2. The crest level of the longitudinal levee bordering the pond at the left side is much lower for the coarsened grids, Grid 1 and Grid 1c, than the crest level of the levee in the reference situation. Moreover, in the coarsened grids the edges of the pond are shallower than in the reference model. Averaging-out of geometrical information at this location is more pronounced since the sides of the pond are modelled as bed levels, instead of weirs. Figure 2.24 to Figure 2.26 presents the initial bed topography of the reference model and the models of Grid 1 and Grid1c. The lower levees in Grid 1 and Grid1c lead to more frequent and more extensive inflow in to the open water area yielding a decrease in main channel discharge at km 908 in comparison to the reference model, see Figure 2.12.

In other words, the averaging-out of the geometrical information in Grid 1 and Grid1c significantly affects the position and height of weirs and levees. Moreover it influences the initial bed topography of the new models.

Both resulted in a mismatch of the main channel discharge between km 907 and km 909. The model of Grid 1c performs better than the model of Grid 1. This emphasizes the importance of gradually coarsening the grid covering the floodplain. Moreover, the figures emphasise the need for a hydraulic calibration tool to reduce or eliminate local deviations in discharge distribution induced by grid coarsening.

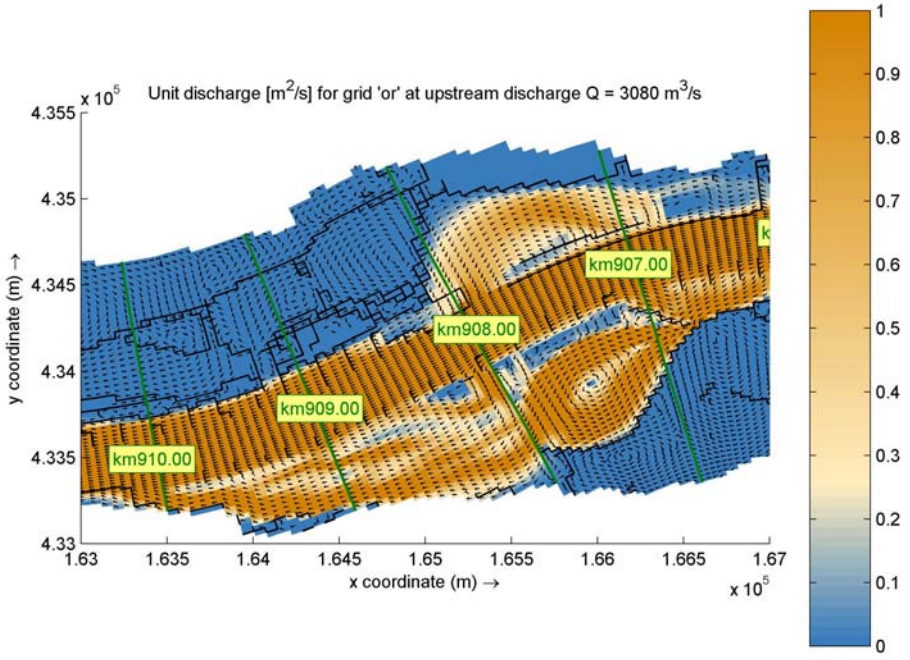

Figure 2.21 Flow pattern, indicating the depth-averaged flow velocity during a discharge of 3080 m^3/s, along with the unit discharge, presenting the discharge per unit of grid cell width for the reference model.

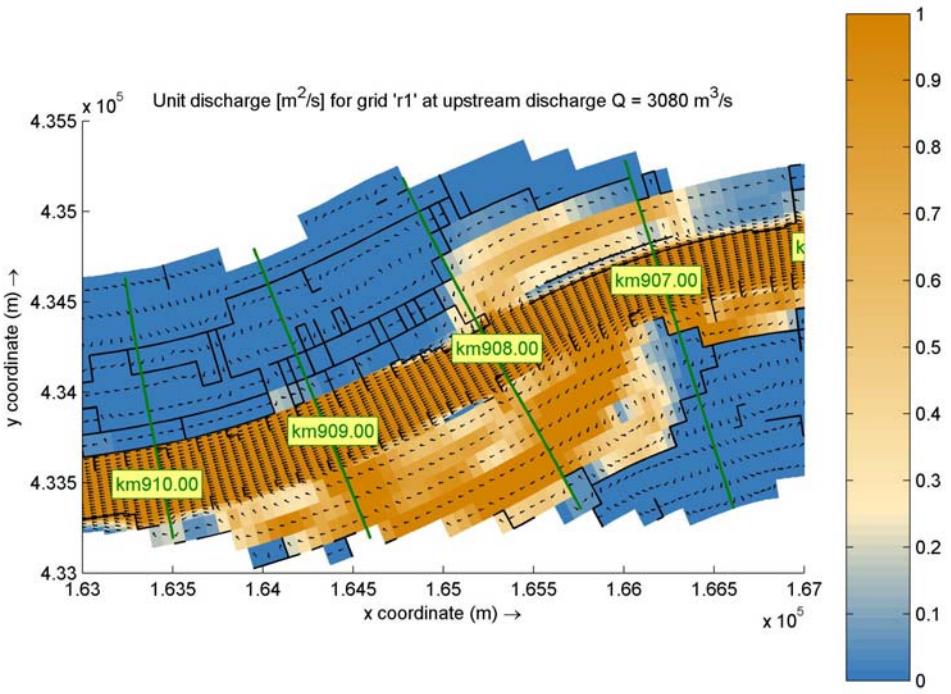

Figure 2.22 Flow pattern, indicating the depth-averaged flow velocity during a discharge of 3080 m^3/s, along with the unit discharge, presenting the discharge per unit of grid cell width for the model of Grid 1.

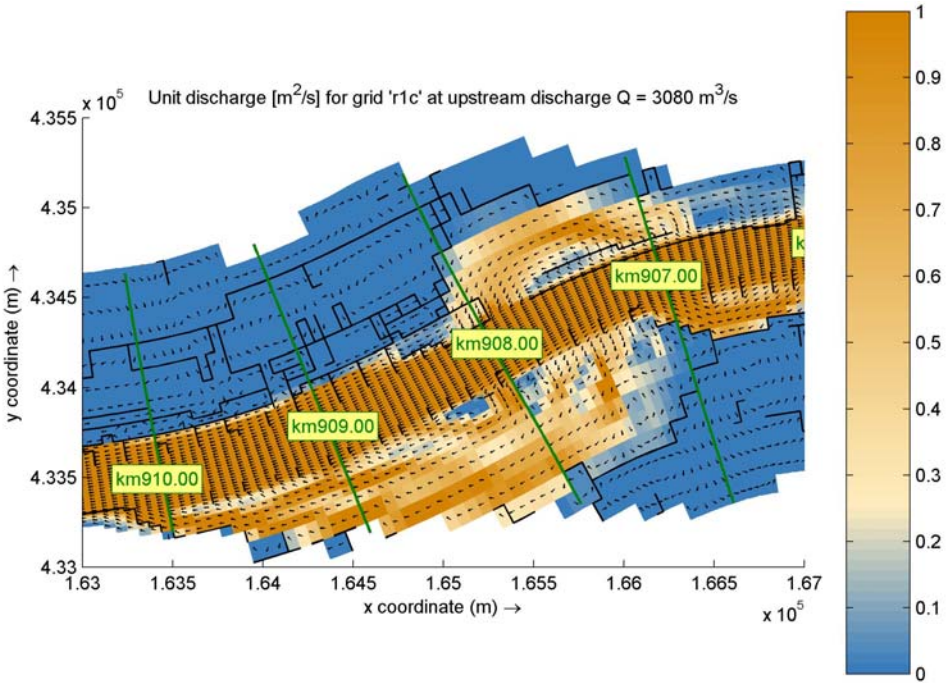

Figure 2.23 Flow pattern, indicating the depth-averaged flow velocity during a discharge of 3080 m^3/s, along with the unit discharge, presenting the discharge per unit of grid cell width for the model of Grid 1c.

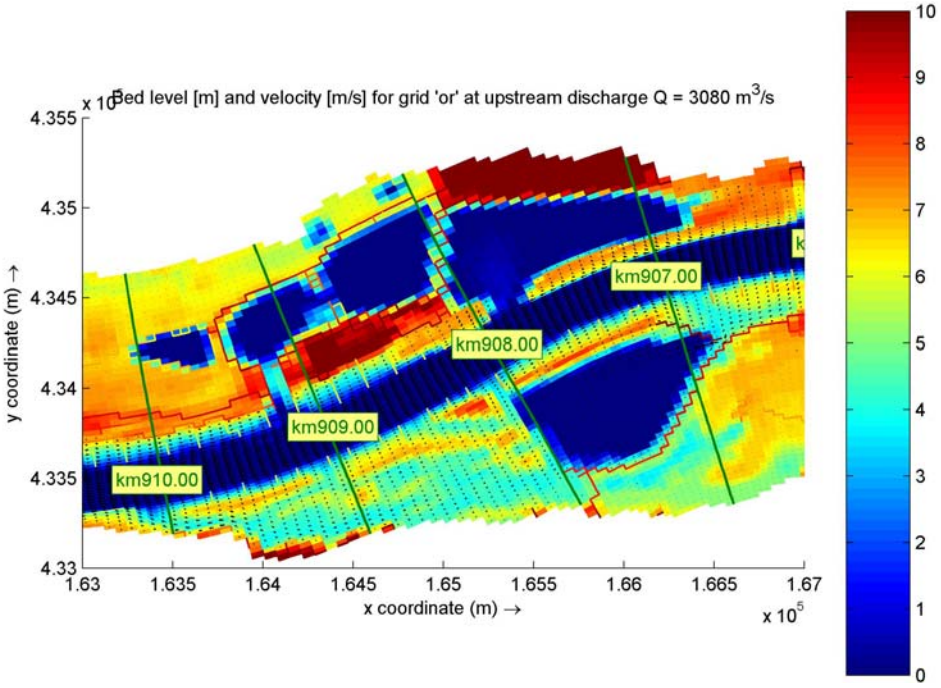

Figure 2.24 Initial bed level, weir heights and flow pattern indicating the depth-averaged velocity of the reference model.

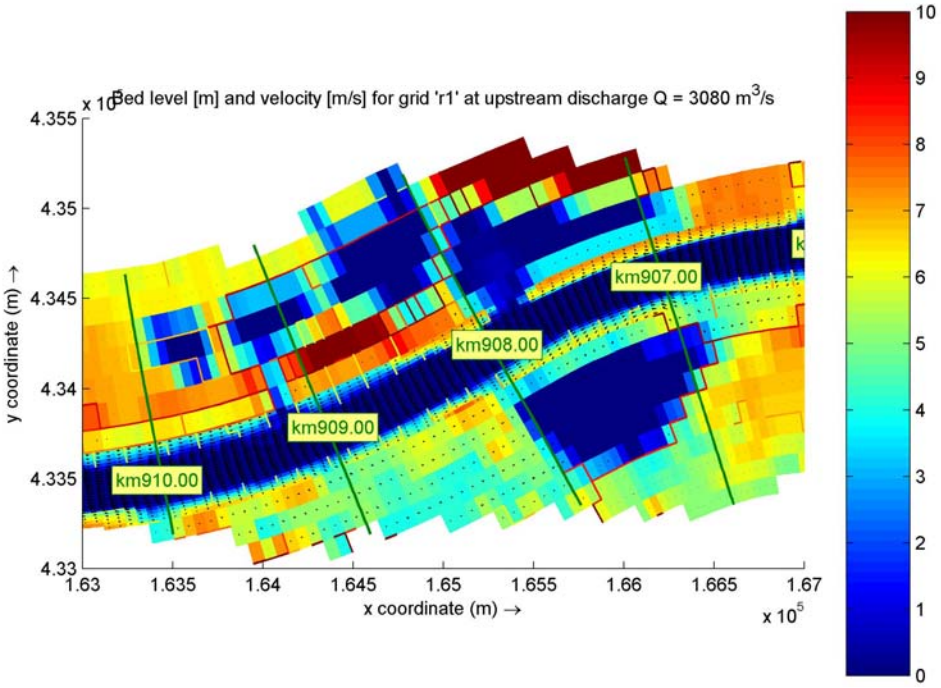

Figure 2.25 Initial bed level, weir heights and flow pattern indicating the depth-averaged velocity of the model of Grid 1.

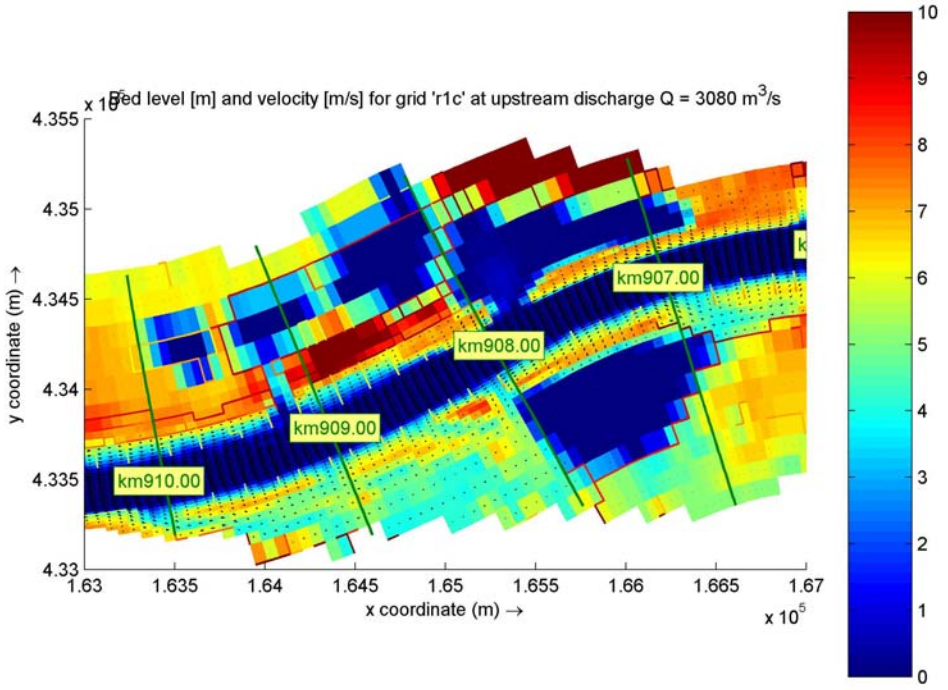

Figure 2.26 Initial bed level, weir heights and flow pattern indicating the depth-averaged velocity of the model of Grid 1c.

In correspondence with Grid1c, Grid 5 show more or less the same flow pattern, see Figure 2.27. As indicated in 2.3.4 the differences in main channel discharge can be reduced by a calibration tool .

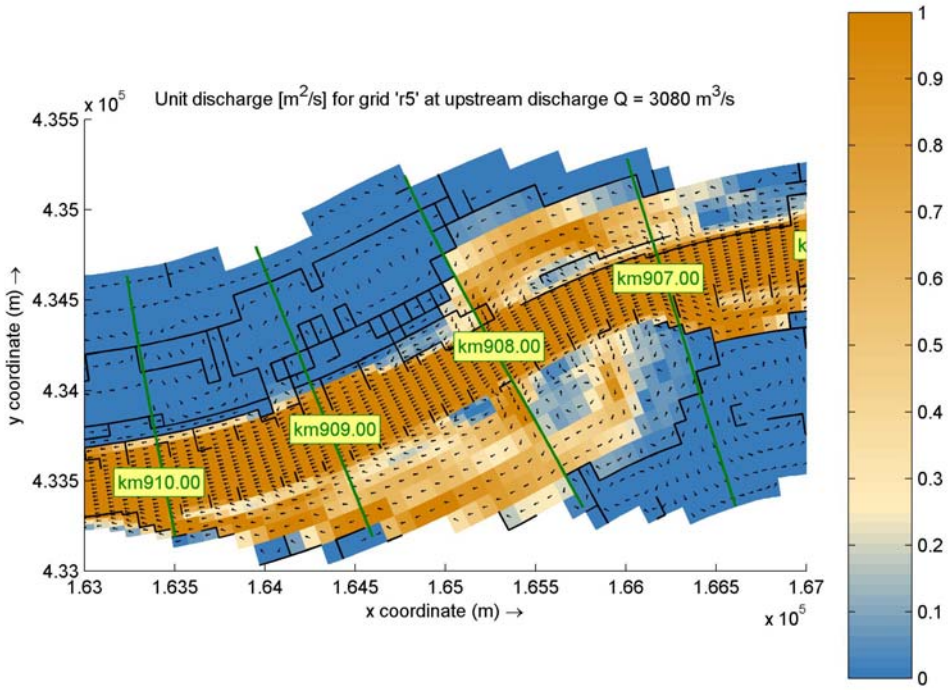

Figure 2.27 Flow pattern, indicating the depth-averaged flow velocity during a discharge of 3080 m^3/s, along with the unit discharge, presenting the discharge per unit of grid cell width for the model of Grid 5.

River reach Gamerensche Waarden km 937-939

Figure 2.28 shows an aerial photograph of the floodplain area Gamerensche Waarden. The photograph illustrates the location of open water areas between km 937 and km 938. In this example, we are interested in the left side of the floodplain. The inflow of water into the open water area is partly restricted by some higher situated levees at left side of the river.

Figure 2.28 Aerial photograph of the Gamerensche waard (source: Google Earth).

The discharge distribution between main channel and floodplain for the reference model and the model of Grid 1c looks very similar. Though, there is a large deviation in main channel discharge from these models for the model of Grid 5, see Figure 2.16 to Figure 2.19.

Figure 2.29 to Figure 2.31 show a similar picture. The figures show the flow pattern, indicating the depth-averaged flow velocity during a discharge of 3080 m^3/s, and the unit discharge, presenting the discharge per unit of grid cell width for the reference model, the model of Grid 1c and the model of Grid 5. The unit discharge is curtailed at 1 m^3/s, since the focus is on discharge entering and leaving the main channel.

The figures illustrate that the flow pattern and unit discharge pattern in the model of Grid 5 deviates considerably from those of the model of Grid 1c and the reference model. In accordance with the example of Ochten, at a certain degree of grid coarsening results in an averaging-out of geometric information. In Grid 5 there is a gap between weirs levees in the floodplain at the left side at km 937, whereas these weirs are connected in the reference grid and Grid 1c. The difference in the schematisation of weirs is indicated by the red circles in the figures. The opening between the weirs in Grid 5 allows water flowing into the floodplain at discharges of above but also beneath bankfull. As a consequence, in comparison to the reference model a local decrease in main channel discharge is predicted at km 937, see Figure 2.19. Again, the example illustrates the need for a hydraulic calibration tool, that enables to reduce discharge deviations introduced by grid coarsening.

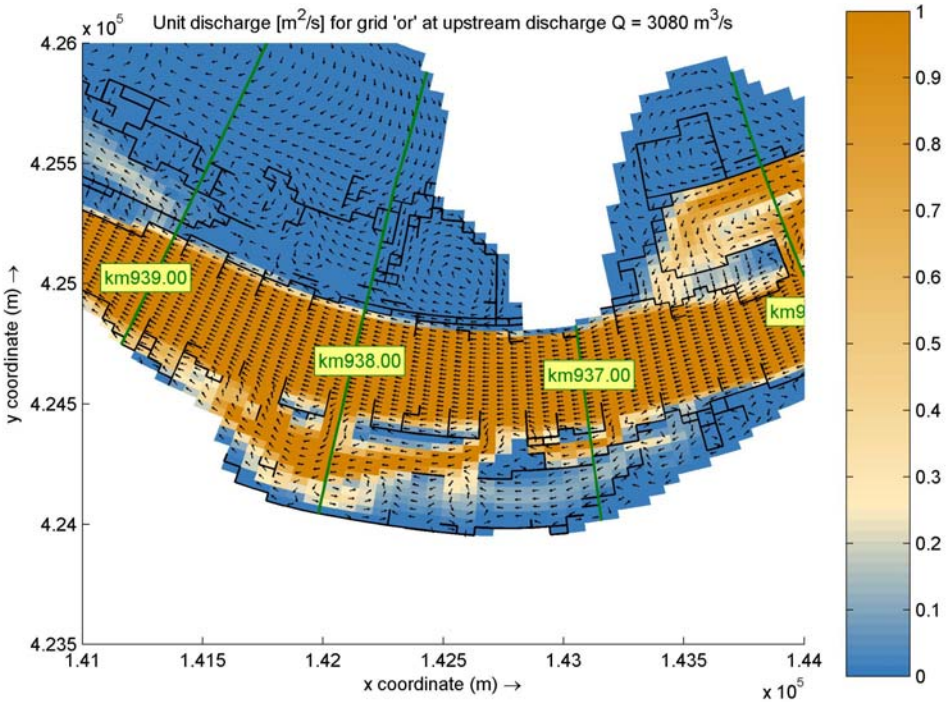

Figure 2.29 Flow pattern, indicating, indicating the depth-averaged flow velocity during a discharge of 3080 m^3/s, along with the unit discharge, presenting the discharge per unit of grid cell width for the reference model.

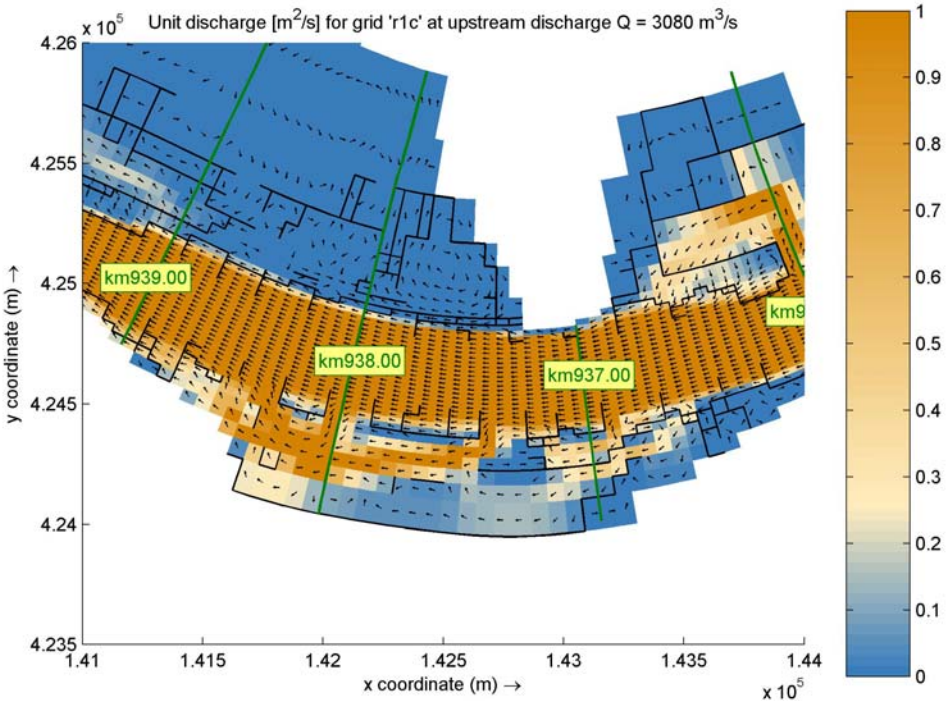

Figure 2.30 Flow pattern, indicating, indicating the depth-averaged flow velocity during a discharge of 3080 m^3/s, along with the unit discharge, presenting the discharge per unit of grid cell width for the model of Grid 1c.

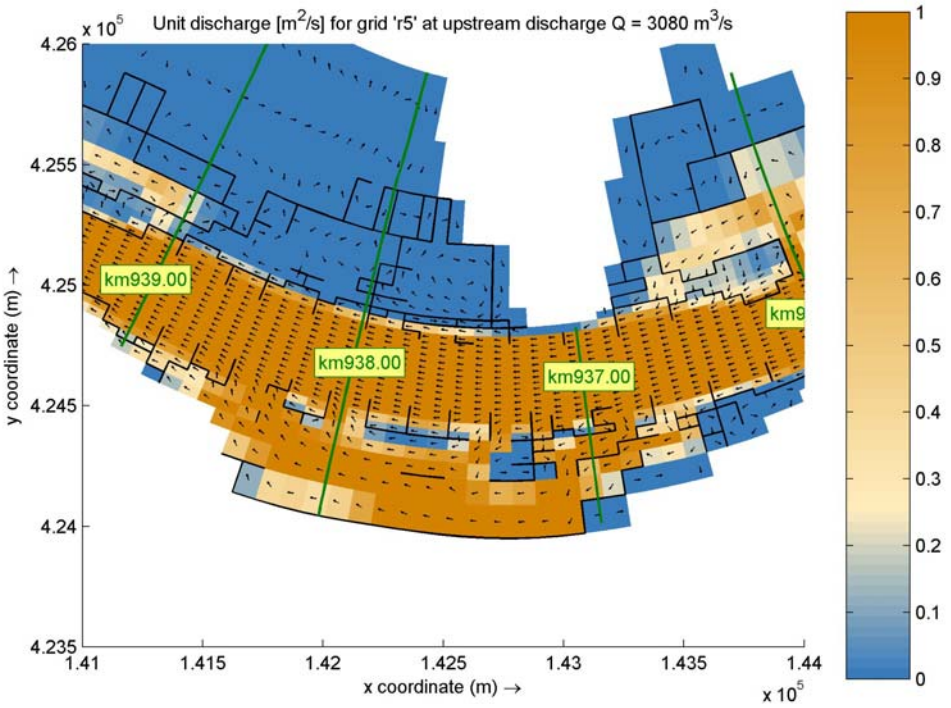

Figure 2.31 Flow pattern, indicating, indicating the depth-averaged flow velocity during a discharge of 3080 m^3/s, along with the unit discharge, presenting the discharge per unit of grid cell width for the model of Grid 5.

2.4 Assessment of grid coarsening: differences in morphology

2.4.1 Introduction

The objective of this section is to give a first indication of the difference in morphodynamic response between the reference model and the models of the new generated grids. In Section 2.3 the need for a hydraulic calibration tool to fine tune the discharge distributions and eliminate discharge deviations introduced by grid coarsening became apparent. The degree in which the deviations could be sufficiently reduced or eliminated strongly depends on the quality of the calibration tool. The hydraulic analysis in Sections 2.3 pointed out that gradual coarsening in transverse direction yield less deviations in discharge distribution. Moreover, the analysis showed a larger coarsening factor results in deviations that become more structural instead of isolated deviations at single river locations. Bearing this all in mind, we expect that the discharge deviations of Grid 1c and Grid 5 could be easily removed with a new (to be developed) calibration tool. As will be indicated in Section 5.3 the tool for imposing lateral discharges could be used for calibration purposes. The question whether this tool is able to reduced the stronger deviations introduced in Grid 2, 3 and 4, remains to be be answered.

The present section focuses on the differences in morphodynamic response for Gird 1c and Grid 5. Note that at a few river reaches the differences in main channel discharge for these grids exceed the limit of acceptability in Section 2.3.3. Since these differences occur at single river locations, we belief that these differences can be eliminated or reduced by

calibration. Model studies of Delft Hydraulics in the past show that imposing lateral discharge extractions and supplies is a useful way to assess the impact of secondary channels in the Rhine near Gameren, Heesselt and Afferdensche and Deetsche waarden.

Calibration is not part of this research study. Therefore, the assessment of the difference in morphology took place with the uncalibrated models. This may have a larger impact on the morphodynamic results of the model of Grid 5 than for Grid 1c, since the uncalibrated model of Grid 5 performs from hydrodynamic point of view less than the uncalibrated model of Grid 1c.

The assessment is split in two steps. First, the difference in the morphological response after a period of 10 years is addressed in Section 2.4.2. Subsequently, in Section 2.4.3 is evaluated whether these bed level difference are acceptable.

2.4.2 Comparison of the bed level after a period of 10 years

Figure 2.32 to Figure 2.34 show the bed level after a period of 10 years of morphological simulation for the reference model and the model of Grid 1c, for three river reaches: the Boven Waal (km 867-896), the Midden Waal (km 896-924) and the Beneden Waal (km 924-954). Grid 1c shows a very similar behaviour as the reference model. Small differences occur in the river reach near Ochten (km 907-910).

Figure 2.32 Resulting bed levels 80 meters left, 80 meters right and on the river axis for the reference model and the model of Grid 1c after a period of 10 years of morphological simulation: Boven Waal (km 867-896).

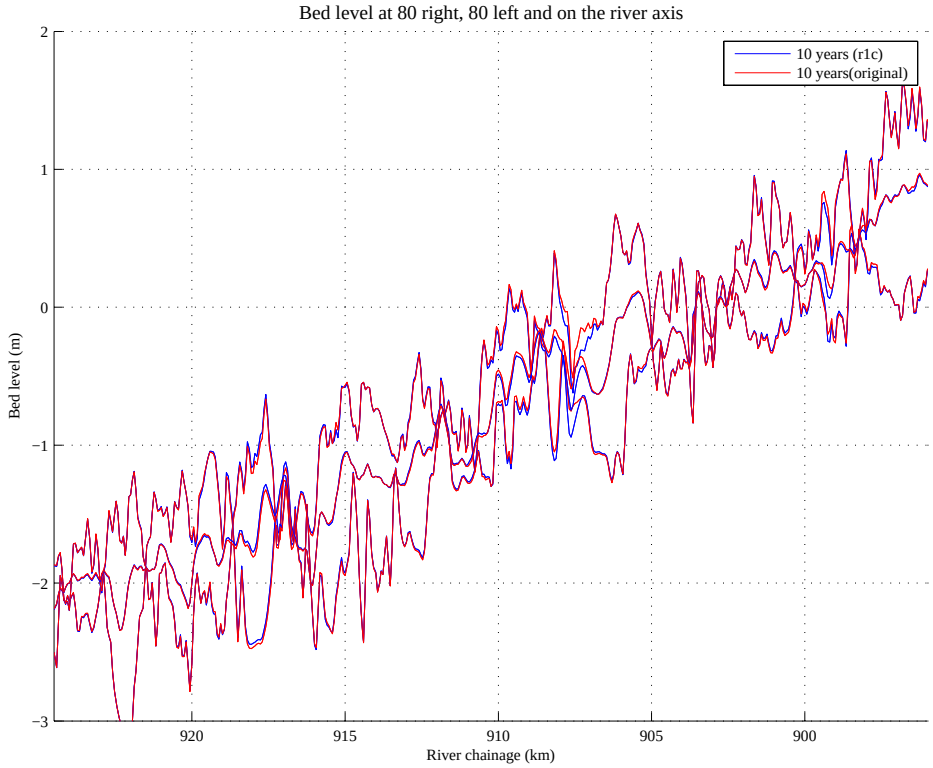

Figure 2.33 Resulting bed levels 80 meters left, 80 meters right and on the river axis for the reference model and the model of Grid 1c after a period of 10 years of morphological simulation: Midden Waal (km 896-924).

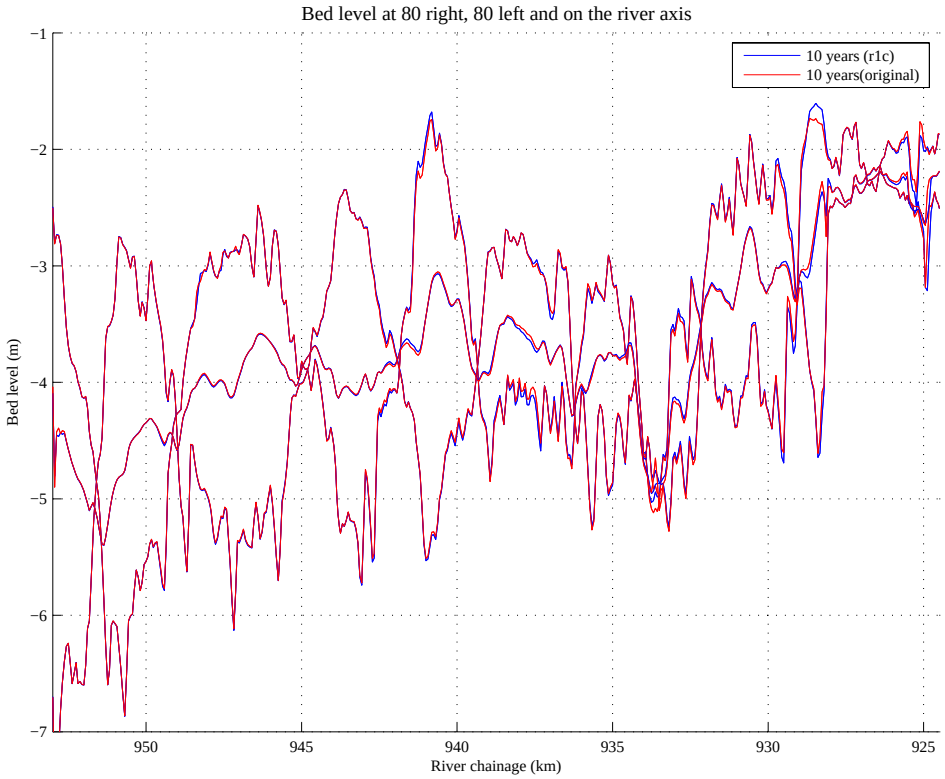

Figure 2.34 Resulting bed levels 80 meters left, 80 meters right and on the river axis for the reference model and the model of Grid 1c after a period of 10 years of morphological simulation: Beneden Waal (km 924-954).

Figure 2.35 to Figure 2.37 present similar figures for Grid 5 as for Grid 1c. The figures show an increase in bed level differences after a period of 10 years with respect to the reference model. Although, differences in main channel discharge for Grid 5, except from a few locations, do not exceed the limit of acceptability as illustrated in Figure 2.16 to Figure 2.19, they do lead to bed level differences in the order of 10 cm to 30 cm after a period of 10 years. Reducing the differences in main channel discharge by calibration, will also reduce the differences in computed bed levels.

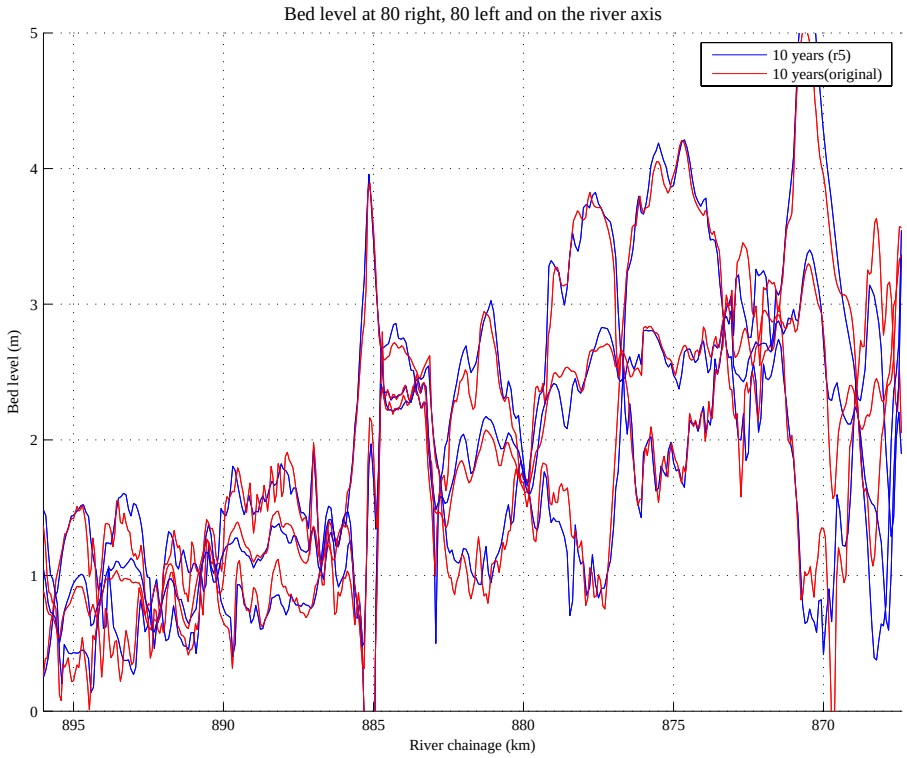

Figure 2.35 Resulting bed levels along the river axis and 80 meters left and 80 meters right from the river axis for the reference model and the model of Grid 5 after a period of 10 years of morphological simulation: Boven Waal (km 867-896).

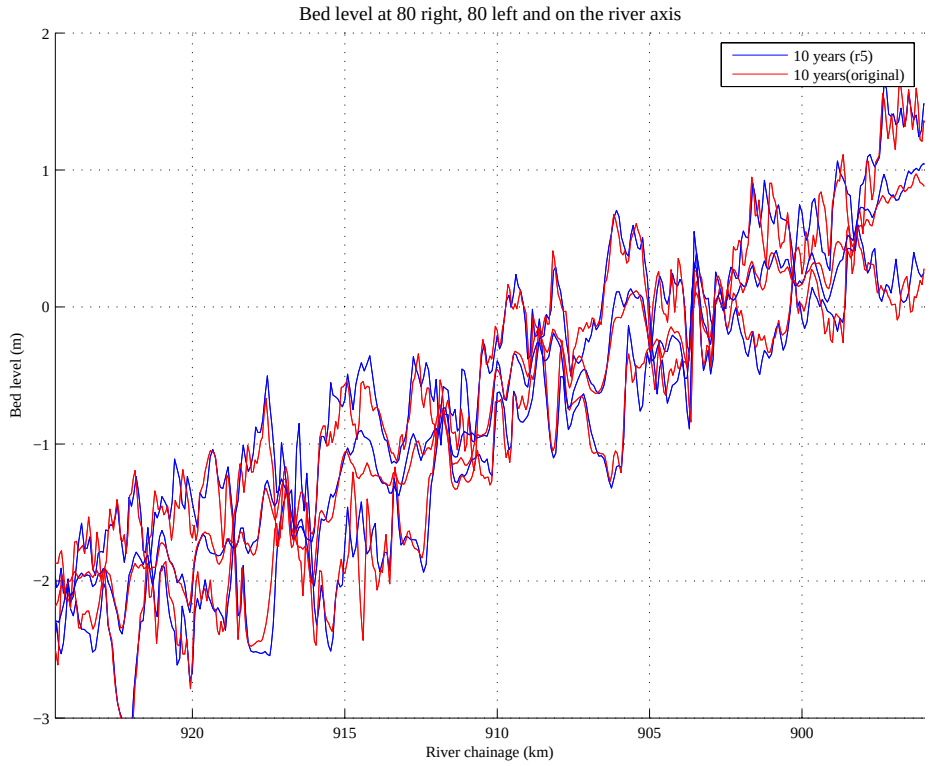

Figure 2.36 Resulting bed levels along the river axis and 80 meters left and 80 meters right from the river axis for the reference model and the model of Grid 5 after a period of 10 years of morphological simulation: Midden Waal (km 896-924).

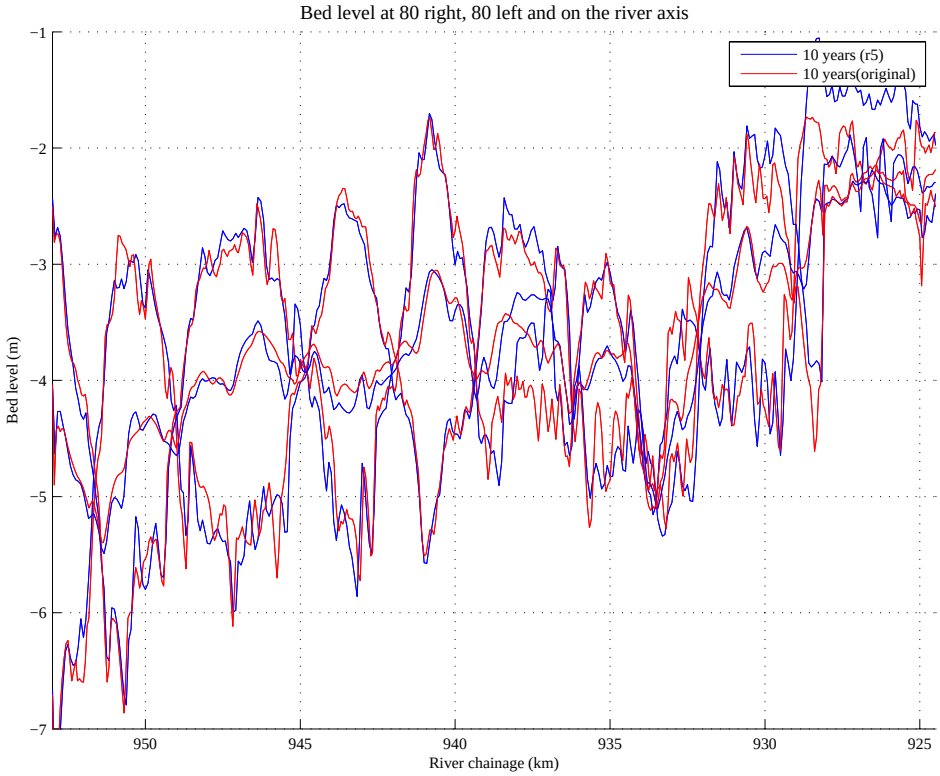

Figure 2.37 Resulting bed levels along the river axis and 80 meters left and 80 meters right from the river axis for the reference model and the model of Grid 5 after a period of 10 years of morphological simulation: Beneden Waal (km 924-954).

2.4.3 Temporal variation of the bed level

In order to evaluate whether the bed level difference in the previous section are acceptable, in this section a limit of acceptability is defined. To that end, the difference between the time-averaged bed level during the 10th year of the model of Grid 1c and Grid 5 ánd the reference model, is related to the temporal variation during the 10th year in the reference model. This temporal variation is taken equal to the difference between minimum and maximum bed level position during the 10th year. The temporal variation is an indication for the natural variability of the river bed. The differences in the time-averaged bed level are acceptable if they fall in the range of this temporal variation.

Figure 2.38 to Figure 2.40 show the difference in time-averaged bed level at 1) the river axis, 2) 80 m left of the river axis, and 3) 80 m right of the river axis, during the 10th year between the reference model and the model of Grid 1c (blue line) and Grid 5 (black line), ánd the temporal variation during the 10th year in the reference model (grey shaded area). The figures indicate that the differences in time-averaged bed levels for Grid 1c (blue line) lie in between the minimum and maximum bed level of the original grid in the 10th year (shaded grey). For grid 5, the difference in time-averaged bed levels (black line) does not always fall in the range of the temporal variation of the reference simulation. In other words, at some locations, the bed level seems to converge to a slightly different solution. But, as indicated before, the simulation is carried out with an uncalibrated model. We expect that most of the bed level differences can be eliminated or reduced by calibration.

Grid 5 yields an acceleration factor AF of 2.4. This means a computation time reduction of:

$$P = \frac{AF - 1}{AF} \times 100\% = 58\%$$

Since the computation time reduction of Grid 1c is only 17%, it is recommended to use Grid 5 as optimal grid.

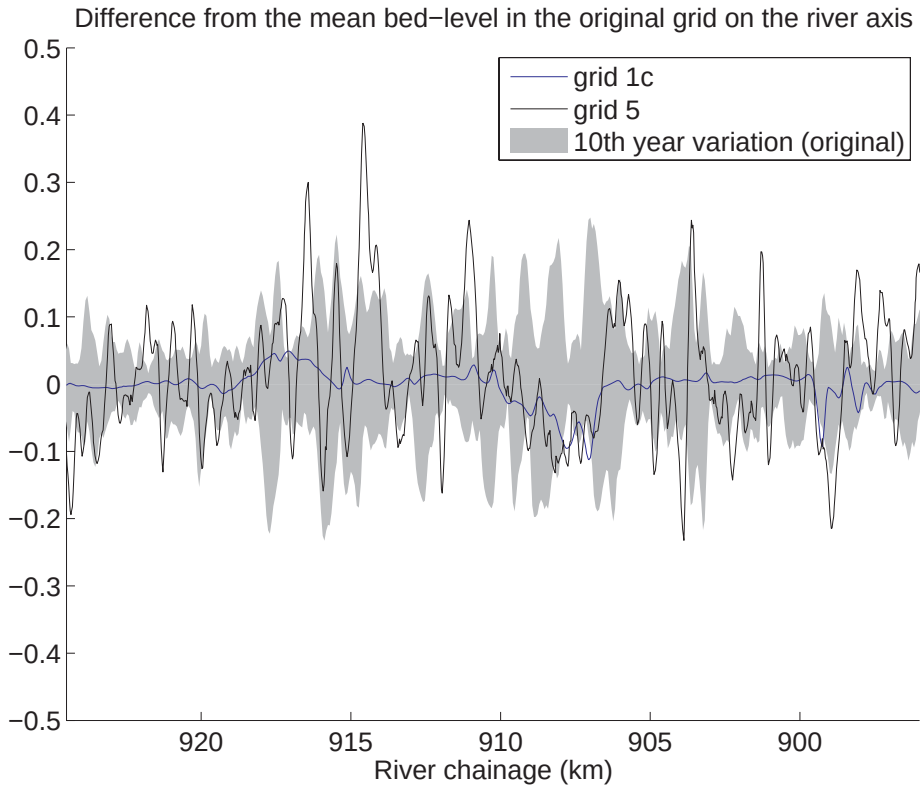

Figure 2.38 Difference in time-averaged bed level at the river axis during the 10th year between the reference model and the model of Grid 1c (blue line) and Grid 5 (black line), ánd the temporal variation during the 10th year in the reference model (grey shaded area).

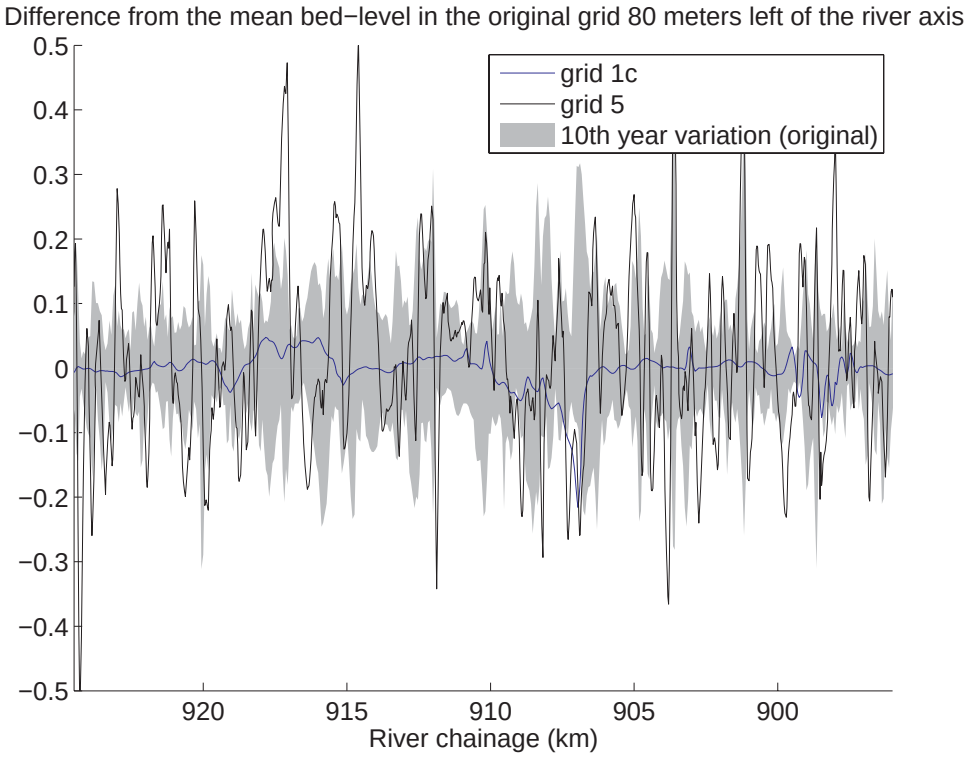

Figure 2.39 Difference in time-averaged bed level 80 m left of the river axis during the 10th year between the reference model and the model of Grid 1c (blue line) and Grid 5 (black line), ánd the temporal variation during the 10th year in the reference model (grey shaded area).

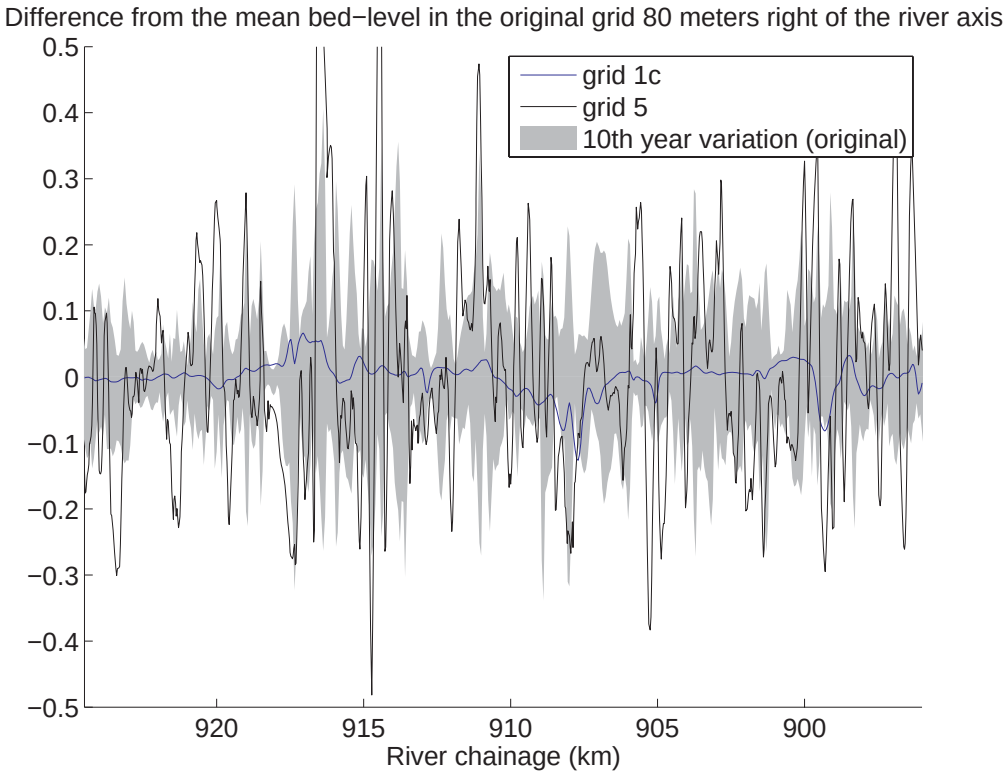

Figure 2.40 Difference in time-averaged bed level 80 m right of the river axis during the 10th year between the reference model and the model of Grid 1c (blue line) and Grid 5 (black line), ánd the temporal variation during the 10th year in the reference model (grey shaded area).

2.5 Conclusions

A number of grids are created by coarsening the original, fine grid in transverse and longitudinal direction by different factors. For the impact assessment of grid coarsening, the difference in 1) discharge distribution between the main channel and floodplains, and 2) morphodynamic response is analysed for each new generated grid.

With respect to grid coarsening the following aspects appear to be important:

1. When coarsening the grid covering the floodplain in transverse, one should acknowledge the importance of gradually coarsening. The transition zone between the main channel and the floodplain, including the groyne section, should be modelled with quite some detail to make sure that the lateral flow exchange between main channel and floodplain is preserved. In particular the schematisation of groynes and summer levees turn out to be important. The averaging-out of geometric information induced by grid coarsening will be reduced when gradually coarsening the grid. Bearing this in mind coarsening the grid up to a factor 4 is allowed. The most important zone appears to be the first 100 m of the groyne section and floodplain area at either side of the main channel. A too abrupt change in grid size in this zone will inevitably lead to strong deviations in the lateral discharge distribution.

2. When coarsening the main channel grid in transverse direction, it is important to keep at least 8 grid cells in this section, in order to preserve a good representation of the cross-section, i.e. the transverse bed slope and pointbar pool development in the inner- and outer bend.

3. When coarsening the grid in transverse direction, the resolution of the grid should be such that it still captures the location of the weirs. The grid cell length should not exceed 100 m.

For defining the limit of acceptability of the difference in discharge distribution, the spatial variation of the discharge flowing through the main channel in the reference model, is taken as a reference. Differences up to 3-5% seem justified.

For the grid-choice, it is important to distinguish between the criteria for grid dimensions and the calibration-targets. The latter focusses on the possibility of the preservation of the lateral flow exchanges and is very important for the grid-choice eventually. The choice for a certain grid should be based on the performance of a hydraulic calibration tool that enables to remove discharge deviation introduced by grid coarsening. This tool should indicate to what extent grid coarsening is possible, in other words the tool should give insight to what extent deviations can be eliminated and reduced by calibration. The decision should be based on the combination of the hydrodynamic performance after calibration and the computation time reduction. Since the calibration tool is not available yet (only a first attempt of such a tool is presented in Section 5.3), the choice for the ‘best’ grid is difficult to make at the moment. The main channel discharge starts to deviate from the reference model along the entire Waal branch for Grid 2 (the grid with the maximum allowed dimensions), 3 and 4. Deviations become more structural instead of isolated single river locations. Whether these deviations are too large to be removed by a hydraulic calibration depends on the quality of the calibration tool. We have the impression that the deviations induced by the grid are difficult to be removed entirely with a calibration tool. Therefore, it is not recommended to proceed with these grid for the moment. Although this decision could actually not be made in this stage of the project, it is recommended to proceed with Grid 5 for the remainder part of the project. A final choice can be made in future, after the development of a calibration tool. Therefore, it is recommended to revise the choice in a later stage of the DVR project.

The ratio between computation time required with the reference model and the model of Grid 5 is 2.4. In other words, Grid 5 yields a computation time reduction of 58%.

3 Optimisation computation time step and morphological acceleration factor

3.1 Method

In this chapter it is investigated how much the computation time for Waal model can be reduced by increasing the simulation time step and the morphological acceleration factor. The aim is to find maximum values for both parameters for which the accuracy of the model results is still acceptable.

Model tests are carried out using the domain of the Waal as example. Grid 5 is used as computational grid, since this grid is recommended in Section 2.5 as optimal grid.

First the time step is optimised (Section 3.2). Different criteria to theoretically assess the maximum possible time step are described in Section 3.2.1. In the next step model simulations are carried out, for which time step is increased gradually, starting from the value originally applied in the Waal model (reference case) up to and beyond a time step that is reasonable according to the theoretical criteria. The size of the time step primarily affects the hydraulic behaviour of the model, which in turn influences morphological processes. Therefore, with respect to the time step optimisation, we focus on the impact on the hydrodynamics. The deviations of the model results for bigger time steps from those of the reference case are evaluated and the gains in computation time are assessed.

In Delft3D all processes (water movement, sediment transport and adaptation of the bed level) are simulated with one time step (flow time step). One of the complications inherent in carrying out morphological projections on the basis of hydrodynamic flows is that morphological developments take place on a time scale several times longer than typical flow changes. One technique for approaching this problem is to use a morphological acceleration factor (*morfac*) whereby the speed of the changes in the morphology is scaled up. Effectively, this means that the morphological development is simulated using a, for instance 10 times, larger time step than the hydrodynamics, or phrased more correctly the hydrodynamics is simulated at a 10 times faster rate. This leads to a significant reduction in simulation time. However one should take care that by speeding up the hydrodynamic forcings one does not substantially change the nature of the overall hydrodynamic and morphological development.

In Section 3.3 it is analysed to what extent the morphological acceleration factor (*morfac*) of the Waal model can be increased without significant influencing the model results. To this end, morphodynamic simulations are carried out for a period of five years. Since, we also investigated the impact of a simulation without a morphological acceleration factor, i.e. the case *morfac* =1, the Waal model is reduced in length, see Figure 3.1, i.e. the model covers the river chainage between km 918 and km 953.

The following simulations are carried out:

a) for four constant discharges and four values for *morfac*, starting with *morfac* = 1 (reference case);
b) for the discharge hydrograph shown in Figure 2.1; and
c) for the same situation as b), but with a trench in the main channel.

Table 3.1 gives an overview 2of the discharge levels and the morphological acceleration factors used in the simulations. The results of the simulations are compared to the reference case with focus on the bed level differences along the river axis and along two gridlines 80 m left and 80 m right of the axis, after a period of 5 years.

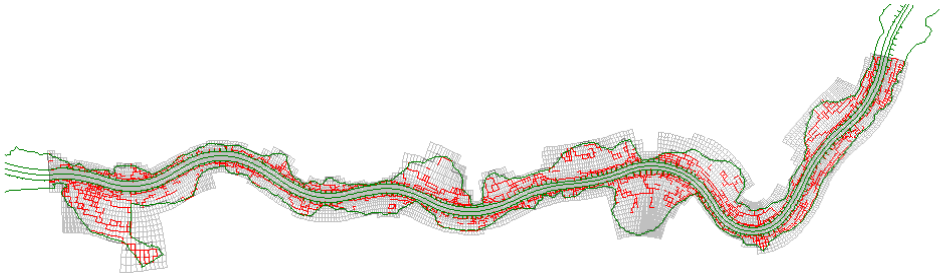

Figure 3.1 Reduced model of the Waal (from km 918 to the downstream boundary).

Table 3.1 Overview of morphological acceleration factors used in the simulations.

Discharge (m^3/s)	**Morfological acceleration factor (-)**			
	simulation #1	simulation #2	simulation #3	simulation #4
1187	1	50	100	200
2000	1	40	80	160
3080	1	20	40	80
4422	1	5	20	40

3.2 Time step optimisation

3.2.1 Theoretical point of view

Generally the time step for a simulation can be chosen based on accuracy arguments only, in most cases stability is not an issue. The accuracy is, among several other parameters, such as the reproduction of the important spatial length scales by the numerical grid, dependent on the Courant number, defined by:

$$C_r = \frac{\Delta t \cdot \left(u \pm \sqrt{gh}\right)}{\{\Delta x, \Delta y\}} \qquad (3\text{-}1)$$

where Δt is the time step (in seconds), g is the acceleration of gravity, h is the water depth, and {Δx, Δy} is a characteristic value (in many cases the minimum value) of the grid spacing in either direction. Generally, the Courant number should not exceed a value of 1+10 = 11.

Applying the right side of the Courant formula with h = 10 m, g = 9.81 m/s^2, Δx = 60 m and Δt = 60 s, Cr becomes 9.9, which is an acceptable value. So for the time step optimisation time steps around one minute seem to be reasonable, while so far a time step of 0.4 minutes has been used.

3.2.2 Model computations

To assess the influence of the time step size on model results, hydraulic simulations with the Waal domain (grid 5) are carried out applying time steps of 0.4 (reference case), 0.6, 0.8, 1.0, 1.5, 1.8 and 2.0 minutes for discharges of 1187, 2000, 3080 and 4422 m^3/s.

When using a time step of 1.8 or 2 minutes the computation crashes right after the start. A time step of 0.8 minutes results in smoothly developing results while for a time step of 1.5 minutes results show small irregularities, but the computation is stable. This can be seen in Figure 3.2 and Figure 3.3, in which the discharge at the downstream end of the model (Werkendam) and the water level at the upstream end of the model (Pannerdensche Kop) are presented for the three higher discharge levels. Figure 3.4 and Figure 3.5 show a magnified part of the same graphs, namely the transition between the discharge levels Q = 3080 m^3/s and Q = 4422 m^3/s. For a discharge of Q = 4422 m^3/s and a time step of 1.5 minutes a water level difference of 2 cm with respect to the reference case occurs.

So, in conclusion increasing the time step from 0.4 minutes to 1.5 minutes gives 1) some transient effects on discharges, but no persistent effect, and 2) small differences in water levels that can be neglected for morphological purposes. Therefore, a time step of 1.5 minutes is chosen for further simulations.

The acceleration of the simulation due to the use of bigger time steps than 0.4 minutes is presented in Table 3.2. For a time step of 1.5 minutes the simulations are 3.4 times faster than the reference case.

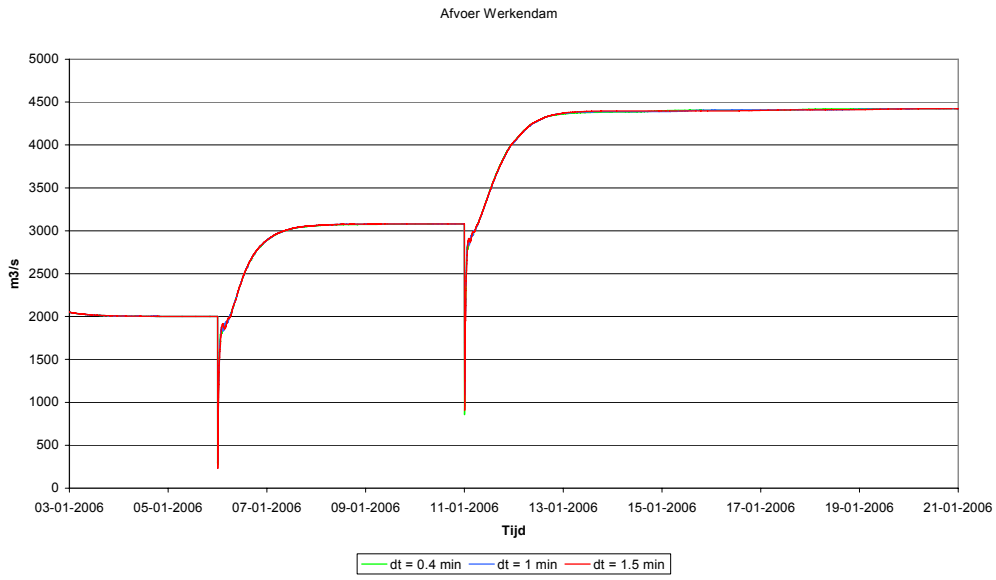

Figure 3.2 Discharge at the downstream boundary of the Waal for simulations using different time steps.

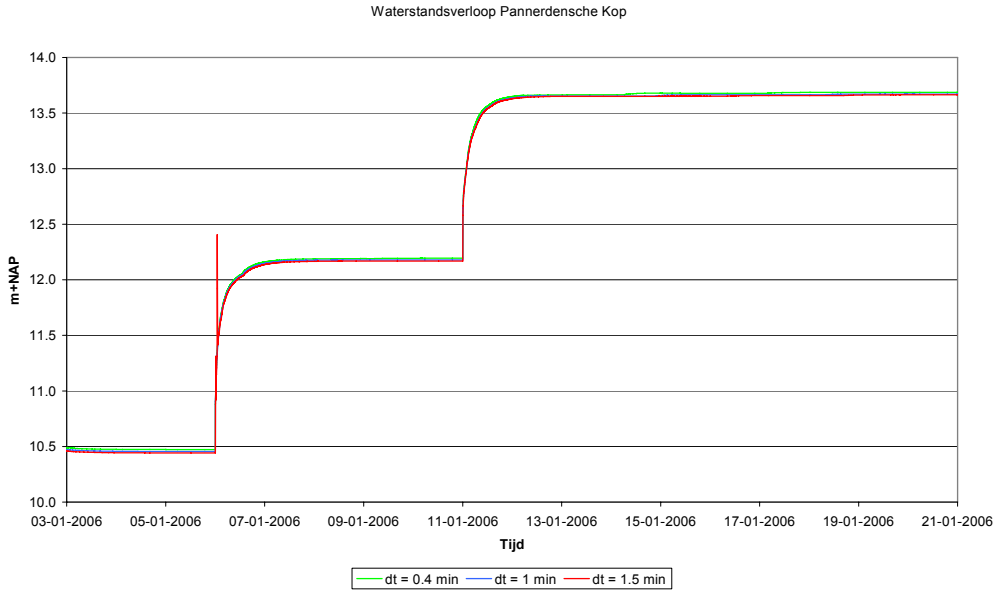

Figure 3.3 Water level at the upstream boundary of the Waal for simulations using different time steps.

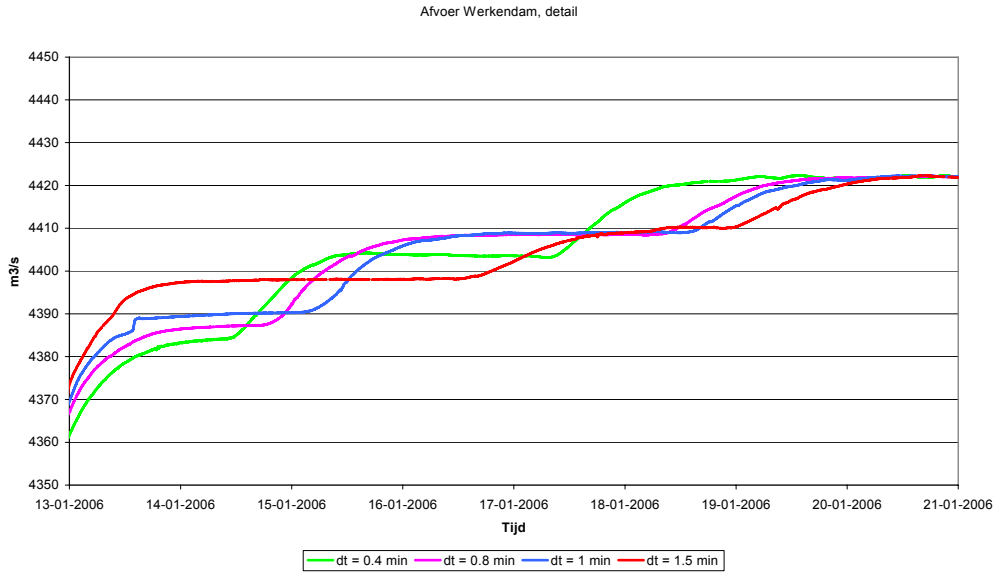

Figure 3.4 Discharge at the downstream boundary of the Waal for simulations using different time steps (transition between the discharge levels Q = 3080 m^3/s and Q = 4422 m^3/s).

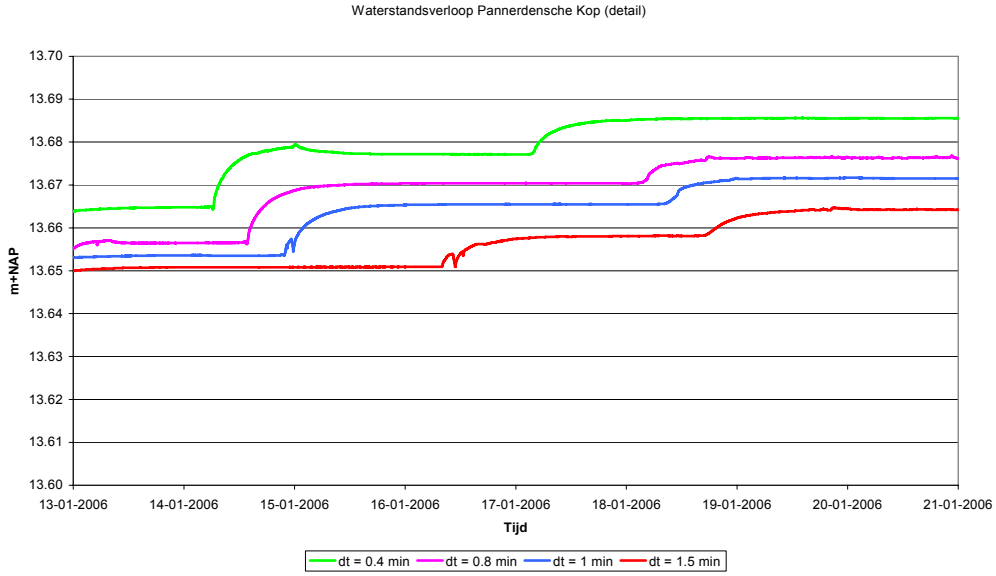

Figure 3.5 Water level at the upstream boundary of the Waal for simulations using different time steps (transition between the discharge levels Q = 3080 m^3/s and Q = 4422 m^3/s).

Table 3.2 Acceleration of the computations with bigger time steps with respect to the reference case with a time step of 0.4 minutes.

Time step (minutes)	Simulation time (hours)	acceleration w.r.t. the reference simulation
0.4	12:55	1.0
0.6	8:04	1.5
0.8	6:21	1.9
1.0	5:01	2.4
1.5	3:31	3.4

3.3 Morphological acceleration factor

3.3.1 Morphodynamic simulations with constant discharge

In order to determine a maximum acceptable value of the morphological acceleration factor, first simulations are carried out using different values of this parameter for four constant discharges (Table 3.1). The model results are compared to the results of simulations with a *morfac* = 1, which is the reference case. The focus lies on the bed level differences along the river axis and along two gridlines 80 m left and 80 m right of the axis after a period of five years.

Figure 3.6 and Figure 3.7 show the bed level differences between the reference case and the simulations with higher morphological acceleration factors after five years of morphological simulation for Q = 1187 m^3/s and Q = 4422 m^3/s as example. It becomes evident that the bed level differences hardly exceed 3 cm, which also holds true for the other two discharge levels.

Besides the impact of the *morfac* on differences in bed levels, the following criterion was looked at: the value of the morphological acceleration factor should be such that the transport layer does not erode by more than 5% of the water depth in one time step.
In Figure 3.8 the maximum bed level changes per time step in terms of percentage of the water depth are presented for a discharge of Q = 4422 m^3/s. It reveals that the criterion is amply fulfilled as the ratio between morphological change and the water depth does not exceed 0.10 %. This holds true for the other discharge levels, too.

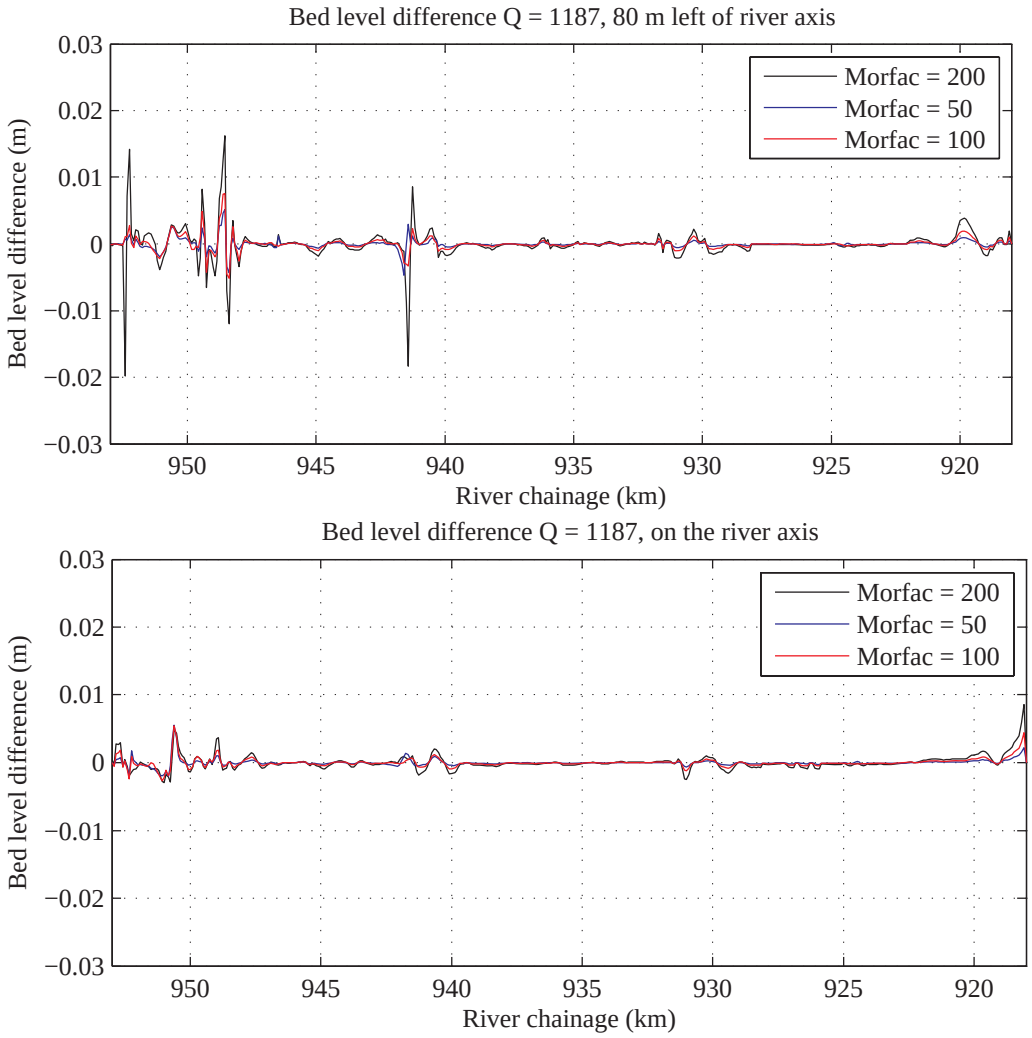

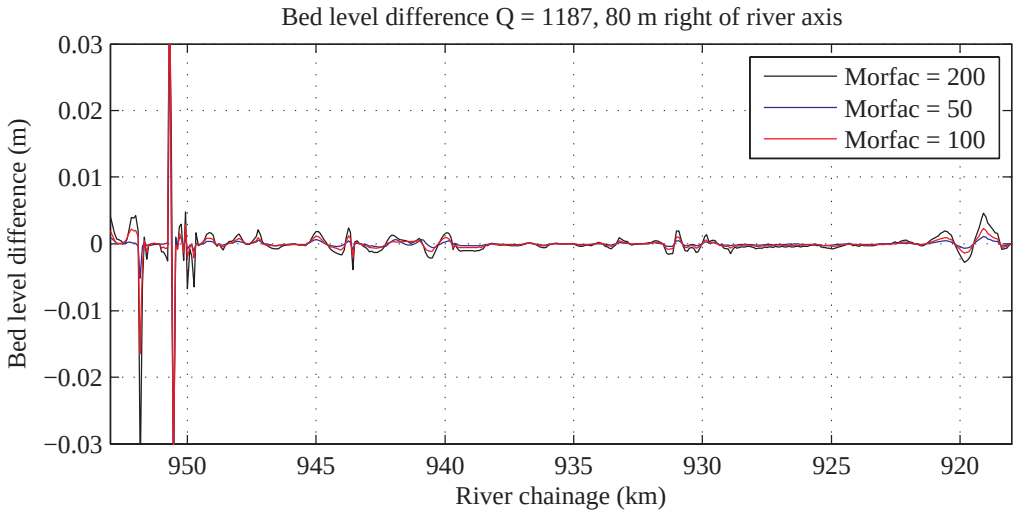

Figure 3.6 Bed level differences between the reference case and simulations using different morphological acceleration factors after 5 years of morphological simulations (Q = 1187 m^3/s).

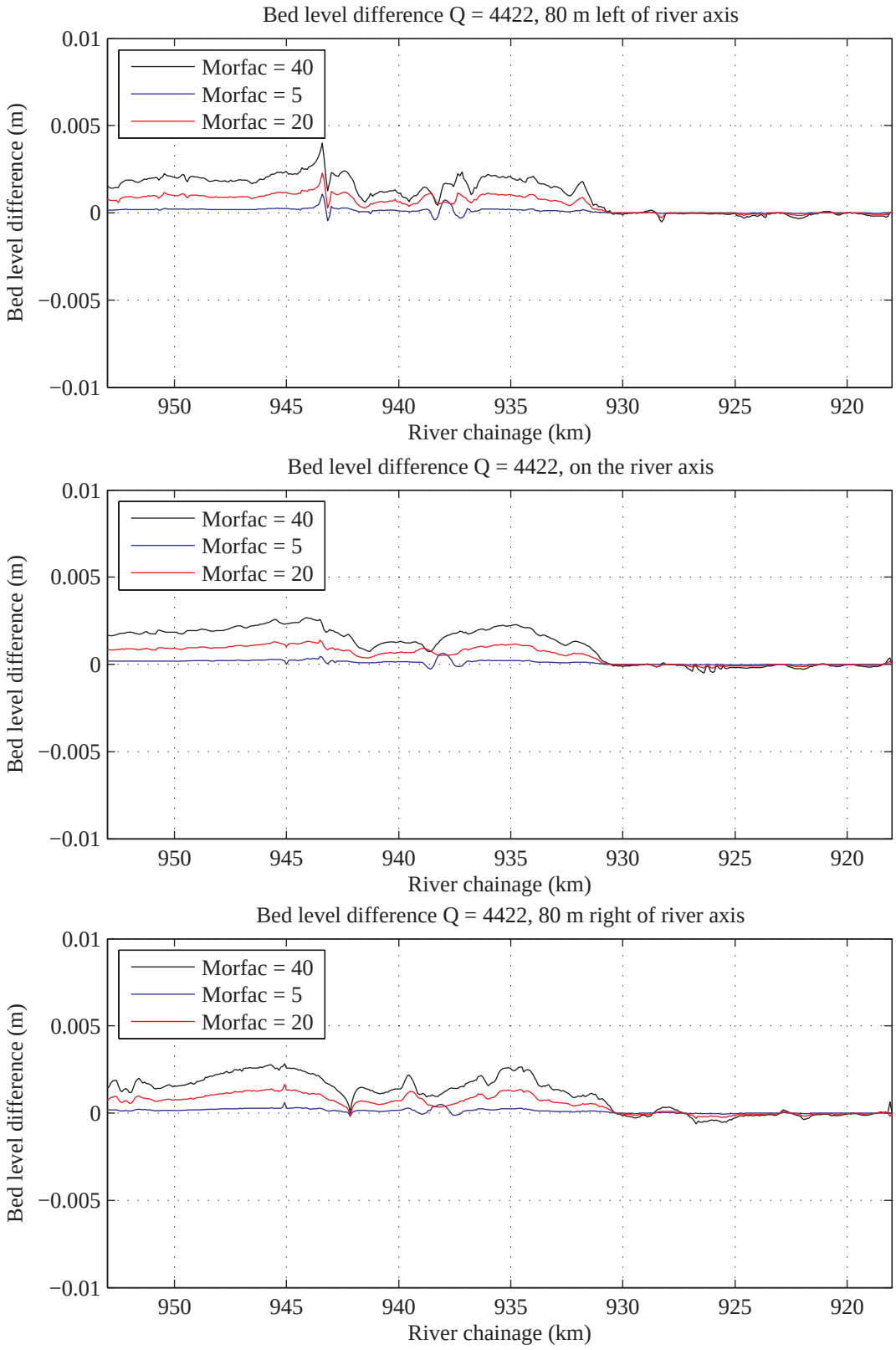

Figure 3.7 Bed level differences between the reference case and simulations using different morphological acceleration factors after 5 years of morphological simulations (Q = 4422 m^3/s).

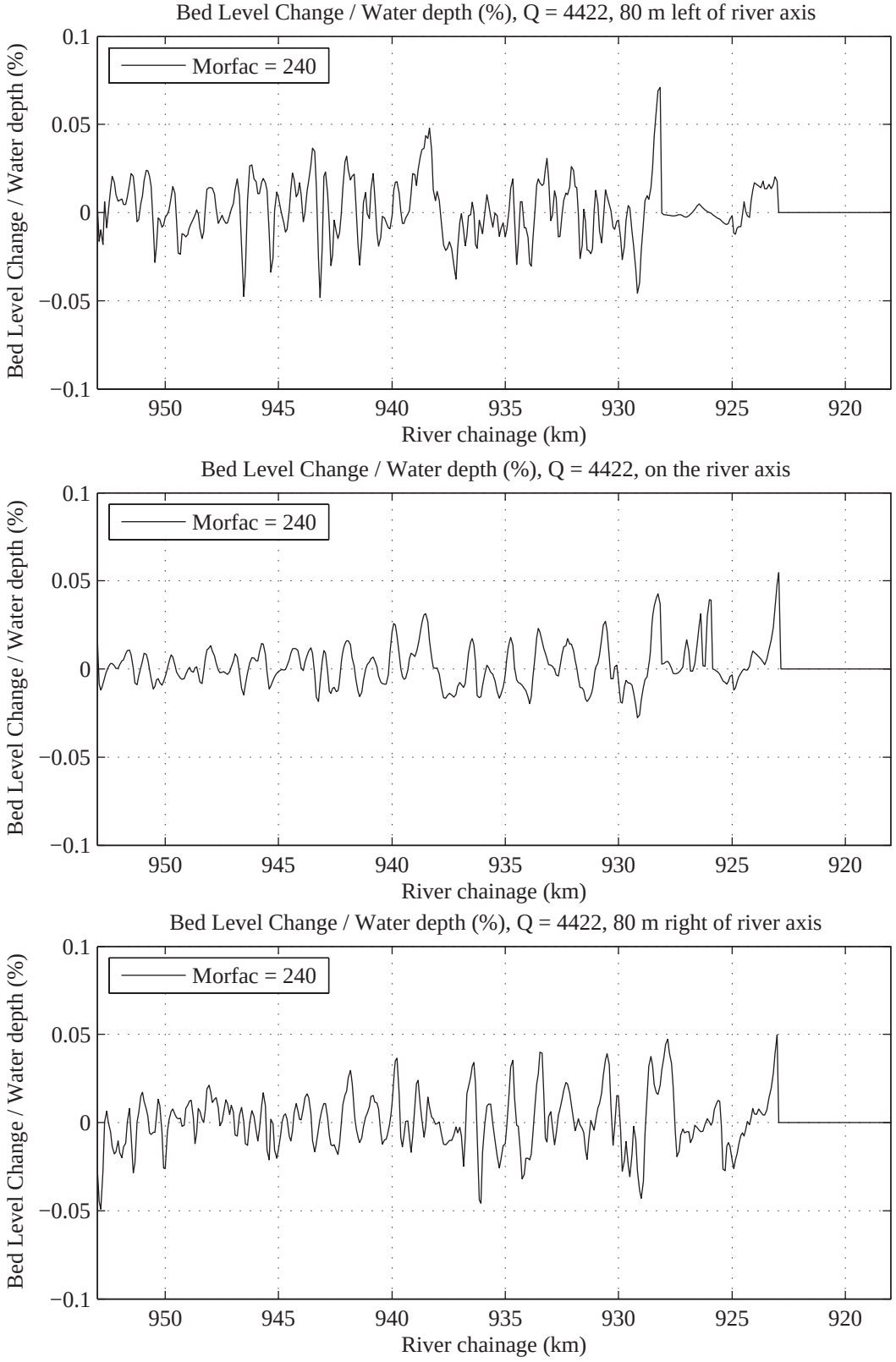

Figure 3.8 Maximum bed level changes per time step in terms of percentage of the water depth for a discharge of Q = 4422 m^3/s.

3.3.2 Morphodynamic simulations with discharge hydrograph

Beside the test simulations with constant discharges, calculations using a discharge hydrograph are carried out. The discharge hydrograph is shown in Figure 2.1. Since the deviations between the simulations with and without *morfac* are small for the constant discharges, two additional sets of extreme *morfac* values are tested, see Table 3.3.

Table 3.3 Additional sets of morphological acceleration factors.

Discharge (m^3/s)	Morfological accerelation factor	
	simulation #5	simulation #6
1187	300	600
2000	240	480
3080	100	200
4422	60	120

Figure 3.9 shows the bed level difference between the reference case (*morfac* = 1) and the simulations with higher morphological acceleration factors after five years of morphological simulation with a discharge hydrograph. The deviations appear to be even smaller than for constant discharges. Even for the extreme values of *morfac* they are below 2 cm.

Table 3.4 shows the factors by which the simulations are accelerated for the different *morfacs*. The case with values of 100, 80, 40 and 20, respectively, is used as reference because these are the factors used so far for the model of the Rhine branches. For the most extreme set of morphological factors an acceleration by a factor of 1.6 is achieved. This seems small at first sight, but it can be explained with the nature of discharge hydrograph simulations. These calculations are actually treated as a series of constant discharge simulations. In contrast to the actual computation time the start-up time needed for each constant discharge simulation can of course not be reduced by the *morfac*.

A interesting question for further research could be ‘what if we use stabilised flow patterns for each discharge stage derived prior to morphodynamic simulations and completely neglect the feedback to flow during the morphodynamic simulation?’

Table 3.4 Acceleration of the computations for different combinations of morphological acceleration factors with respect to the simulation with *morfacs* of 100/80/40/20.

Simulation #	Morfological accerelation factor (1187, 2000, 3080, 4422 m^3/s)	Simulation time (hours)	Acceleration w.r.t. ‘100/80/40/20’
1	1/1/1/1	150:35	0.03
2	50/40/20/10	6:34	0.58
3	100/80/40/20 (reference)	3:50	1.00
4	200/160/80/40	2:52	1.33
5	300/240/100/60	2:26	1.58
6	600/480/200/120	2:23	1.60

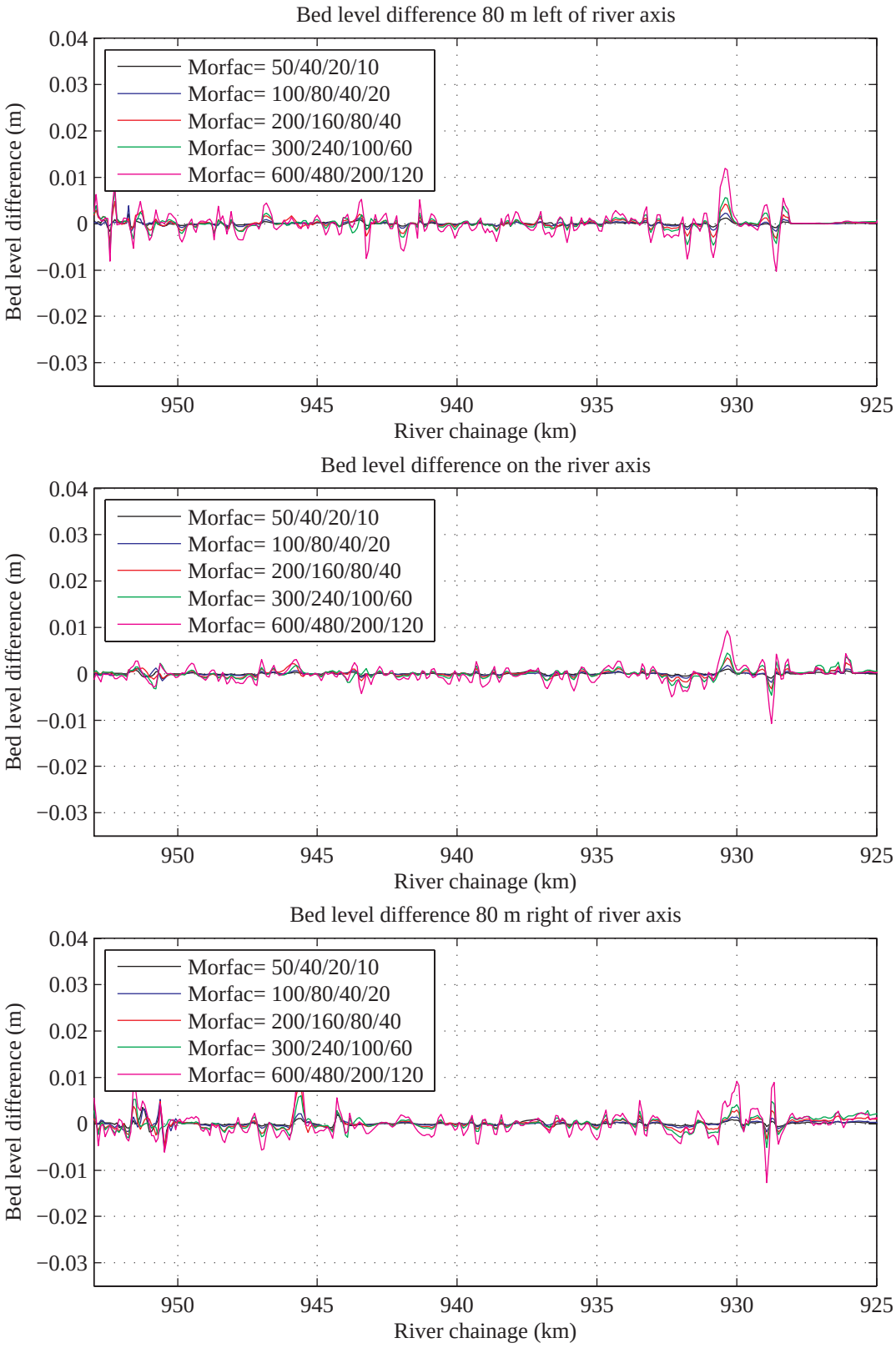

Figure 3.9 Bed level differences between the reference case and simulations using different morphological acceleration factors after a period of 5 years (discharge hydrograph).

3.3.3 Morphodynamic simulations with discharge hydrograph and trenches

In this part of the study it is tested if the value of the morphological acceleration factor significantly influences the evolution of a trench along the river. For this test the same discharge hydrograph and morphological acceleration factors as in Section 3.3.2 are used.

Figure 3.10 shows the trench in its initial state (black line) as well as its evolution in time for the case with *morfac* = 1 (reference case). The bed level around the trench is presented with respect to the initial bed level without trench. In Figure 3.11 the evolution of the trench is compared for the different morphological acceleration factors. Again the deviations from the reference case are small even for the extreme morphological acceleration factors. This can also be seen in Figure 3.12, in which the bed level differences with respect to the reference case that have developed after a period of five years are presented for all simulations.

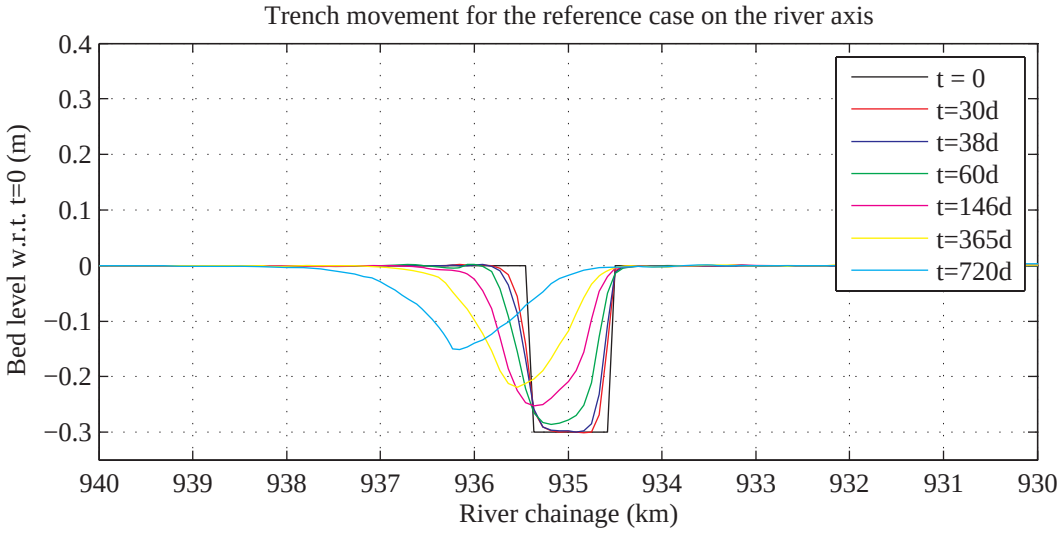

Figure 3.10 Evolution of the trench for the reference case (*morfac* = 1).

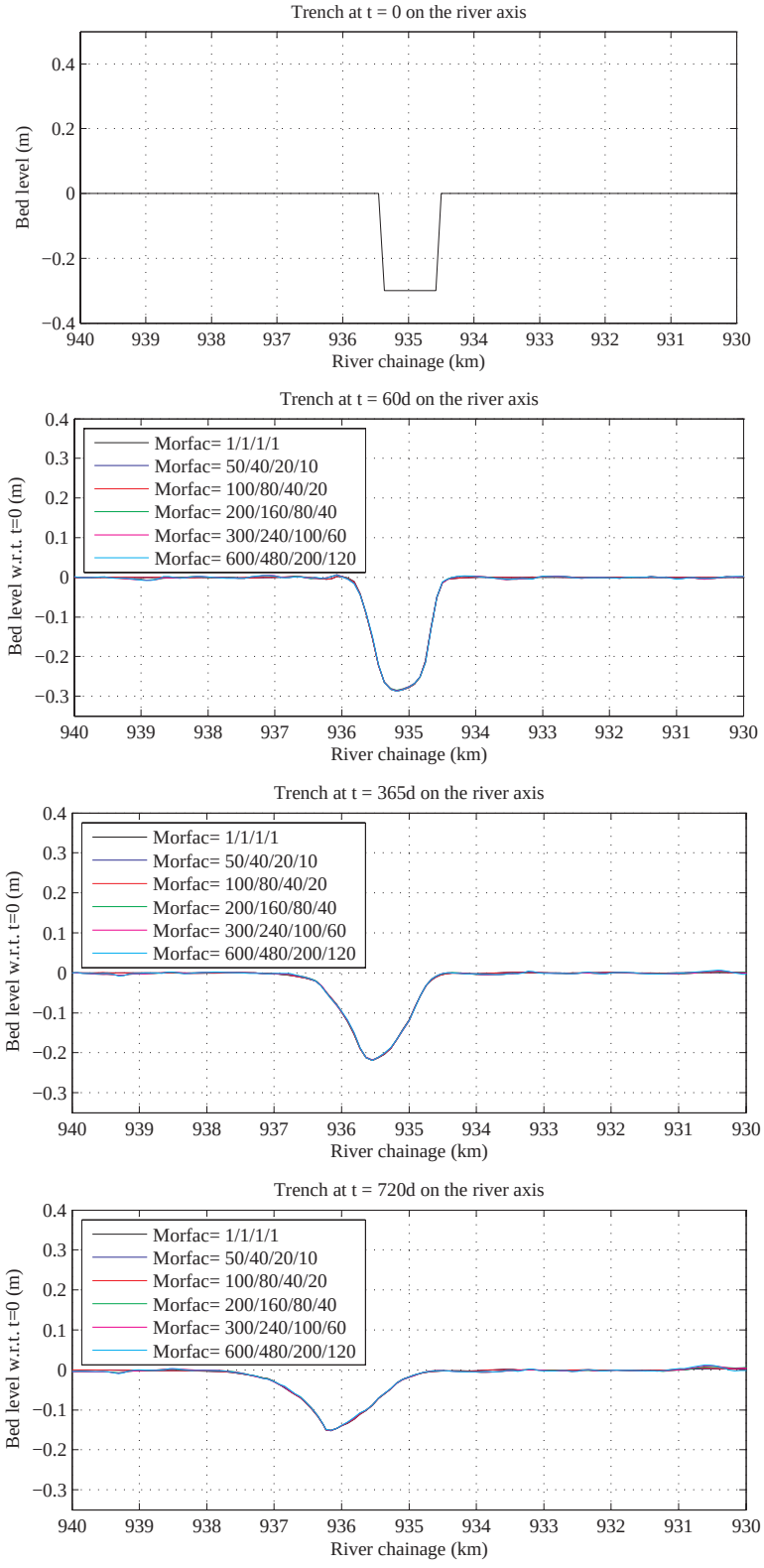

Figure 3.11 Comparison of the evolution of the trench for different morphological acceleration factors.

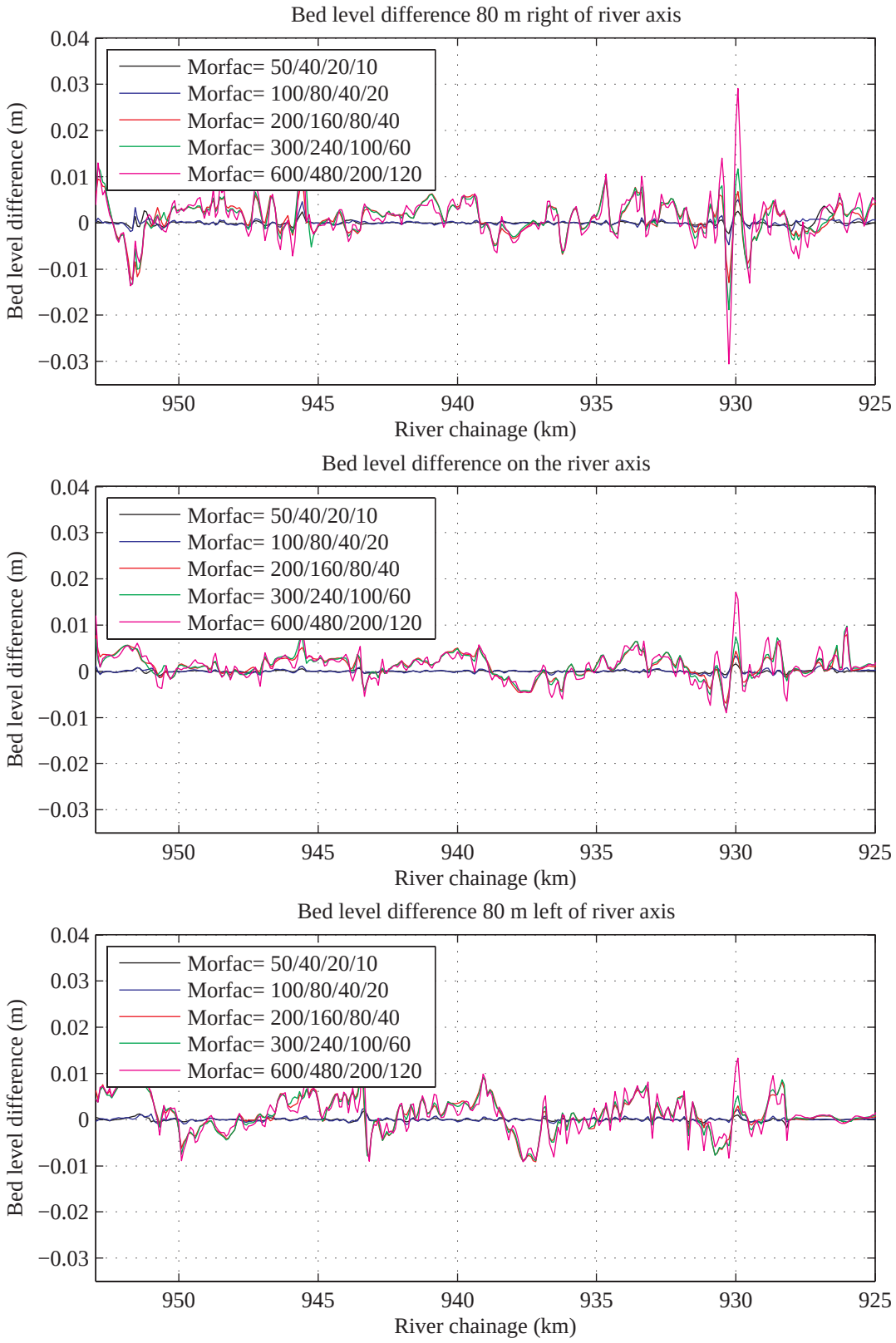

Figure 3.12 Bed level differences between the reference case with a trench and simulations using different morphological acceleration factors after a period of 5 years (discharge hydrograph).

3.4 Conclusions

The time step analysis in Section 3.2 shows that stable simulations yielding smoothly developing results are achieved with time steps of up to 1.5 minutes. Since the deviations of the model results for this time step from the time step used so far ($\Delta t = 0.4$ min) are acceptable, a time step of 1.5 minutes is used for future calculations. This results in an acceleration of the simulations by a factor of 3.4.

The analysis of the morphological acceleration factor in Section 3.3 shows that the factors used so far can be increased significantly without considerable loss in accuracy of the model results. Therefore the maximum factors tested (Table 3.5) are used in further simulations. This speeds up further the simulation time by a factor of 1.6.

Table 3.5 Morphological acceleration factors to be used in future simulations.

Discharge (m^3/s)	Morfological acceleration factor (-)
1187	600
2000	480
3080	200
4422	120

The investigation of the morfac setting for both constant discharge levels and for discharge time series for the DVR model of the Waal domain is rather complete. This does however not imply that the ultimate state with respect to the morfac setting has been reached. For instance, the morfac setting should be revised when running the entire Rhine branches model with the 5 domains. Besides, the morfac setting is not investigated in the light of detailed flood waves. Nor is the setting addressed in relation to graded sediment processes. From experiences in Mosselman et al. (2007) concerning the graded sediment model used for the case study of sediment nourishments in de Bovenrijn, it is known that the morfac had to be brought down to 10 in order to achieve stable simulations. This implies that the setting derived for the uniform sediment model is most probably not optimal for a model with graded sediment processes.

4 Application of parallel computation

4.1 Method

The objective of this chapter is to investigate the possibility to reduce the computation time by the application of parallel computation. For parallel computation, the technique of domain decomposition is used. Domain decomposition is a technique in which a model domain is subdivided into several smaller model domains, which are called sub-domains. The computations can be carried out separately on these sub-domains. The communication between the sub-domains takes place along internal open boundaries, or so-called domain boundaries. If these computations are carried out concurrently, we speak of parallel computing. The objective of parallel computing is to reduce the computation time via multiple domain simulations.

Earlier attempts in Van Vuren et al. (2006) & Yossef et al. (2006) showed that parallel computations using a cluster of 70 computers with dual processors, the h3 cluster, resulted in an opposite effect: an increase in computation time. This was mainly due to the fact that the communication between the sub-domains run at separate processors counteracted the reduction of computation time achieved by parallel computation.

In the current research a different computer with 8 processors ánd a shared memory, the Mordax machine, is used. The shared memory creates a faster communication between the processors used for the sub-domains. Table 4.1 gives the specifications of the Mordax machine and the h3 cluster.

Table 4.1 Overview of the two machines used for the comparison for parallel computations.

Machine	Processors	Memory
Mordax Machine	8 AMD processor machine	16 Gb of shared RAM
H3 cluster (a cluster of 70 pc's)	dual processor AMD Ath64 X2 AM2 2200 (a total of 140 jobs can be run)	4 Gb ddr2 memory

The impact of parallel computation is evaluated on the basis of the following test simulations with the DVR model of the river Waal at the Mordax machine:

1. a reference simulation with a single domain for the Waal branch between river chainage km 867.40 to km 953;

2. simulations for which the Waal domain has been split into four domains that were run in parallel. The four domains cover the following river chainages:

a) domain 1: km 867.4 to km 889.0;
b) domain 2: km 889.0 to km 910.1;
c) domain 3: km 910.1 to km 931.6;
d) domain 4: km 931.6 to km 953.0.

For the simulations with the DVR model of the Waal, Grid 2 (see Section 2.2.2) is used as a reference. For the simulation with parallel computation, Grid 2 is split into four sub-grids. Table 4.2 gives an overview of the characteristics of the sub-grids. The communication between the sub-domains takes place along three internal open boundaries. To test the performance at the domain boundaries, two additional simulation (one with a single domain and one with the four sub-domains) are carried out with a trench in order to evaluate the evolution of the trench over the domain boundary.

Table 4.2 Characteristics of the sub-grids of the Waal.

Gridname	Waal	Waal 1	Waal 2	Waal 3	Waal 4
number of grid cells	64 x 702	64 x 177	64 x 177	64 x 178	64 x 176
number of grid cells	44928	11328	11328	11392	11264
river chainage	867.4 - 953	867.4 - 889	889 - 910.1	910.1- 931.6	931.6 - 953
relative size in simulation	100 %	25 %	25 %	25 %	25 %

At the upstream inflow boundary at the Pannerdensche Kop a constant discharge of 1580 m^3/s and a constant bed level degradation equivalent to 2 cm per year is imposed. At the downstream boundary a constant water level of 95 cm was used, based on the rating curve in Mosselman et al. (2006). The simulations run for a period of 20 years. In Section 4.2.1, the Waal simulations are compared by simulation time as well as the differences in the computed results after 20 years, viz. the differences in morphological response and flow pattern.

The performance of the new Mordax machine is evaluated by repeating the test simulation of the Waal on the h3 cluster. In addition, a simulation with the complete model including the five Rhine branches Bovenrijn, Waal, Pannerdensche Kanaal, IJssel and Nederrijn is run on both the Mordax machine as the h3 cluster. Table 4.3 gives an overview of the number of grid cells of the grids in the complete Rhine branches model.

Table 4.3 Characteristics of the original fine grids of the Rhine branches model (Van Vuren et al. (2006)).

Gridname	Bovenrijn	Waal	Pan. Kanaal	IJssel	Nederrijn
number of grid cells	90 x 237	124 x 1402	96 x 184	182 x 405	93 x 179
number of grid cells	21330	173848	17664	73710	16647
relative size in simulation	7 %	57 %	6 %	24 %	5 %

The complete Rhine branches model is run for a period of 10 years, driven by a constant discharge of 2500 m^3/s and a bed degradation of 2 cm per year at the upstream boundary of the Bovenrijn. At the downstream boundaries a discharge outflow at the Nederrijn of 444 m^3/s, a water level of 5.80 m at the IJssel and a water level of 1.04 m at the Waal are imposed. For other model settings, we refer to Van Vuren et al. (2006). The comparison between the Mordax machine and the h3 cluster is restricted to the difference in computation time, see Section 4.2.2.

Table 4.4 gives an overview of all simulations in this chapter.

Table 4.4 Overview of the simulation used for testing the application of parallel computation.

# simulation	# domains	# nodes	machine	grid	description
From a single Waal domain to four sub-domains					
1.	1 domain	1	Mordax	wl grid 2	a) with and b) without trench
2.	4 domains	4	Mordax	wl grid 2	a) with and b) without trench
Parallel computation with h3 cluster and Mordax machine					
3.	1 domain	1	h3	wl grid 2	-
4.	4 domains	4	h3	wl grid 2	-
5.	4 domains	1	h3	wl grid 2	-
6.	5 domains	1	h3	br, w1, pk, ijs, nr	grids of the original Rhine branches model, see Van Vuren et al. (2006)
7.	5 domains	5	Mordax		

4.2 Impact of parallel computation

4.2.1 From a single domain to parallel computation with four sub-domains

In this section the difference between a simulation with the Waal schematised with a single domain and four sub-domains is discussed. We focus on differences in flow pattern, indicating the depth-averaged velocity and the morphological response after a period of 20 years.

Figure 4.1 shows the depth-averaged velocity along the river axis after a period of 20 years of morphological simulation, for a single and multiple domain simulation. The differences in depth-averaged velocity along the river axis and 80 m left and 80 m right from the river axis are presented in Figure 4.2. At the domain boundary differences in the order of 0.1 m/s occur. Figure 4.3 illustrates the flow pattern near one of the domain boundary, after a simulation period of one day. The red arrows show the flow pattern for the single domain simulation, the blue and green arrows indicate the flow pattern for the multiple domain simulation. The small difference in flow pattern seems to be induced by a difference in the spiral flow intensity, as indicated in Figure 4.4.

Figure 4.5 shows the morphological evolution after a period of 20 years for the single and the multiple domain simulation. The bed level difference between both simulations is presented in Figure 4.6.
The bed level differences along the river axis, 80 m left and 80 m right from the river axis, are less than 0.1 m. In other words, they are very small as compared to the natural variation presented in Section 2.4.3. Figure 4.7 shows the evolution of a trench over the domain boundary. Despite, the differences in flow pattern, the trench appears to smoothly pass the domain boundary.

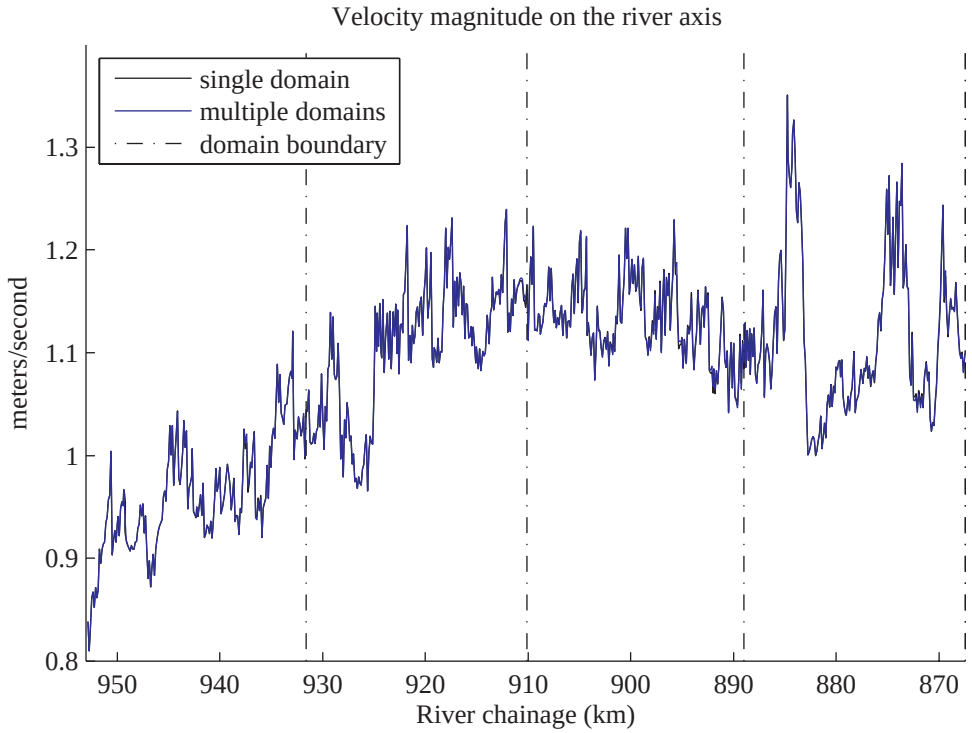

Figure 4.1 Depth-averaged velocity along the river axis after a period of 20 years using a single domain and four sub-domains.

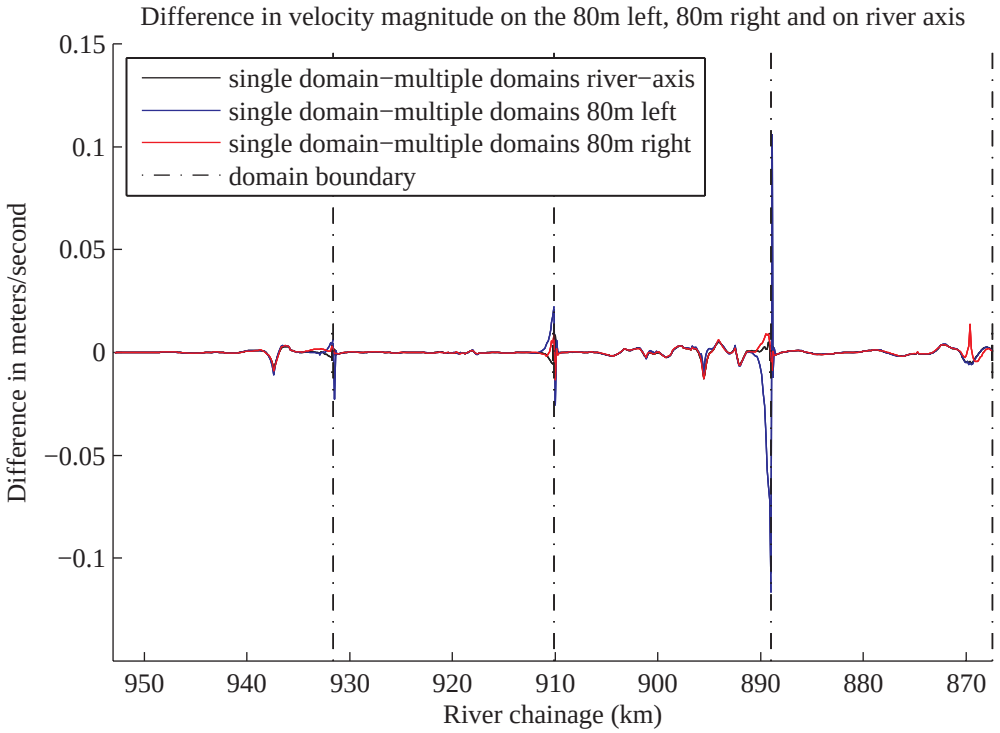

Figure 4.2 Difference in depth-averaged velocity along the river axis, 80 m left and 80 m right from the river axis, after a period of 20 years using a single domain and four sub-domains.

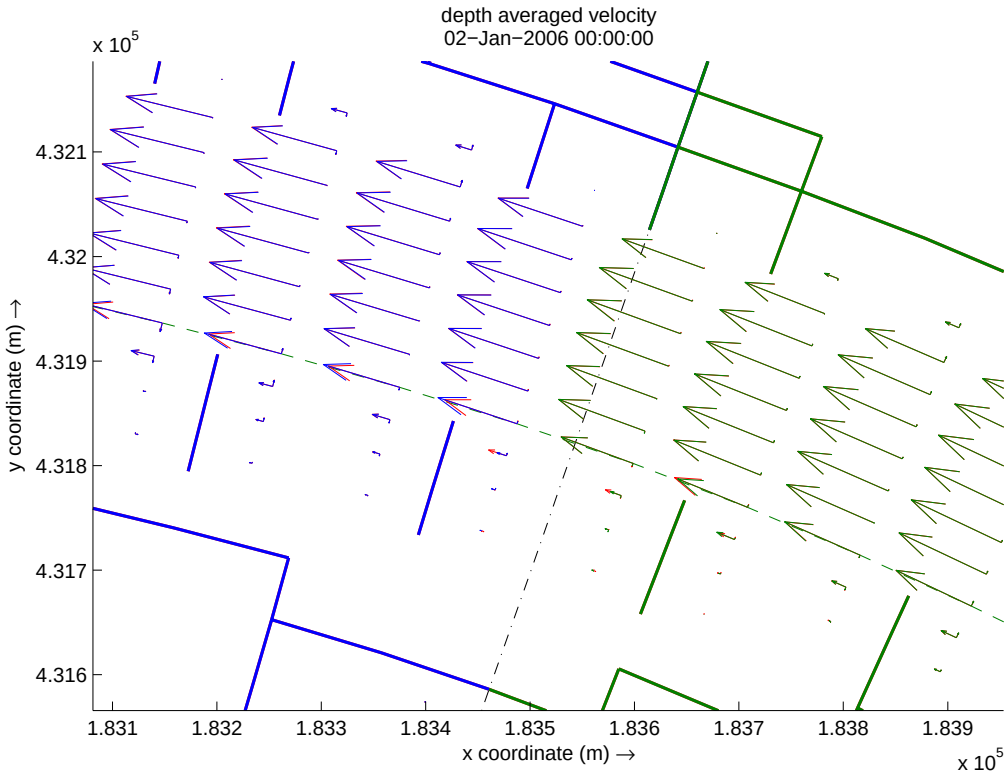

Figure 4.3 Flow pattern, indicating the depth averaged velocity after a simulation period of 1 day using a single domain (red arrows) and four sub-domains (blue and green arrows). The blue and green show the position of the groynes. The black dash-dot line is the domain boundary.

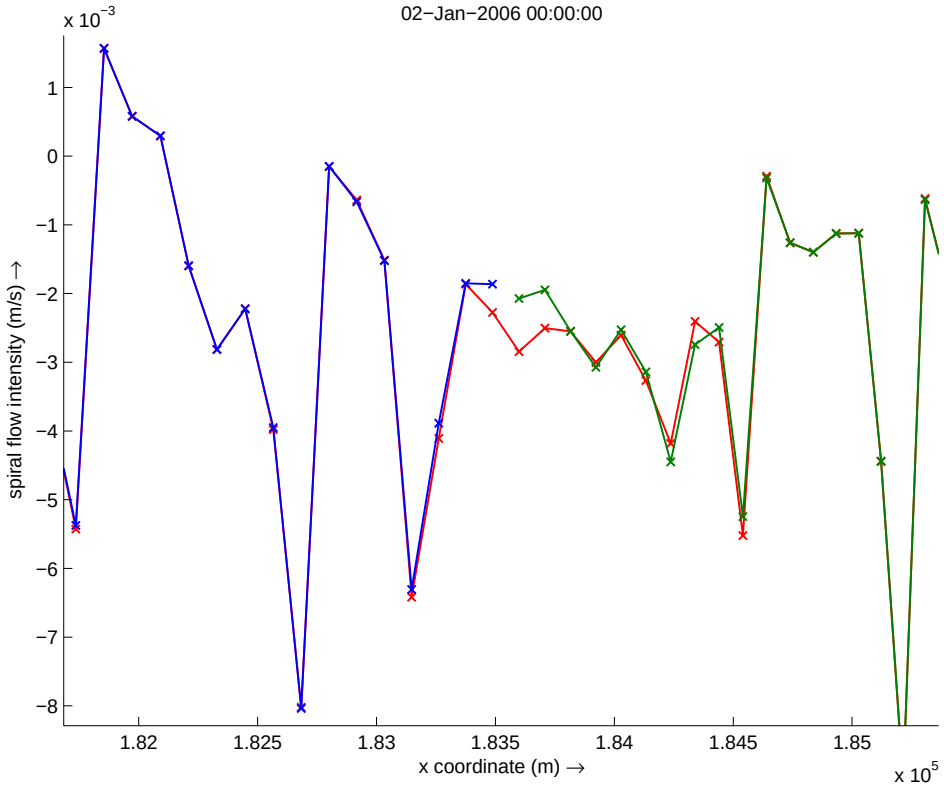

Figure 4.4 Spiral flow intensity after a simulation period of 1 day for a simulation with a single domain (red lines) and four sub-domains (blue and green lines).

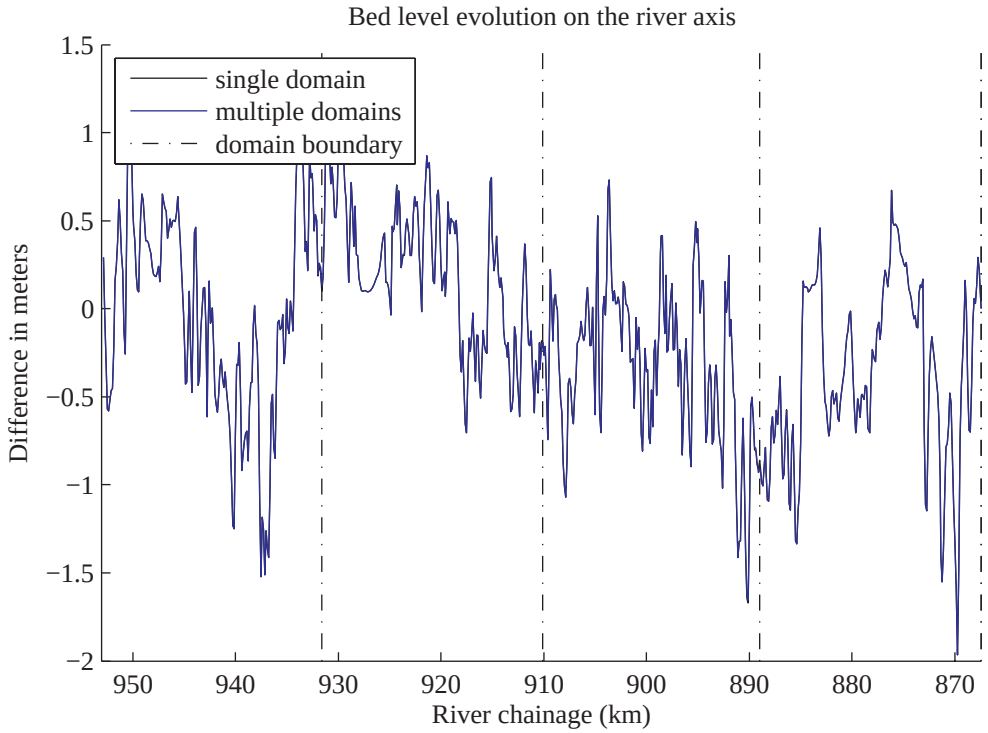

Figure 4.5 Resulting bed levels along the river axis, after a period of 20 years, for a simulation with a single domain (black line) and four sub-domains (blue line). The black dash-dot line is the domain boundaries.

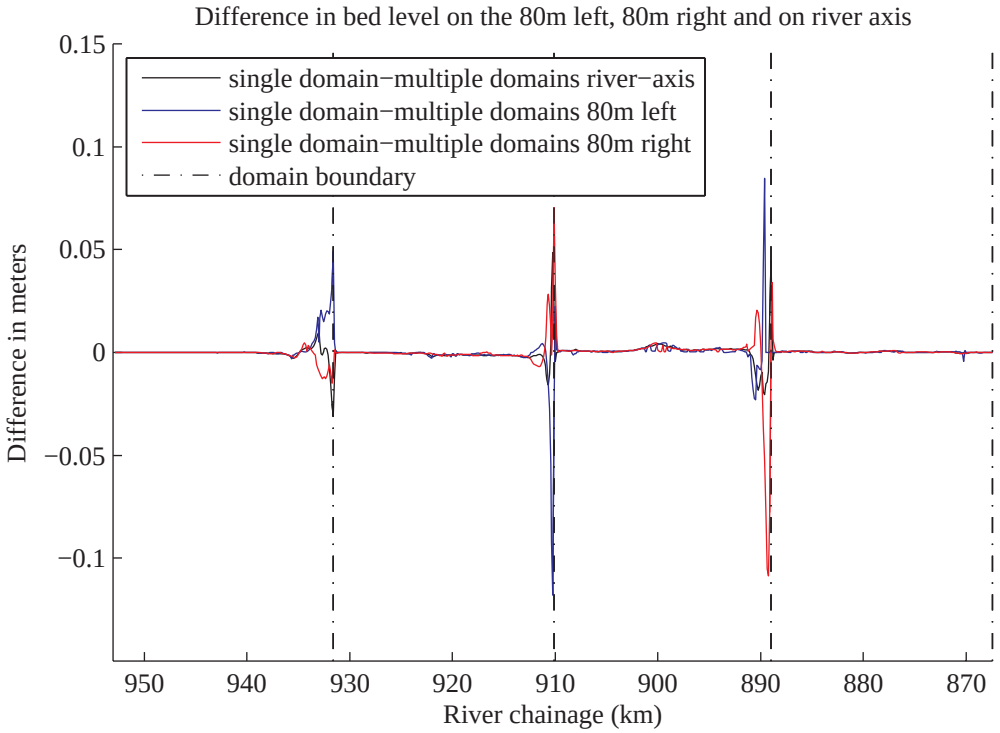

Figure 4.6 Difference in resulting bed levels along the river axis, after a period of 20 years, between the simulation with a single domain and with four sub-domains. The black dash-dot line is the domain boundaries.

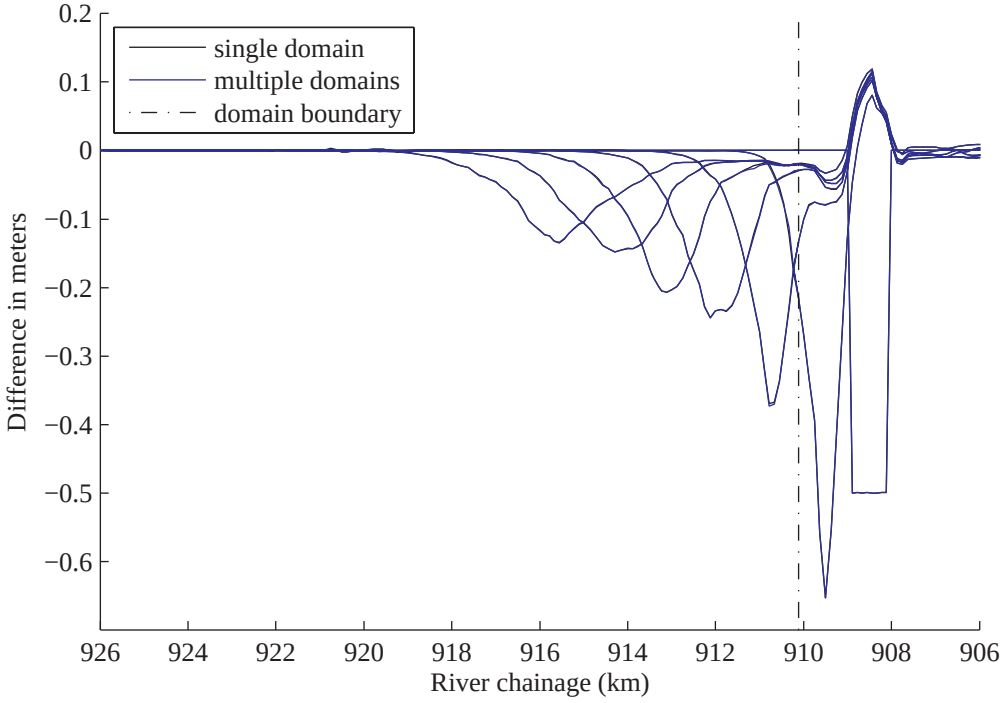

Figure 4.7 The evolution of a trench in the Waal after a period of 2 years for a simulation with a single domain (black line) and four sub-domains (blue line). The black dash-dot line is the domain boundary.

The results show that the accuracy lost by the application of parallel computation is negligible. As indicated in Table 4.5 parallel computation accelerates the computation with a factor 2.3, yielding a 56% computation time reduction.

Table 4.5 Overview of the simulation time and acceleration.

# simulation	# domains	# nodes	machine	Simulation time (hours)	Acceleration w.r.t. the reference model (-)
1.	1 domain	1	Mordax	10:46:39	reference model
2.	4 domains	4	Mordax	4:38:25	2.3

4.2.2 Parallel computation with h3 cluster and Mordax machine

Since, the difference in hydrodynamics and morphology between the single and multiple domain simulations turn out to be limited, we focus in this section purely on the computation time reduction between simulations at the h3 cluster and the Mordax machine. The simulations of the Waal and the complete Rhine branches model at the h3 cluster using a single computation node are taken as a reference.

Table 4.6 gives an overview of the simulation time, and the ratio between the reference simulation and the other simulations.

Table 4.6 Overview of the simulation time and acceleration.

# simulation	# domains	# nodes	machine	Simulation time (hours)	Acceleration w.r.t. the reference model (-)
Waal model					
1.	1 domain	1	Mordax	10:46:39	1,08
2.	4 domains	4	Mordax	4:38:25	2,51
3.	1 domain	1	h3	11:39:45	reference model
4.	4 domains	4	h3	10:55:45	1,07
5.	4 domains	1	h3	18:01:39	0,65
Complete Rhine Branches model					
6.	5 domains	1	h3	196:58:07	reference model
7.	5 domains	5	Mordax	175:33:54	1,12

The Mordax machine appears not to be significantly faster when running a single domain simulation (simulation number 1). However, a significant computation time reduction is achieved by a parallel multiple domain simulation at Mordax machine in comparison with a multiple domain simulation at the h3 cluster. Running the Waal model with four sub-

domains yields at the h3 cluster a computation time reduction of 7% (when using 2 computers with dual processors, simulation number 4), whereas at the Mordax machine a reduction of 60% is reached (simulation number 2).

The difference in computation time between a single and a multiple domain simulation using a single computation node (one processor) indicates that the communication at the domain boundaries is time-consuming (simulation number 5). By choosing boundaries at river sections with the minimum number of grid cells in transverse direction, the across communication can be minimised.

A simulation of the complete Rhine branches model at the Mordax machine yields only a slight increase in performance: a computation time reduction of 11% (simulation number 7). This speed up is quite small when compared with the reduction of 60% of the multiple domain simulation of the Waal model at the Mordax machine (simulation number 2). This is due to the fact that the Waal domain contains 57% of the grid cells in the complete Rhine branches model, see Table 4.3. This means that the simulations of the other processors are waiting every time step for the processor of the Waal domain to be finished. Cutting the Waal grid into 4 equal parts would further reduce the computation time. Considering also the share of the IJssel domain in total number of grid cells, it is recommended to optimize the sub-domains in such a way that the load is more or less evenly balanced over the processors. This optimisation is however not part of the present study.

4.3 Conclusions and recommendations

Domain decomposition in combination with parallel computation turns out to be a useful technique to reduce the computation time. It appears to be important to use a computer with a number of processors sharing the same memory, such as the Mordax machine.
In comparison with the h3 cluster with several computers with dual processors, a significant reduction is achieved by the Mordax machine. Splitting the Waal domain in four sub-domains and run them in parallel on the Mordax machine results in a reduction of 60%, whereas the same simulations at the h3 cluster reduces the computation time only by 7%. This appears to be due to the extra time required for communication between the sub-domains run at separate processors, counteracting the reduction of computation time achieved by parallel computation.

It is recommended to use the Mordax machine for future projects. Moreover it is recommended to optimise the sub-domains of the complete Rhine branches model in such a way that the load is more or less evenly balanced over the number processors.

The communication at the domain boundaries is time-consuming. Therefore, it is recommended to choose the domain boundaries at the river sections with the minimum number of grid cells in transverse direction. In this way the across communication can be minimised.

There appears to be still some physical restrictions for the domain decomposition. The simulations in Section 4.2.1 shows that information about spiral flow intensity is not transferred across domain boundaries. To minimise the impact of this aspect, it is

recommended to place the domain boundary is a more or less uniform river reach. The functionality of weirs and thin dams at domain boundaries is also an untested feature (personal communication with Bert Jagers), so it is recommended to avoid these structures at the domain boundary.

5 Application of a more efficient description of flow through the floodplain

5.1 Introduction

In this chapter, we investigate whether the flow through the floodplain area can be dealt with in a more efficient way. Two different approaches has been investigated:

1. Two grid approach: an approach in which a grid covering only the main channel section is used for discharges below the bankfull discharge, whereas the entire model is used for discharges above bankfull. In this way, the flow through the floodplain is updated less frequent than the flow through the main channel;

2. Lateral water extraction & supply approach: an approach in which the model is reduced in size by cutting off the floodplain section. The discharge exchange between the cut-off floodplain and the remainder part of the model is imposed via lateral discharges along the boundaries of the other model. This discharge exchange is derived from a simulation with the complete model, and should be updated on a regular basis.

The two approaches are discussed in the sections below.

5.2 Two grid approach

The objective of the two grid approach is to reduce the computational time by using a grid that covers the main channel and the groyne section for discharges below bankfull, and using the entire model grid including the floodplain sections for discharges above bankfull. We refer to the first grid as ‘SMALL’ grid, and the second grid as ‘LARGE’ grid (see Figure 5.1).

To be able to perform this calculation the code for the discharge hydrograph (Yossef et al. (2006) had to be adapted such that the ‘SMALL’ and ‘LARGE’ grid could be used in sequence for the same hydrograph simulation. This involves the copying of data from the ‘LARGE’ grid on to the ‘SMALL’ grid when moving from a higher than bankfull discharge level to a lower than bankfull discharge level. Similarly information from the ‘SMALL’ is copied to the ‘LARGE’ domain when proceeding to a higher than bankfull discharge from a lower than bankfull discharge.

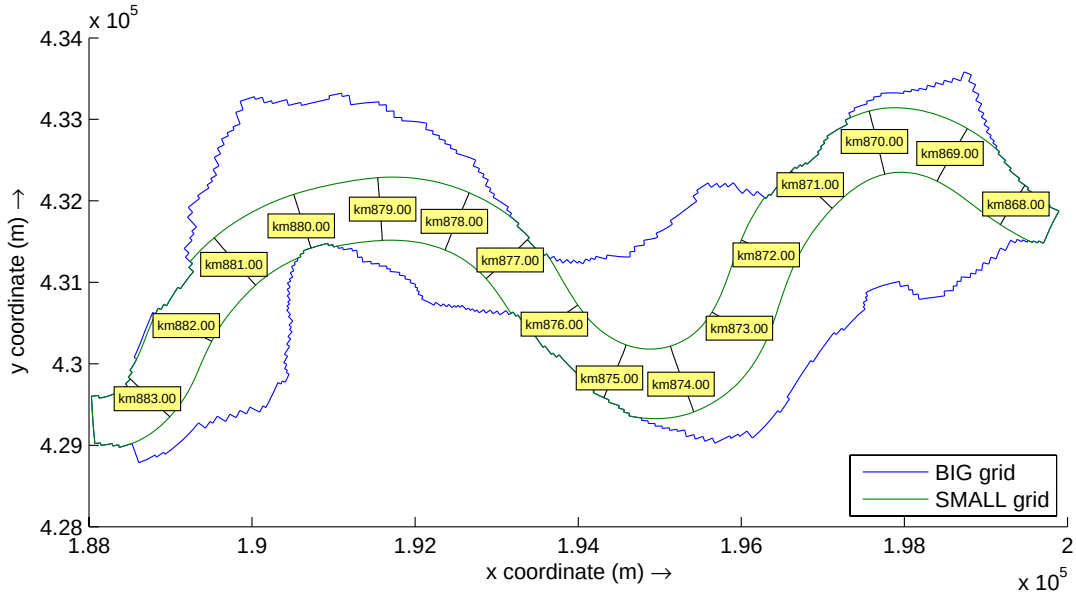

Figure 5.1 The outlines of the 'SMALL' and 'LARGE' grid for the Boven Waal models.

Initial testing of the newly developed code took place with the Bovenrijn model. In Mosselman et al. (2007), the Bovenrijn grid was already split in two grids, a 'SMALL' and a 'LARGE' grid. The tests showed that the 'SMALL' grid should be slightly wider than the section covering the main channel and the groyne fields. It appears important to include the flow pattern near the groyne fields to avoid large deviations in flow patterns with respect to the reference model covering the entire model grid.

Subsequent simulations were all done with the Waal model. We can differentiate between two models. The first model covers the Boven Waal from river chainage km 867 to km 883. The grid is based on the original fine grid and was shortened to speed up the computation time. The second model covers the Beneden Waal downstream of km 918. The latter model was also used in Chapter 4. The Beneden Waal model was based on Grid 5, and was included to investigate suitability of the two grid approach in a river reach characterised by a number of large open water areas in the floodplain and strong confinements of the floodplains by winter dykes. This leads to more lateral discharge exchanges over the cut-off boundary, and may make the two grid approach less appropriate.

Table 5.1 gives an overview of all simulations. For simulation #1 to #3 the Boven Waal model is used, whereas simulation #4 and #5 are performed with the Beneden Waal model. Simulations #2, #3 and #5 use the two-grid approach (i.e. 'SMALL' and 'LARGE'). Simulation #1 and #4 are reference simulations using only the 'LARGE' grid, for the respective cases.

Table 5.2 gives an overview of the number of grid cells for the 'SMALL' and the 'LARGE' grids of both models (see also Figure 5.1).

Table 5.1 Overview of the simulation used for testing the application of the two grid approach.

# simulation	discharge levels simulated with the SMALL grid	description
Boven Waal model		
1.	-	reference simulation
2.	1187 m^3/s	two grid approach
3.	1187 m^3/s and 2000 m^3/s	two grid approach
Beneden Waal model		
4.	-	reference simulation
5.	1187 m^3/s and 2000 m^3/s	two grid approach

The simulations consist of morphodynamic simulation for a period of 5 years, driven by the discharge hydrograph presented in Figure 2.1. Table 5.3 shows the discharge levels of the hydrograph, the number of days the discharge level occur per year, and the morphological acceleration factors that are used for each discharge level. Accounting for the difference in morphological acceleration factors, the fifth column shows the percentage of the hydrodynamic simulation time at each discharge level in the hydrograph during the simulation.

Table 5.2 Characteristics of the sub-grids of the Waal.

Gridname	Boven Waal	Beneden Waal
number of grid cells in 'LARGE' grid	90 x 237 = 32736	49 x 428 = 20972
number of grid cells in 'SMALL' grid	36 x 264 = 9504	24 x 428 = 10272
Relative size of the 'SMALL' grid	29,0 %	49,0 %

Table 5.3 Schematisation of the discharge hydrograph of the Waal.

Schematisation of the discharge hydrograph of the Waal (m^3/s)	Morphological time (days)	Morphological acceleration factor (-)	Flow time (days)	Percentage of the discharge level in the morphodynamic simulation (%)
2000	30	80	0.375	7.9 %
3080	8	40	0.2	4.2 %
4422	14	20	0.7	14.8 %
3080	8	40	0.2	4.2 %
2000	86	80	1.075	22.7 %
1187	219	100	2.19	46.2 %

For the Waal the bankfull discharge is approximately 1560 m^3/s. This implies that in principle the 'SMALL' grids should only be used for the lowest discharge level in the hydrograph, i.e. 1187 m^3/s.

Neglecting spin-up time, 46.2% of the simulation the 'SMALL' should be used. Including the second lowest discharge 2000 m^3/s would result in 77% (≈ 46.2% + 7.9% + 22.7%, see Table 5.3) of the simulation to be run with the 'SMALL' grid. For testing purposes the second lowest discharge (2000 m^3/s) has been included.

The results are discussed in Section 5.2.1. We focus on differences in flow pattern, indicating the depth-averaged velocity, in the morphological response after a period of 5 years, and in computation time.

5.2.1 Results

First, the differences in the morphological response after a period of 5 years, in the flow pattern and in the computation time, are discussed for the Boven Waal model. Figure 5.2 shows the bed level difference after a period of 5 years for the simulations with the two grid approach (simulation #2 and #3) and the reference simulation (simulation #1). The absolute differences are less than 0.1 m, which is small in comparison with the natural variation in the bed level within a period of a year, as presented in Section 2.4.3. The differences in bed level at the inflow and outflow boundary are slightly larger than in the remainder part of the model. This appears to be due to small differences in depth-averaged velocity, see Figure 5.3. This may be caused by slight variations in the boundary segments.

For the Boven Waal models the bed level difference and difference in flow pattern between the simulation using the 'SMALL' model only for the discharge level of 1187 m^3/s (simulation #2) and the simulation using the 'SMALL' model for the discharge level of 1187 m^3/s and 2000 m^3/s (simulation #3), are negligible. Apparently, the discharge of 2000 m^3/s flows in total through the 'SMALL' model area. There is not any lateral flow exchange with the surrounding floodplains at this discharge level.

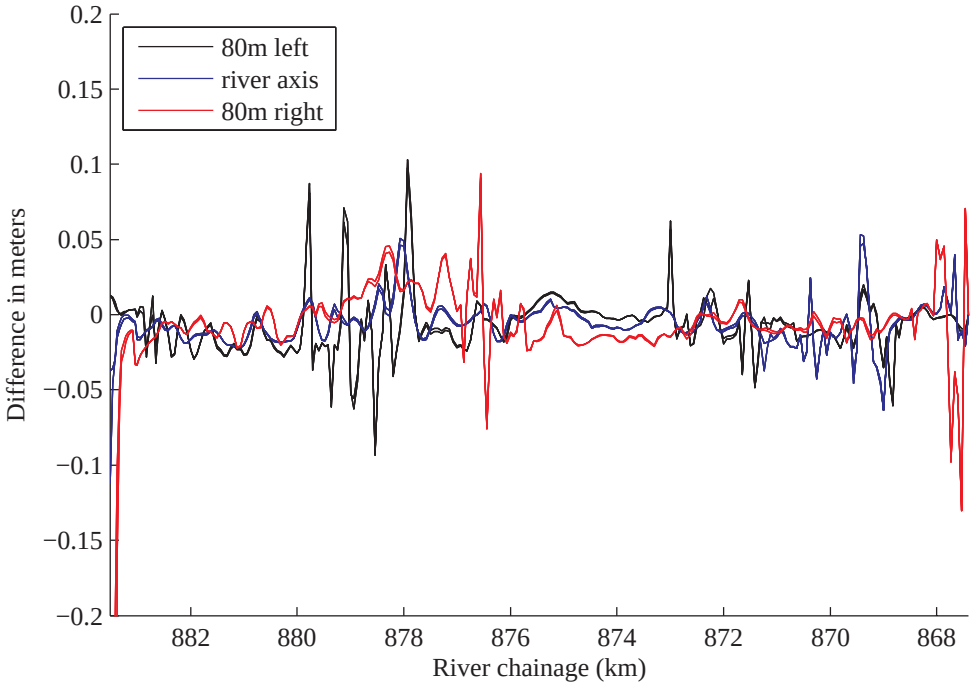

Figure 5.2 Bed level difference in the Boven Waal after a period of 5 years between the simulations using the two grid approach (sim. #2 and #3) and the reference simulation (sim #1) using one grid.

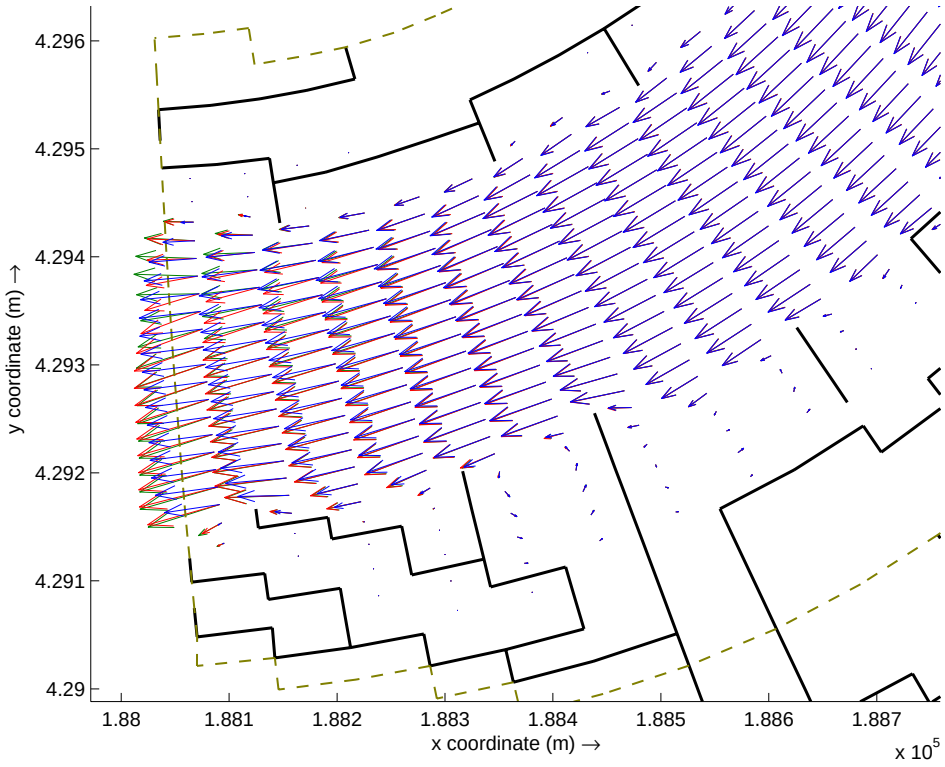

Figure 5.3 Flow pattern, indicating the depth averaged velocity after a period of 5 year, at the outflow boundary for the reference model (simulation #1, blue arrows) and for the simulations with the SMALL model for the discharge of 1187 m^3/s (simulation #2, red arrows), and the discharge of 1187 m^3/s and 2000 m^3/s (simulation #3, green arrows). The green dashed line is the boundary of the SMALL grid. The black dash-dot line is the domain boundary.

Figure 5.4 shows the bed level difference between the reference model (simulation #4) and the simulation with the two grid approach for the Beneden Waal (simulation #5). The difference in bed level after 5 years is in the order of 0.4 m. As indicated by the flow pattern in Figure 5.5 this is due to flooding of the floodplains at the discharge level of 2000 m^3/s. The 'SMALL' grid is not able to accurately capture the flow field at the discharge of 2000 m^3/s. In other words, when using the two grid approach, the 'SMALL' model should only be used for discharges in which the flow is completely contained within the grid (e.g. discharge levels below bankfull).

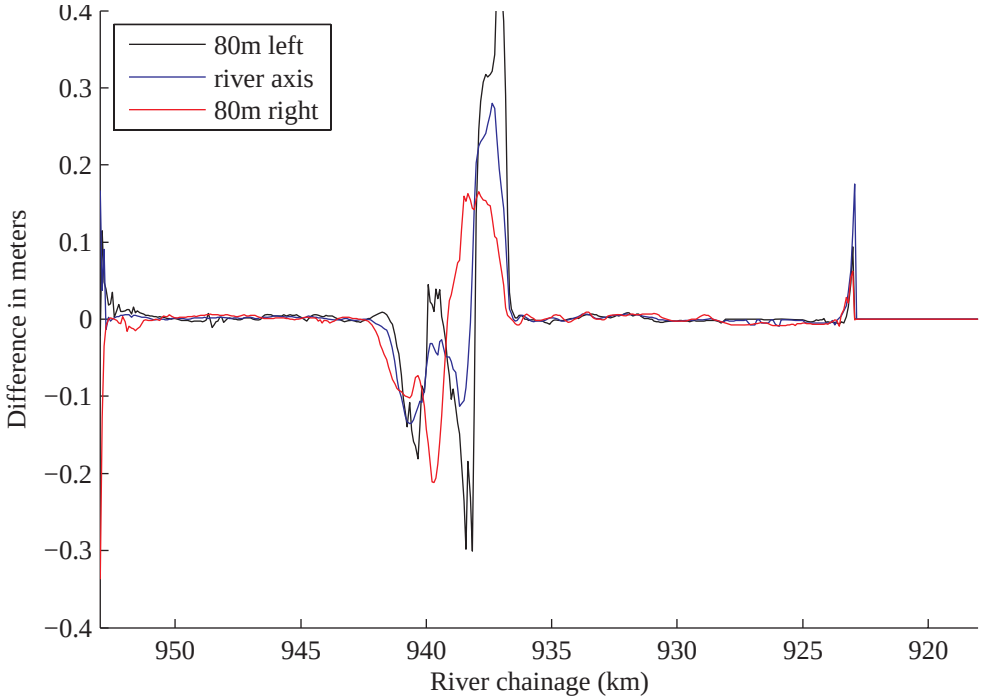

Figure 5.4 Bed level difference in the Beneden Waal after a period of 5 years between the simulation using the two grid approach (simulation #5) and the reference simulation (simulation #4).

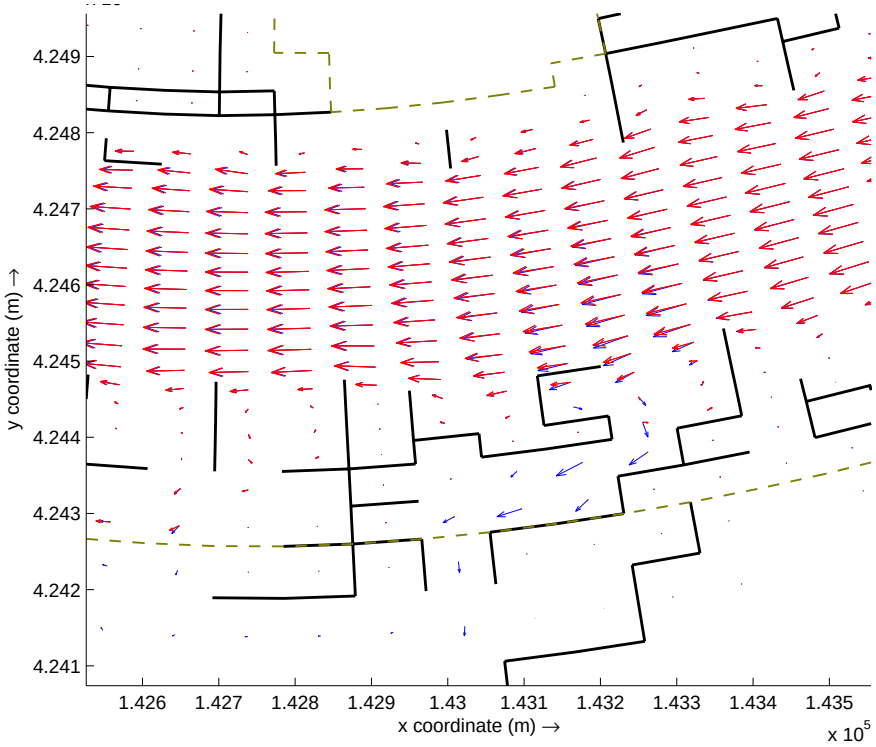

Figure 5.5 Flow pattern, indicating the depth averaged velocity at the discharge of 2000 m^3/s, in the vicinity of river chainage km938 in the Beneden Waal for the reference (sim. #1; blue arrows) and for the simulation (#5) with the two grid approach (red arrows) for the discharge of 2000 m^3/s. The green dashed line is the boundary of the SMALL grid. The black lines give the position of the weirs.

Table 5.4 gives the computation time and acceleration with respect to the reference model. The application of the two grid approach, using the 'SMALL' model for the discharge level of 1187 m^3/s (simulation #2) yields an acceleration of 18% for the Boven Waal model. This acceleration increases to 35 %, when using the 'SMALL' model for the discharge level of 1187 m^3/s and 2000 m^3/s (simulation #3). For the Beneden Waal (simulations #4 and #5) the computation time reduction is 26%.

Table 5.4 Acceleration of the computations for the two grid approach with respect to reference simulations using the complete model.

# simulation	discharge levels simulated with the SMALL grid	description	simulation time (hours)	reduction w.r.t. the reference model
Boven Waal model				
1.	-	reference simulation	15:50:44	-
2.	1187 m^3/s	two grid approach	13:01:46	18%
3.	1187 m^3/s and 2000 m^3/s	two grid approach	10:15:53	35%
Beneden Waal model				
4.	-	reference simulation	3:49:54	-
5.	1187 m^3/s and 2000 m^3/s	two grid approach	2:50:32	26%

A comparison between the reduction in computation time achieved with the two grid approach in simulation #2 for the Boven Waal (35 %) and simulation #5 on the Beneden Waal (26 %) shows the two grid approach is relatively more efficient for the fine reference grid than the optimised grid (Grid 5). The efficiency can be explained by the relative sizes of the grids as shown in Table 5.2. In the Boven Waal (simulations #4 and #5) the percentage of grid cells not used is 71 % and for the Beneden Waal (simulations #2) this percentage is 51% (In Grid 5 the grid covering the floodplain was coarsened up to a factor 4).

5.2.2 Conclusion

The two grid approach is a useful technique to reduce the computation time. When using the two grid approach, the 'SMALL' model should only be used for discharge levels below the bankfull of approximately 1560 m^3/s. Application of the two grid approach to a model of the Boven Waal yields a computation time reduction of 18 %. This may be less than expected, considering the 46% of the simulation is done with the 'SMALL' grid, and the percentage of grid cells that is not considered in the 'SMALL' model simulation (71%). Apparently the computation time involved with communication and morphological spin up is significant.

The test simulations showed that the 'SMALL' grid should be slightly wider than the section covering the main channel and the groyne fields. It appears important to include the flow pattern near the groyne fields to avoid large deviations in flow patterns with respect to the reference model covering the entire model grid.

At low discharges the flow show be totally included in the 'SMALL' grid, otherwise big differences in the morphology will appear. When there is exchange over the domain boundary this should accounted for.
Perhaps the approach of lateral in- and outflow in the proceeding section will offer a solution to prescribing the correct discharges at the cut-off boundary.

5.3 Lateral water extraction & supply approach

The objective of the lateral in- & outflow approach is to reduce the computation time by using a grid that covers only the main channel and groyne section. For discharges above bankfull, the flow and discharge momentum entering the main channel from the floodplain area is schematised by imposing lateral in- and outflows from the floodplain.

In other words, the model is reduced in size by cutting off the floodplain section. The discharge exchange between the cut-off floodplain and the remainder model is imposed via lateral discharges along the boundaries of the remainder model. These lateral discharges, either a supply or an extraction of discharge, are derived from a simulation with the original model. It turned out that to guarantee that the resulting flow field at these exchange locations yields an equivalent flow magnitude and flow direction, the lateral discharges have to be imposed with type "momentum". This implies that the inflowing discharges are introduced having a prescribed momentum, i.e. discharge rate, flow velocity and angle with respect to North. Furthermore it is relevant to preserve the total mass balance of the model.

Since, the morphological response in the main channel will affect the discharge distribution between the main channel and the floodplains, the discharge distribution will be updated periodically. This means that the full model has to be run again with the changed bed topography (hydraulically) to simulate the new flow patterns at flood condition. It is expected that a five to ten-year interval for updating the discharge distribution is sufficient.

The aim of this approach is to modify the flow in model with reduced grid along the boundaries in such a way that discharges, flow velocities and direction of flow in this boundary reach are identical to those in the full model. It is then expected that the internal flow field in the reduced model (notably the flow in the main channel) will also become identical to the full model results. However, it is not possible in Delft3D to replace the flow in grid cells along the boundary exactly with that of the full model (this type of functionality is not available). Nevertheless, by using the lateral discharges it is possible to force the near-boundary flow in such a way that the resulting flow field in the reduced model is approximating the flow field in the full model very well. Lateral discharges of the momentum-type are introduced into the momentum and continuity equation for flow in Delft3D as source terms. Therefore they act as forces that modify the existing flow field. They can be used to more or less push or draw the existing flow lines in the direction and magnitude that fits the full model results. It has been found that it was necessary to add a double row of lateral discharges, combined with a series of thin dams along the boundary, to get the best approximation.

In Figure 5.6 the definition of grid administration of the Delft3D staggered grid, and the relevant parameters are presented. The direction of the grid and flow quantities are shown for the typical model-schematisation of the DVR models.

The required functionality has been derived by testing different approaches for introducing the lateral inflows on a simplified testmodel. The model consist of a rectangular channel with a constant discharge.
The left part of the channel has a higher elevation than the right part, to reproduce a flood plain. The flood plain is raised in two steps downstream, such that the flood plain flow is forced to enter the main channel (see Figure 5.7). The model is clipped at the flood plain (cutting a row of two cells wide from the flood plain). Note that in this model the n and m-coordinates are rotated 90º with respect to Figure 5.6 (coincidently).

The relevant settings of the model are summarised in the following table.

Setting	**Value**
grid full model	n = 1 to 10; m=1 to 17
grid small model	n = 1 to 8; m=1 to 17
bed slope	1.67E-4 m/m
bed roughness (Chézy value)	50 $m^{1/2}/s$
inflow discharge (full model)	3500 m^3/s
inflow discharge (small model. from full model)	2988 m^3/s
water depth (lower water level)	8.5 m
bed-level main channel	0.5 to 0 m
bed-level flood plain	5 m; 6 m; 8 m resp.

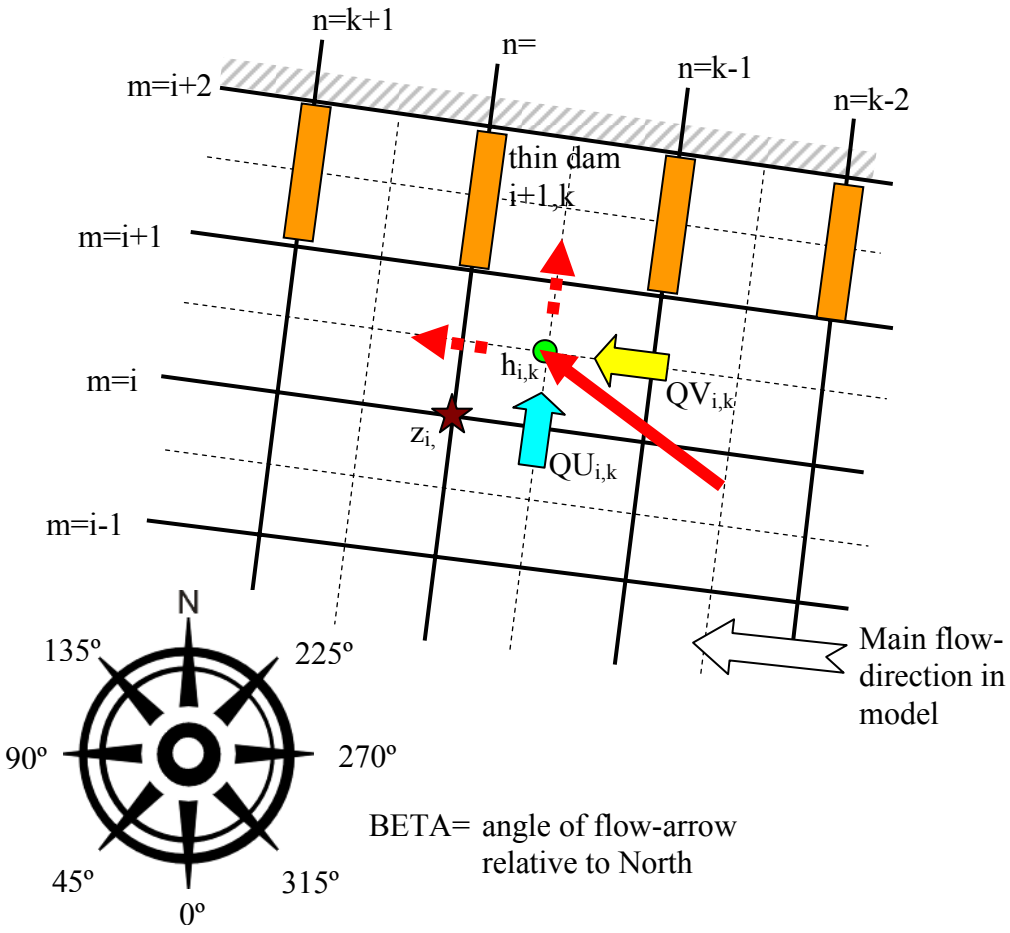

Figure 5.6 Schematic representation of staggered grid in Delft3D (drawn line = morphological grid, dashed lines = hydrodynamic grid), representative quantities and their location for index number i,k (water level h, bed level z, discharge QU, discharge QV). The red arrow indicates location of an inflow-discharge at cell i,k, and the red dashed arrows indicate to which exchanges the components of this discharge are projected. The definition of the angle of inflow discharge is shown in the compass rose. Orange block indicate thin dams located along the boundary of the reduced grid.

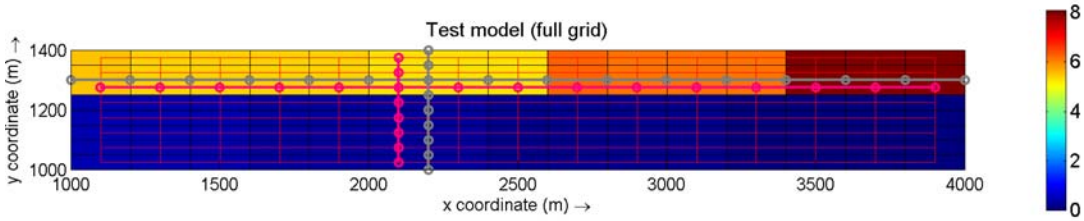

Figure 5.7 Topview test model showing bed topography (m) and coordinates of grid lines for the full grid. Flow is from left to right. The model is clipped at the gray grid line indicated horizontally in the plot (cutting a row of two cells wide from the flood plain).

The best results were obtained using the following method:

1. The first two rows of grid cells along the left boundary of the reduced model are defined as exchange area. Using lateral inflows it is necessary to adjust the flow field in this zone, such that the flow in the rest of the model fits the flow in the full model.
2. At the inflow boundary the discharge is imposed that is computed with the full model for the sections that coincide with the small grid (substract the inflow to the flood plain).
3. Introduce a row of thin dams along the exchange boundary in the reduced model (blocking flow along the boundary). In this zone we only allow transverse discharges, which we impose as lateral inflows. From the full model only the QV (transverse) values at the boundary are used for the laterals in this row of grid cells.
4. For the second row of grid cells the longitudinal flow QU is replaced by taking it out using a normal lateral discharge (no momentum, so without direction and velocity), and replacing it back with a momentum lateral discharge with the correct direction and velocity. Discharges used for the lateral are upwinded from the full model output, such that no mass loss or gain is occurring.

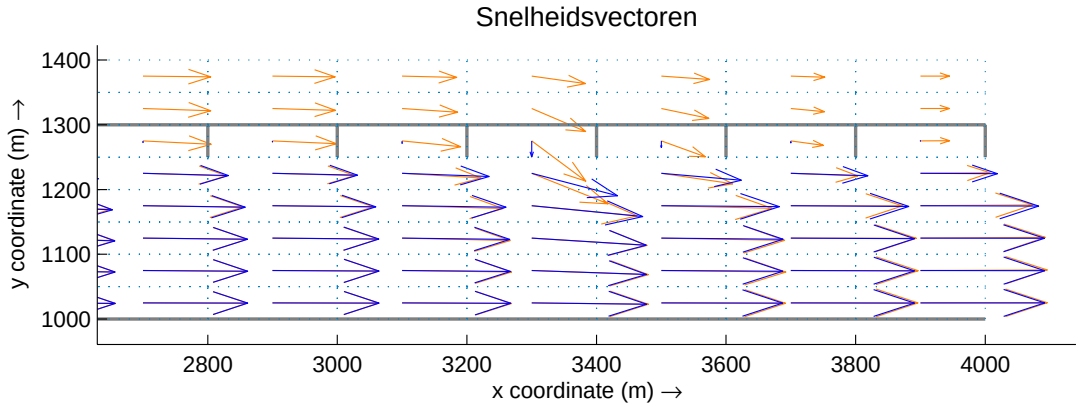

Figure 5.8 Plot of computed velocity vectors at section with flow from flood plain towards the main channel: orange arrows are computed with full grid, blue arrows are computed with reduced model and lateral discharges.

The agreement appeared to be acceptable, especially if noted that this is quite an extreme situation. The gain in computation speed was in the order of 50%.

The procedure is therefore extended and applied to the Waal River model for a discharge of 4422 m^3/s (flood discharge).

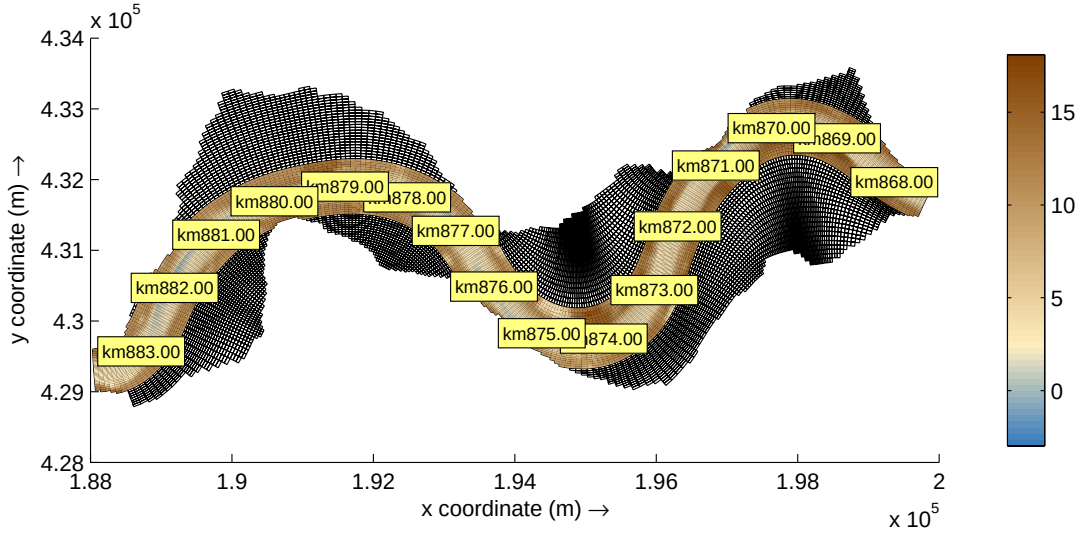

Figure 5.9 Model area applied for test of lateral discharges: colored bed-level section indicates the extent of the reduced grid. Flow is from right to left: grid numbering is n=1 to 264 from upstream to downstream, and m=1 to 124 from left bank to right bank.

The translation from previous results of the full model to discharge tables is programmed in Fortran. Hence it can be applied automatically into the morphology simulations as part of the discharge steps. The following steps have been defined:

- Read information from com-file, according to the following table (for the Waal grid)

	Flow direction	Transverse direction
grid numbering	n (positive downstream)	m (positive from left to right bank)
discharge per cell (com-file)	QV	QU
flow velocity (com-file)	V1	U1
x-coordinate of grid point on morphological grid (m,n)	XCOR	-
x-coordinate of grid point on morphological grid (m,n)	YCOR	-
Active cells KCS=1	KCS	-

Note that in the reduced grid (after clipping) the grid line 2 on the left bank corresponds to grid line 56 in the full grid. Similarly grid line 35 on the right bank corresponds with 89 in the full grid.

- Determine the lateral discharges on the zones along the boundaries in the reduced grid according to the following table (in the example of the Waal i=56 and j=89, k=2 to 264)

n=k	left bank		right bank	
	m=i	m=i+1	m=j-1	m=j
Discharge added QIN	$QIN_{i,k}=0$ if $QU_{i,k}\leq 0$ else $QIN_{i,k}=QU_{i,k}$	$QIN_{i+1,k}=0$ if $QU_{i,k}>0$ else $QIN_{i+1,k}=\lvert QV_{i+1,k}\rvert$ if $QV_{i,k}\geq 0$ else $QIN_{i+1,k}=\lvert QV_{i+1,k-1}\rvert$ if $QV_{i,k}<0$	$QIN_{j-1,k}=0$ if $QU_{i,k}<0$ else $QIN_{j-1,k}=\lvert QV_{j-1,k}\rvert$ if $QV_{j,k}\geq 0$ else $QIN_{j-1,k}=\lvert QV_{j-1,k-1}\rvert$ if $QV_{j,k}<0$	$QIN_{j,k}=0$ if $QU_{j,k}\geq 0$ else $QIN_{j,k}=QU_{j-1,k}$
Discharge substracted QOUT	$QOUT_{i,k}=0$ if $QU_{i,k}\geq 0$ else $QOUT_{i,k}=QU_{i,k}$	$QOUT_{i+1,k}=-QIN_{i+1,k-1}$	$QOUT_{i+1,k}=-QIN_{j-1,k-1}$	$QOUT_{j,k}=0$ if $QU_{j,k}\leq 0$ else $QOUT_{j,k}=QU_{j,k}$
Velocity of added discharge UIN	$UIN_{i,k}=0$ if $QIN_{i,k}=0$ else $UIN_{i,k}=U1_{i,k}$	$UIN_{i+1,k}=0$ if $QIN_{i+1,k}=0$ else $UIN_{i+1,k}=V1_{i+1,k}$ if $QV_{i+1,k}\geq 0$ else $UIN_{i+1,k}=U1_{i+1,k-1}$ if $QV_{i,k}<0$	$UIN_{i,k}=0$ if $QIN_{i,k}=0$ else $UIN_{j-1,k}=V1_{j-1,k}$ if $QV_{j-1,k}\geq 0$ else $UIN_{j-1,k}=U1_{j-1,k-1}$ if $QV_{i,k}<0$	$UIN_{j,k}=0$ if $QIN_{j,k}=0$ else $UIN_{j,k}=U1_{j,k}$
Angle of added discharge ALPHIN	$ALPHIN_{i,k}=BETA_{i,k,left}$	$ALPHIN_{i+1,k}=ALPHA_{i+1,k}$	$ALPHIN_{j-1,k}=ALPHA_{j-1,k}$	$ALPHIN_{j,k}=BETA_{j,k,right}$
Active points	$KCS_{i,k}$	$KCS_{i+1,k}$	$KCS_{j-1,k}$	$KCS_{j,k}$

The computation of grid-angle for gridline i,k (gridline in longitudinal direction) is carried out as follows:

- BETA1 = ATAN[($YCOR_{i,k}$-$YCOR_{i,k-1}$)/($XCOR_{i,k}$-$XCOR_{i,k-1}$)] in degrees;
- Angle of a normal inflowing discharge through this grid line relative to North:
  - For left bank: $BETA_{i,k,\ left}$ = BETA1+180º
  - For right bank: $BETA_{i,k,right}$=BETA1 (or $BETA_{i,k,right}$=BETA1+360º if BETA1<0º)

The computation of flow angle is carried out as follows:

- ALPH1=ATAN($QU_{i,k}/QV_{i,k}$) in degrees; if $QV_{i,k}=0$ and $QU_{i,k}\neq 0$ then ALPH1=90*sign($QU_{i,k}$)
- Left bank: $ALPHA_{i,k}=ALPH1+BETA_{i,k,left}-90$
  - If $ALPHA_{i,k}>360$ then $ALPHA_{i,k}=ALPHA_{i,k}-360$
  - If $ALPHA_{i,k}<0$ then $ALPHA_{i,k}=ALPHA_{i,k}+360$
- Left bank: $ALPHA_{j,k}=ALPH1+BETA_{j,k,right}+90$

- If $ALPHA_{j,k}>360$ then $ALPHA_{j,k}=ALPHA_{j,k}-360$
- If $ALPHA_{j,k}<0$ then $ALPHA_{j,k}=ALPHA_{j,k}+360$

The results have been tested for the 4422 m^3/s simulation of the upper Waal River including morphology. The run is executed for 7200 minutes (flow time, i.e. 20*7200 = 144000 min = 100 days morphological time) for both the reduced and full grid approach, starting from the same bed.

A comparison of the computed flow fields has been presented by means of vector plots in the following plots. From this comparison it has been concluded that the approach is well capable of redirecting the flow in the boundary zone, such that it reproduces very well the flow vectors of the full model.

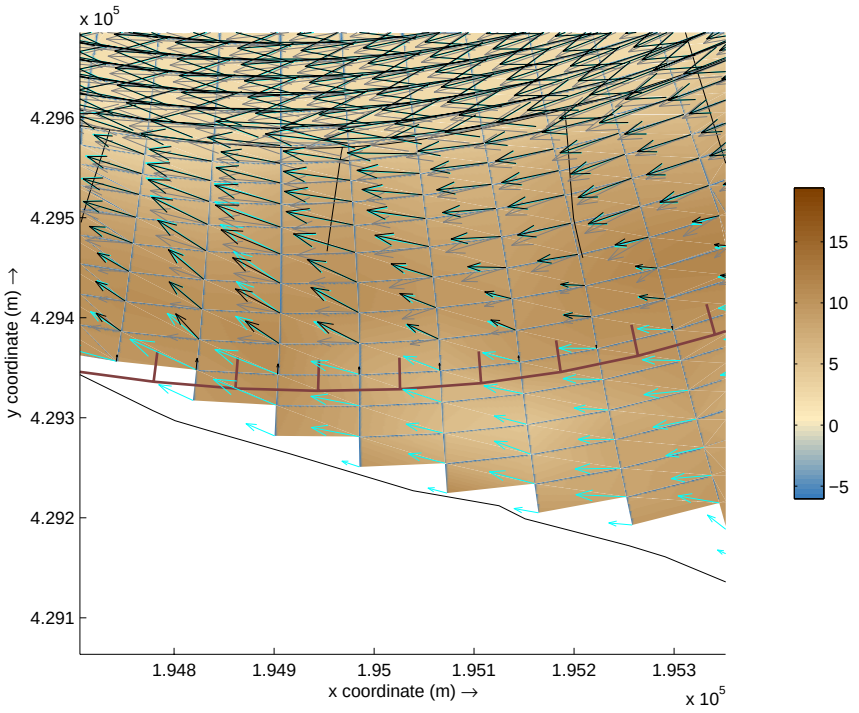

Figure 5.10 Velocity vectors for Waal River km 874: light blue vectors computed for full grid, gray vectors for reduced grid without lateral discharges, black vectors for reduced grid with lateral discharges. Colorbar refers to the bed-elevation in m+NAP presented in this figure.

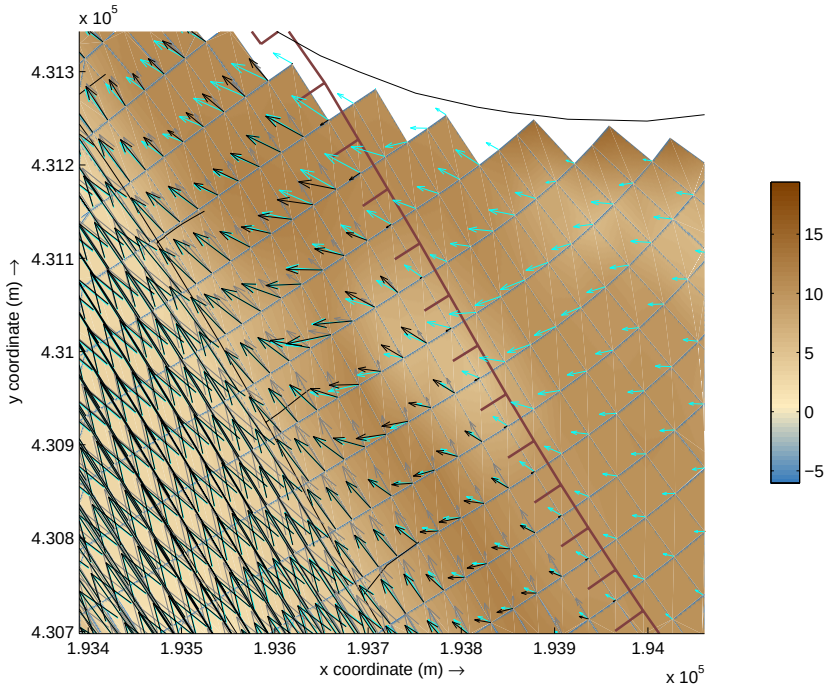

Figure 5.11 Velocity vectors for Waal River km 876.5: light blue vectors computed for full grid, gray vectors for reduced grid without lateral discharges, black vectors for reduced grid with lateral discharges. Colorbar refers to the bed-elevation in m+NAP presented in this figure.

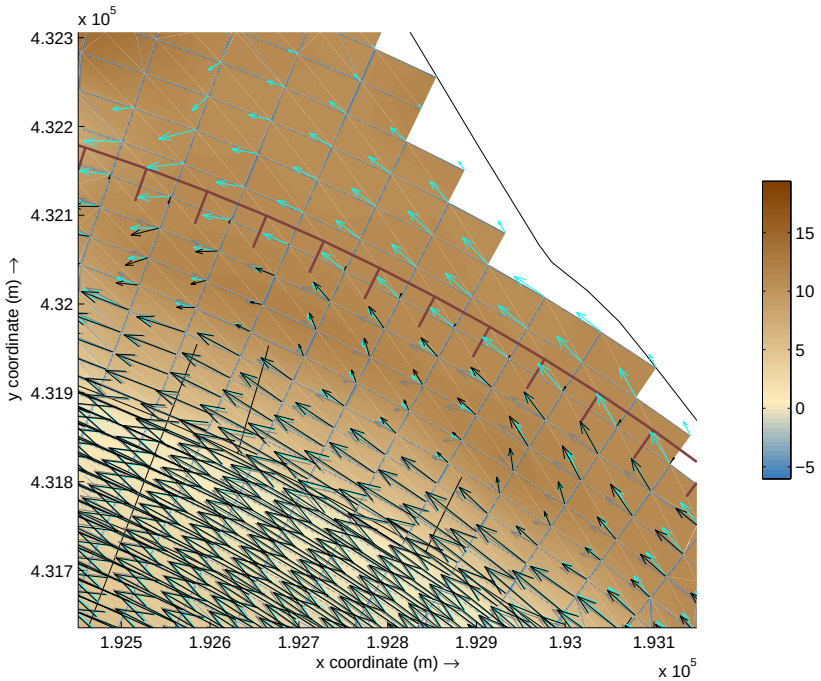

Figure 5.12 Velocity vectors for Waal River km 878: light blue vectors computed for full grid, gray vectors for reduced grid without lateral discharges, black vectors for reduced grid with lateral discharges. Colorbar refers to the bed-elevation in m+NAP presented in this figure.

Similarly a comparison has been made of the bed-level changes computed in the simulation period of 100 days with a constant (steady) discharge of 4422 m3/s (including the lateral discharges). The eventual differences are very small (order of a few centimetres and only at some isolated locations) and do not amplify during the computation (a longer computation will yield the same effects). These small differences cannot be associated directly to the lateral discharges, as their locations are sometimes far away from significant discharge in-/outflows.

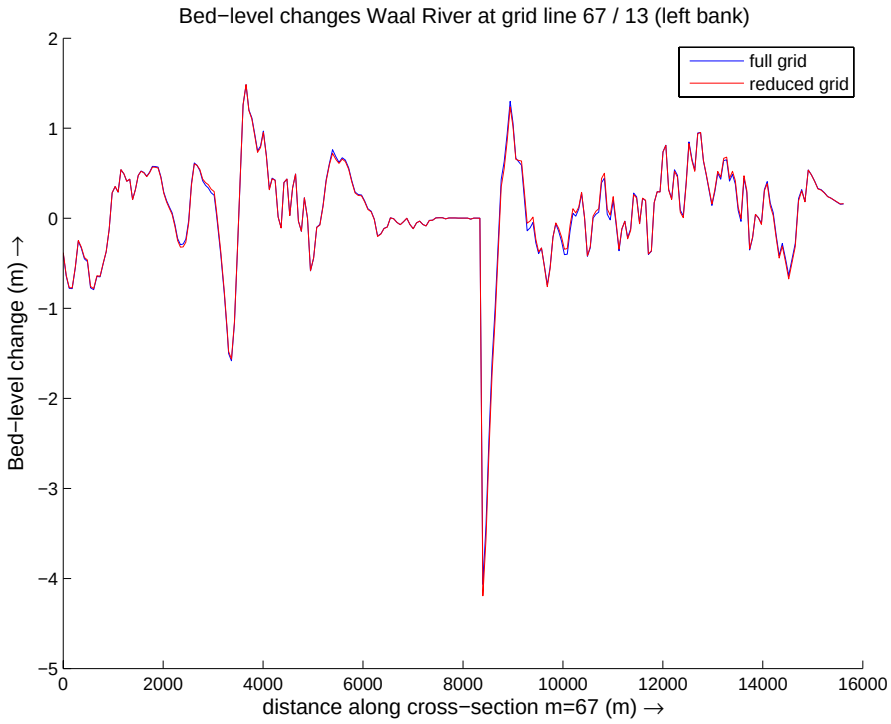

Figure 5.13 Bed-level change computed for a 100 day simulation with 4422 m^3/s: longitudinal section at about 85 m left of river axis.

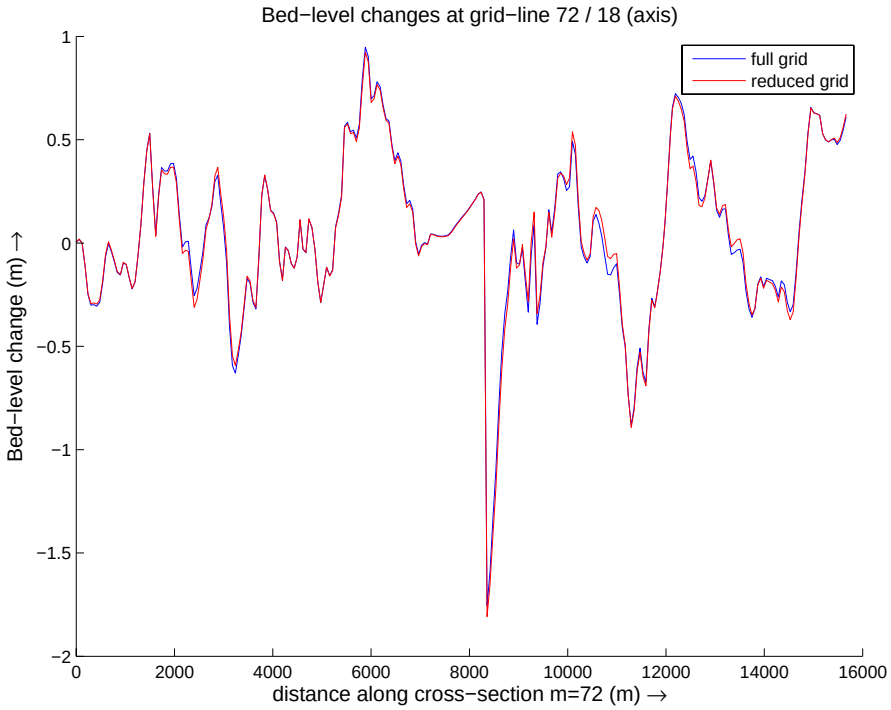

Figure 5.14 Bed-level change computed for a 100 day simulation with 4422 m^3/s: longitudinal section at the river axis.

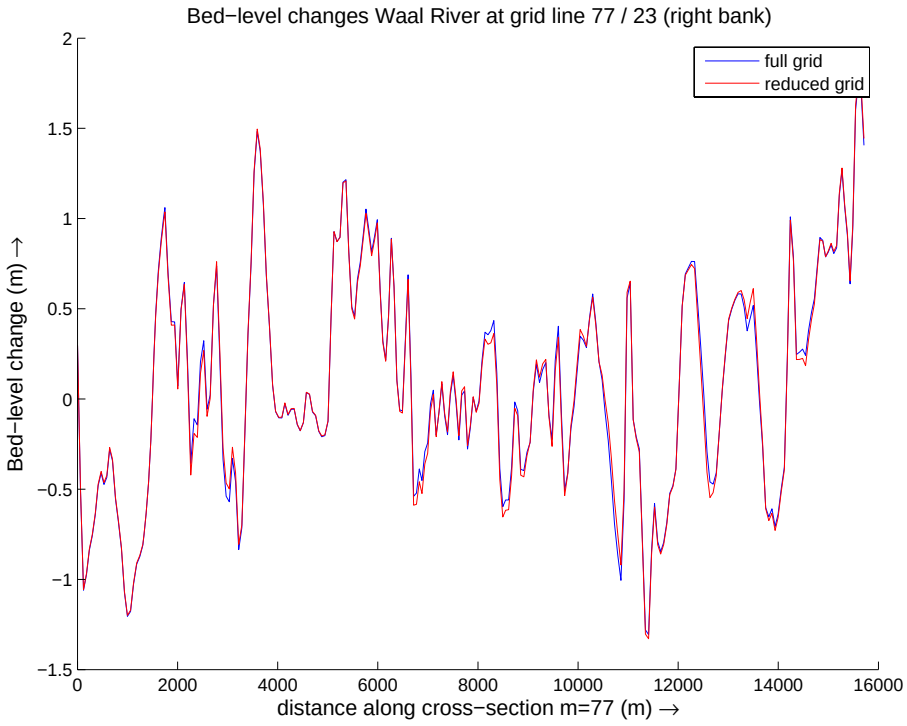

Figure 5.15 Bed-level change computed for a 100 day simulation with 4422 m^3/s: longitudinal at about 85 m right of the river axis.

The computation time for the reduced grid (with or without lateral inflows) is *half* of that of the full grid for this part of the Waal. An increase of computation speed with roughly a factor 2 is expected if this approach is applied to the DVR model in general.

6 Reduction of physical processes in sub-domains

6.1 Introduction

The Rhine is characterised by non-uniform sediment. In the Rhine significant downstream fining and vertical segregation of fine and coarse sediment are observed. Vertical grain sorting and bed armouring with coarse particles covering the fines ones, are important segregation processes in the Bovenrijn, Pannerdensch Kanaal, the upper part of the IJssel and the areas close to the bifurcations. Vertical sorting processes are less important in the Nederrijn and the Waal. In other words, including vertical sorting processes in morphodynamic simulations is not relevant for all Rhine branches.

The possibility of minimising the number of model domains in which graded sediment processes are simulated, is tested in this part of the project. To that end, the Delft3D code has been changed slightly such that at the domain boundary between the upstream domain with graded sediment and the downstream domains with uniform sediment, the sediment transport for the bedload fractions of the domain with graded sediment are summed up and imposed at the downstream situated domain with uniform sediment.

In this study it is analyzed whether it is possible to use graded sediment formulations only in the upstream part of the model, the Bovenrijn, whereas for the other model uniform sediment is used. In order to do this, the Delft3D functionality had to be extended. In Section 6.2 it is briefly analyzed in which circumstances it is necessary to consider graded sediment. In Section 6.3 the new Delft3D functionality is tested. All results are discussed in Section 6.4.

6.2 Theoretical analysis of the necessity of using graded sediment

6.2.1 Method

In this Section a theoretical study is carried out to determine in which cases it is necessary to use a graded sediment formulation for morphological calculations. For this purpose it is studied in how far the total transport rate s and the mean diameter of the transported mixture D_T are influenced by the number of fractions N that has been used in the calculations. Following the method proposed by Ribberink (1987), the behavior of the total transport rate has been studied by calculating $s_{T,N}/s_{T,1}$, where $s_{T,N}$ and $s_{T,1}$ represent the transport rate in the case of N size fractions (graded sediment) and one fraction (uniform sediment) respectively. Concerning the DVR project it is expected that the use of graded sediment formulations is most important in the upstream part of the model, where grain sizes vary over a bigger range. The transport formula that will be applied in the model in future analyses behaves similarly to the formula of Meyer-Peter & Müller in the upstream part of the model.

Therefore the transport formula of Meyer-Peter & Müller is used for the theoretical analysis. The following expression is derived:

$$\frac{s_{T,N}}{s_{T,1}} = \frac{\sum_{i=1}^{N} s_i}{s_{T,1}} = \frac{\sum_{i=1}^{N} \left(\Delta g D_i^3\right)^{1/2} \cdot p_i \cdot 8 \cdot \left(\mu\theta_i - \theta_{cr,i}\right)^{3/2}}{\left(\Delta g D_m^3\right)^{1/2} \cdot 8 \cdot \left(\mu\theta_m - 0.047\right)^{3/2}}, \qquad (6\text{-}1)$$

where D_i is the diameter of sediment fraction i, and p_i is its volume fraction. The Shields value is defined as:

$$\theta_i = \frac{\tau}{\left(\rho_S - \rho\right) \cdot g \cdot D_i} \qquad (6\text{-}2)$$

The critical Shields value in the case of one fraction is 0.047, while the effect of hiding and exposure is included for the case of N size fractions:

$$\theta_{cr,i} = \xi_i \cdot 0.047 \qquad (6\text{-}3)$$

The hiding and exposure coefficient ξ_i is calculated using the improved Egiazaroff exposure correction of Ashida and Michiue (1972).

Similarly the behavior of the mean grain diameter of the transported mixture, D_T, has been studied:

$$\frac{D_{T,N}}{D_{T,1}} = \frac{D_{T,N}}{D_m} = \frac{\sum_{i=1}^{N} D_i \cdot \frac{s_i}{s_{T,N}}}{D_m}, \qquad (6\text{-}4)$$

where $D_{T,N}$ is the diameter of the transported sediment in case of N size fractions (graded sediment) and $D_{T,1}$ is the diameter of the transported uniform sediment, which is equal to the mean diameter D_m. Thus the behavior of the transport rate and the mean diameter of the transported mixture are dependent on the following parameters:

- $\theta' = \mu\theta_m$,
- D_i/D_m,
- p_i,

where θ' is the effective Shields value.

It is assumed that the grain size follows a log-normal distribution. The sediment mixture can then be characterized by its mean and its standard deviation, D_m and σ_D. D_i/D_m as well as p_i can be expressed in terms of N and σ_D/D_m.

The grain size distribution is divided into N size classes according to the following procedure:

- An upper and a lower boundary of the distribution is chosen.
- The range between these boundaries is divided in such a way that the ratio of successive diameters D_{i+1}/D_i is constant. This corresponds to the repartition of sieve diameters.

The theoretical analysis is carried out for the following parameter ranges:

- σ_D/D_m from 0.25 to 2;
- θ' from 0.075 to 0.5;
- N from 1 to 10.

The results of this analysis are presented in the following Section.

6.2.2 Results

Figure 6.1 to Figure 6.3 present the ratio of the transport rate in the case of N fractions and of uniform sediment for three different ratios of σ_D/D_m. Figure 6.4 to Figure 6.6 show the ratio of the mean diameters of the transported sediment.

The ratios $s_{T,N}/s_{T,1}$ and $D_{T,N}/D_m$ are constant for five or more fractions, i.e. the number of fractions used does not have a significant influence on the transport rates and mean diameters of the transported material anymore. So if a graded sediment formulation is used, the use of more than five fractions would not lead to a better reproduction of sediment transport rates. Note that this does not necessarily also hold for bed evolution and sorting processes. To assess this it is advised to run simulations with changing bed and composition, and analyse the evolution and final equilibrium.

The influence of the number of fractions is biggest for sediment mixtures with a high value of σ_D/D_m, i.e. poorly sorted sediment mixtures. Furthermore the transport rate calculated for N fractions is bigger than if it is calculated for uniform sediment, whereas the diameter of the transported sediment is smaller for graded than for uniform sediment. This holds for the complete range of σ_D/D_m and θ' tested in the present study.

The mean diameter of the transported sediment is more sensitive to the number of fractions used than the transport rate. For instance for a $\sigma_D/D_m = 1.25$ the total transport rate for many fractions does not deviate by more than 8% from that for one fraction even for the low effective Shields values (Figure 6.3). The mean diameter of the transported sediment, however, deviates by more than 13% even for high effective Shields values (Figure 6.6).

The transport rate and the diameters derived for one fraction and several fractions deviate most in conditions close to the threshold of motion, i.e. for small effective Shields values θ'. This becomes evident in Figure 6.7 and Figure 6.8, in which the ratios of $s_{T,10}/s_{T,1}$ and $D_{T,10}/D_m$ at different effective Shields values are presented for the lowest and highest ratios of σ_D/D_m tested in the present study. The Figures also show a curve for the upstream part of

the Waal between the Pannerdensch Kop and Nijmegen, for which σ_D/D_m can be estimated to 1.08 (see Section 6.2.3).
The deviations of the transport rates for uniform sediment from the transport rates for graded sediment are relatively small. Only at conditions very close to the threshold of motion and for poorly sorted sediment mixtures they slightly exceed 5%. For higher effective Shields values a state of equal mobility is reached, at which the transport rates for uniform and graded sediment do not differ considerably any more.

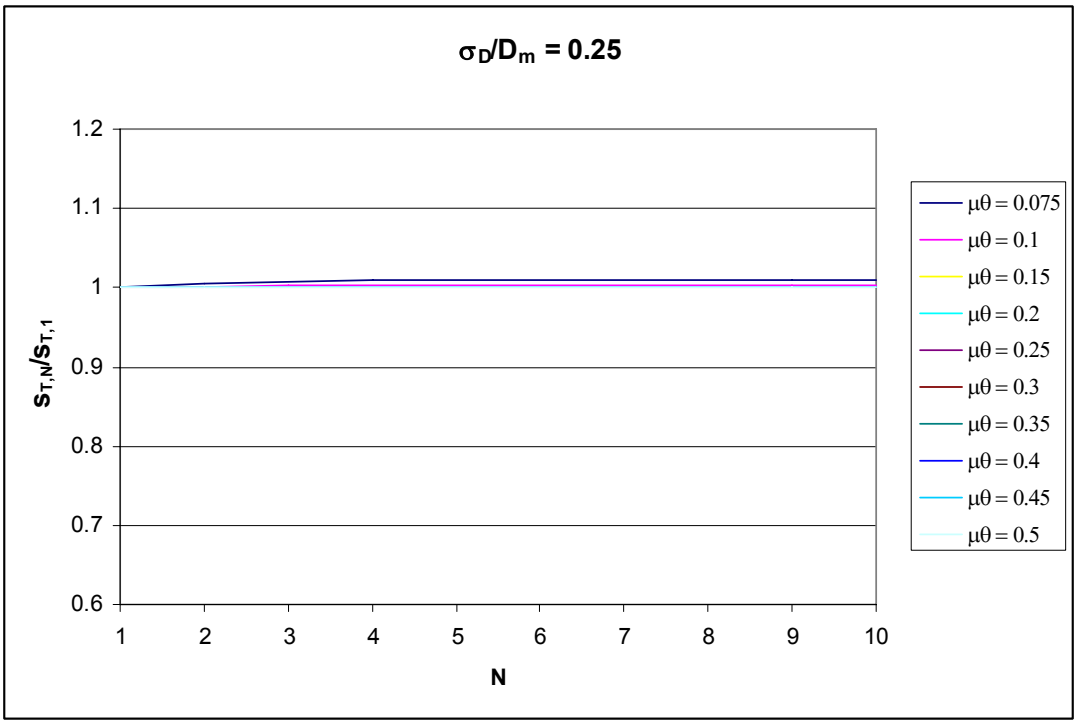

Figure 6.1 Ratio of transport rate in the case of N fractions and of uniform sediment for a ratio of $\sigma_D/D_m = 0.25$ and different effective Shields values.

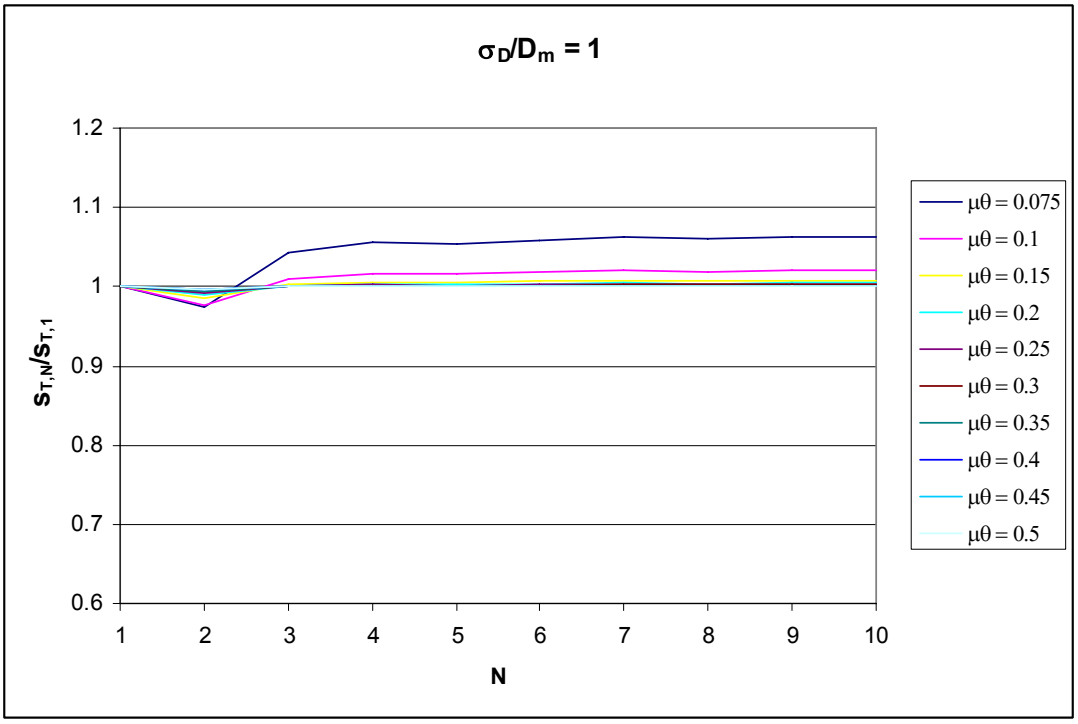

Figure 6.2 Ratio of transport rate in the case of N fractions and of uniform sediment for a ratio of $\sigma_D/D_m = 1.0$ and different effective Shields values.

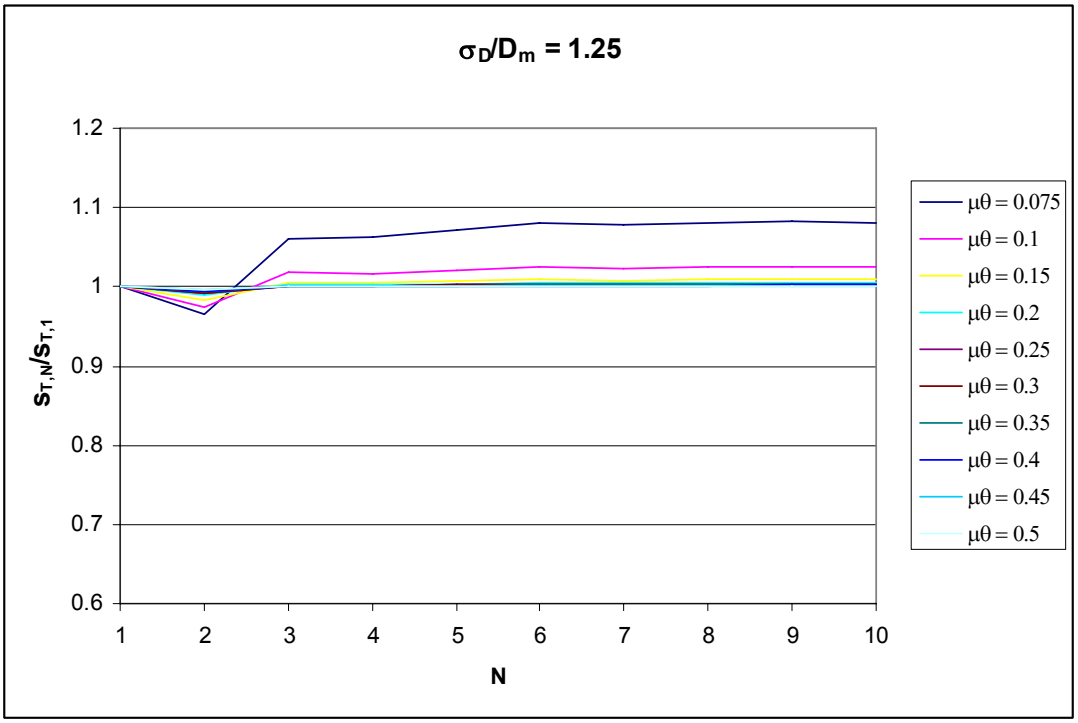

Figure 6.3 Ratio of transport rate in the case of N fractions and of uniform sediment for a ratio of $\sigma_D/D_m = 1.25$ and different effective Shields values.

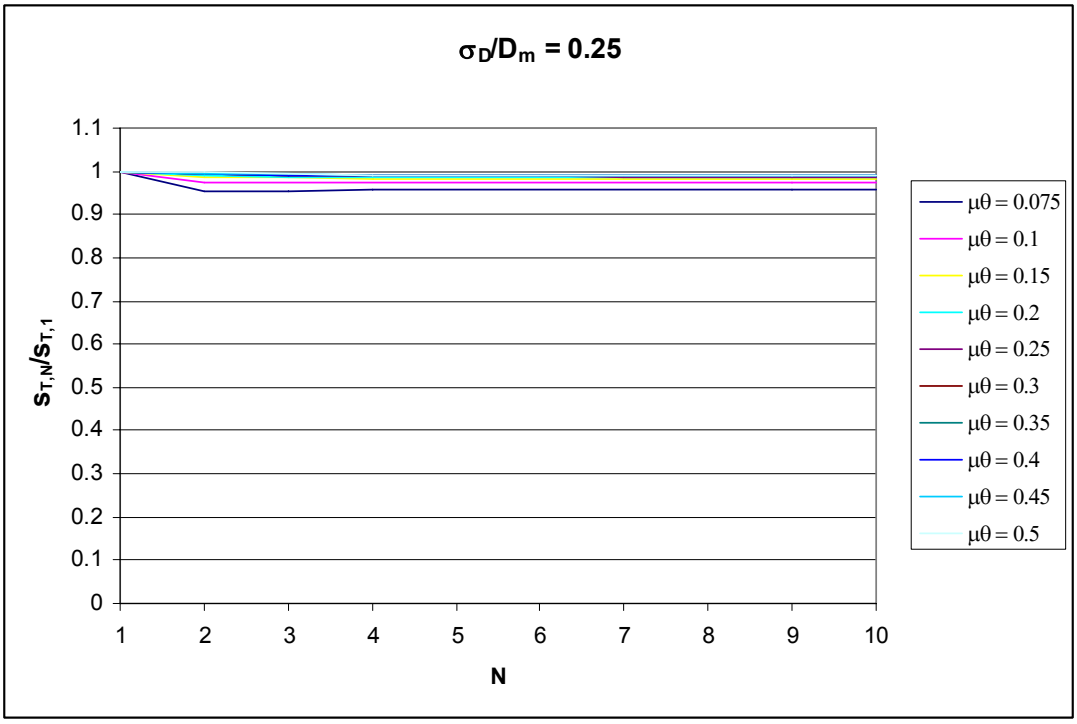

Figure 6.4 Ratio of the mean diameter of the transported mixture in the case of N fractions and of uniform sediment for a ratio of $\sigma_D/D_m = 0.25$ and different effective Shields values.

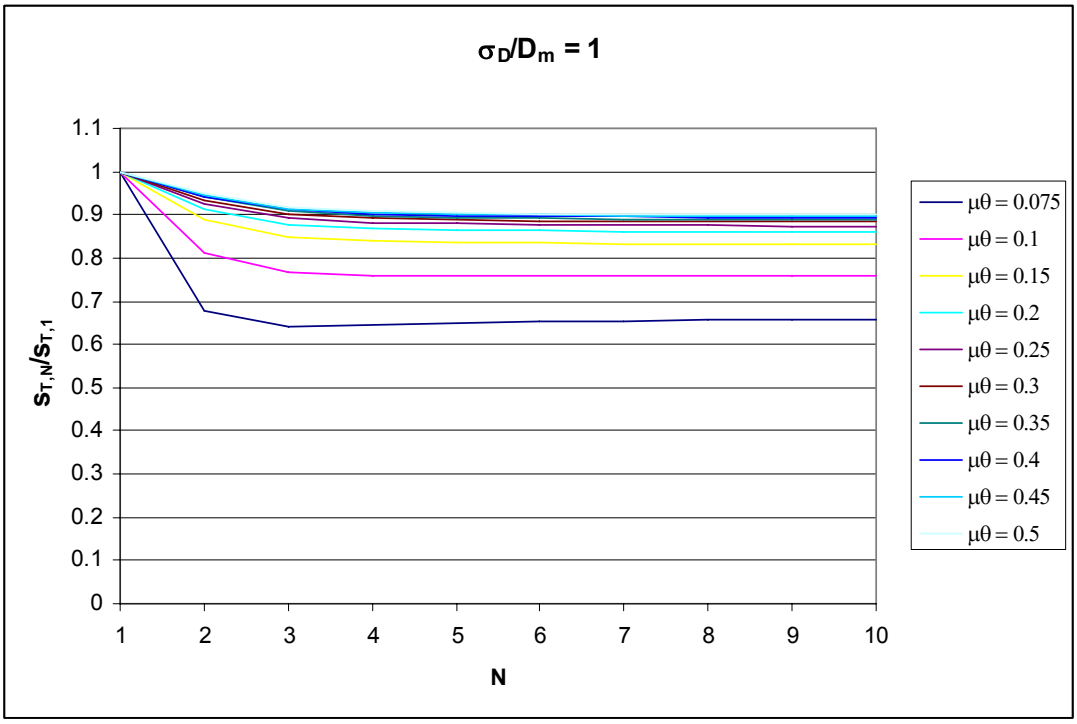

Figure 6.5 Ratio of the mean diameter of the transported mixture in the case of N fractions and of uniform sediment for a ratio of $\sigma_D/D_m = 1.0$ and different effective Shields values.

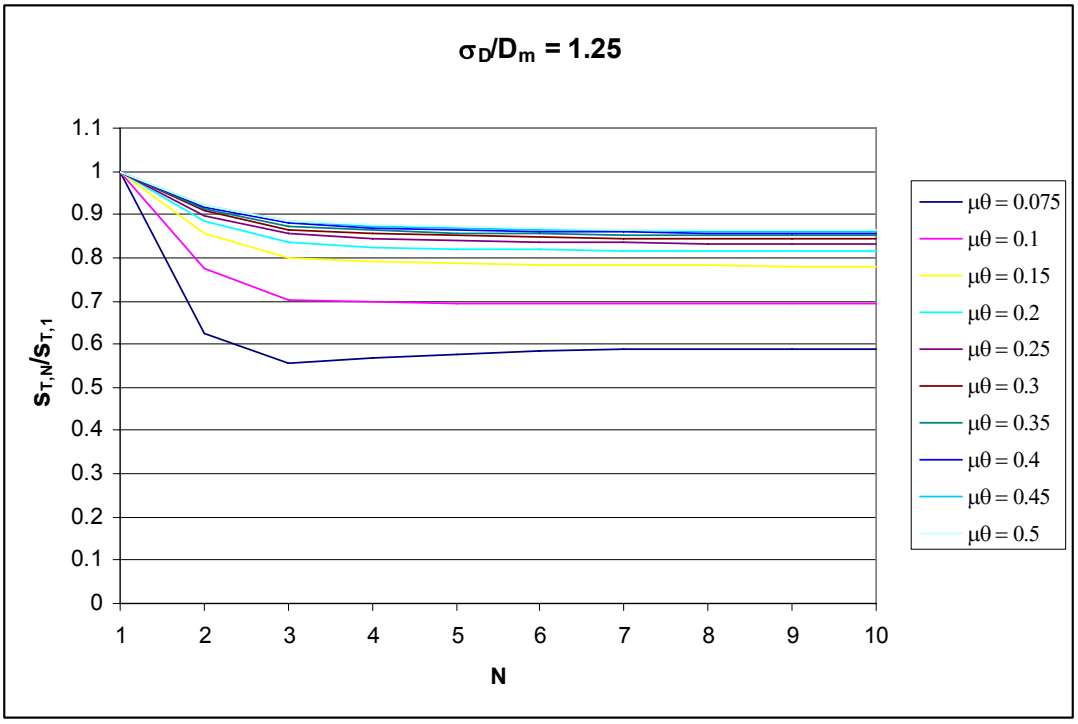

Figure 6.6 Ratio of the mean diameter of the transported mixture in the case of N fractions and of uniform sediment for a ratio of $\sigma_D/D_m = 1.25$ and different effective Shields values.

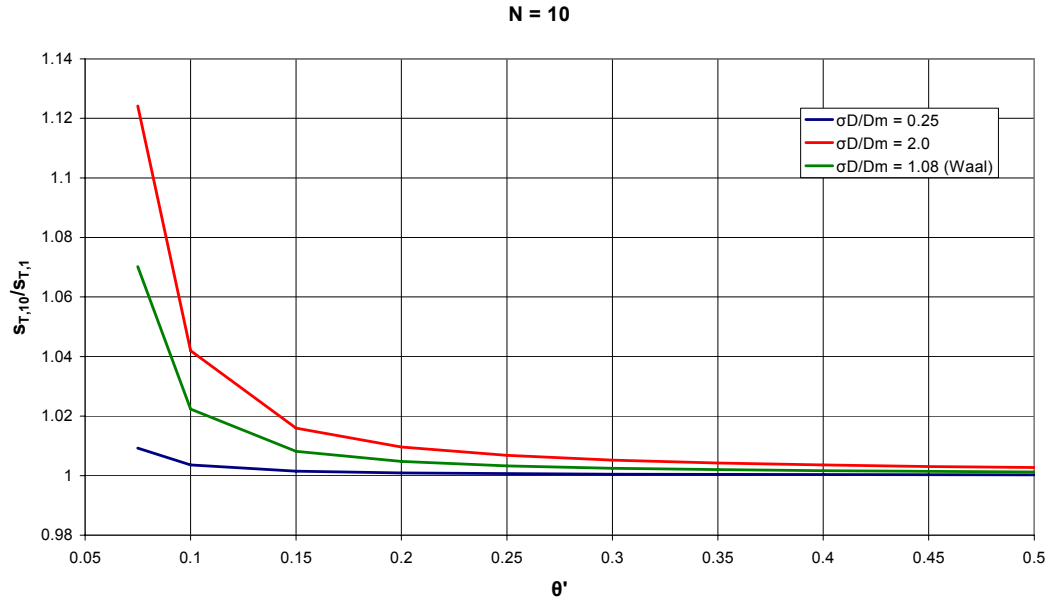

Figure 6.7 Ratio of transport rate in the case of 10 fractions and of uniform sediment for different effective Shields values and the minimum and maximum ratios of σ_D/D_m tested in the present study as well as the ratio of σ_D/D_m for the Waal.

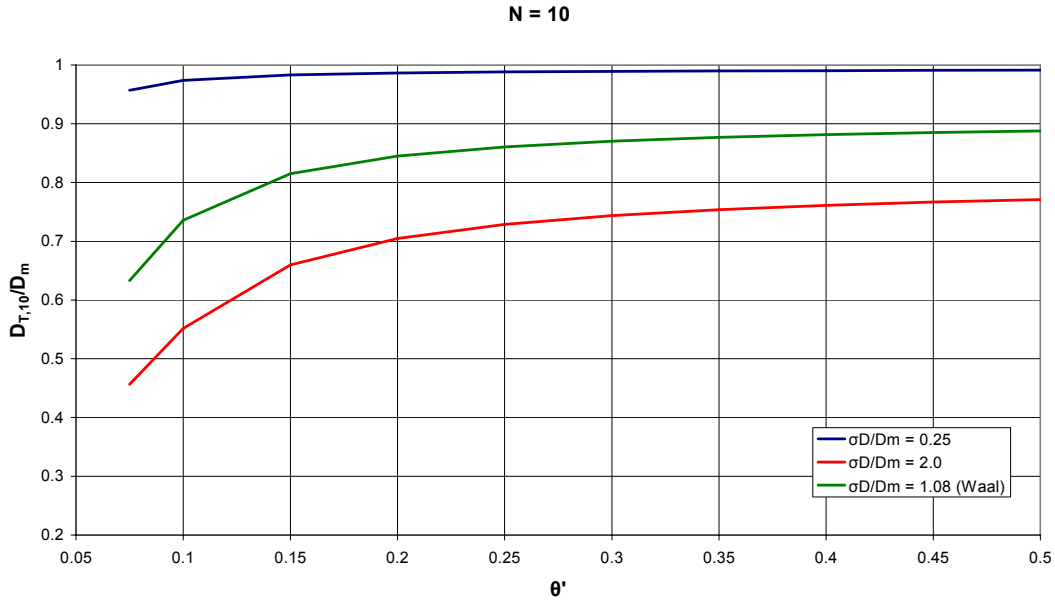

Figure 6.8 Ratio of the mean diameter of the transported mixture in the case of 10 fractions and of uniform sediment for different effective Shields values and the minimum and maximum ratios of σ_D/D_m tested in the present study as well as the ratio of σ_D/D_m for the Waal.

The analysis shows that at low effective Shields values it is important to use graded sediment formulations. Further analyses have shown that furthermore the choice of the hiding and exposure formulation has a significant influence on the outcome. If for instance the formulation of Egiazaroff (1957 and 1965) is used instead of the one by Ashida & Michiue (1972) the transport rates for graded sediment are lower than the ones for uniform sediment at high values of σ_D/D_m (see Ribberink, 1987). The choice of the reference diameter in the hiding and exposure formulation as well as in the transport formula also has a significant impact on the outcome of the study. The diameters and hiding and exposure formulation chosen for this study are consistent with the formulations in the DVR-model in Delft3D.

6.2.3 Discussion

The results of the theoretical analysis show that it is necessary to use a graded sediment formulation if the combination of effective Shields values and spreading of the sediment mixture (characterized by σ_D/D_m) in the model lead to differences in the transport rates and the diameters of the transported material that exceed a certain limit. This is explained in the following using the upstream part of the Waal from the Pannerdensche Kop to Nijmegen as example.

Based on the sediment diameters derived by Vuren et al. (2006) the mean diameter and standard deviation of the sediment mixture, D_m and σ_D, are estimated. The grain sizes are assumed to follow a log-normal distribution. Figure 6.9 shows the resulting profile of σ_D/D_m. This parameter ranges between 1.04 and 1.13, with an average of 1.08.

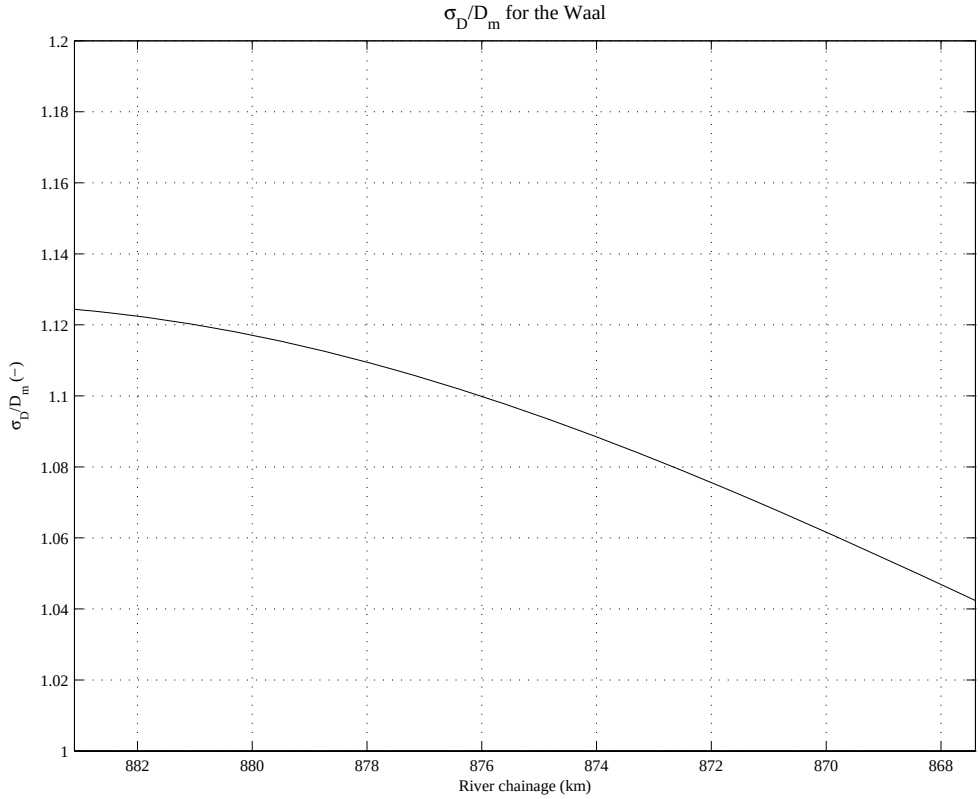

Figure 6.9 Profile of σ_D/D_m for the upstream part of the Waal between the Pannerdensche Kop and Nijmegen.

Furthermore the effective Shields values θ' occurring in the Waal at a total upstream discharge in the Bovenrijn of Q = 2500 m^3/s, i.e. a discharge of Q = 1739 m^3/s in the Waal, are calculated:

$$\theta' = \mu \cdot \theta, \qquad (6\text{-}5)$$

with

$$\theta = \frac{u^2}{C^2 \cdot \Delta \cdot D_m} \qquad (6\text{-}6)$$

and

$$\mu = \left(\frac{C}{C_{90}} \right)^{3/2} = \left(\frac{C}{18 \cdot \log\left(\frac{12h}{3D_{90}} \right)} \right)^{3/2}. \qquad (6\text{-}7)$$

Width-averaged values are used for the flow velocity u and the water depth h. The Chézy value is calculated using

$$C = 18 \cdot \log\left(\frac{12h}{k_s} \right), \qquad (6\text{-}8)$$

where k_s is the alluvial roughness height. The values of u, h and k_s are taken from Delft3D-calculations. Table 6.1 lists the estimated parameter values at the upstream boundary of the Waal domain. It becomes evident that using the standard version of the Meyer-Peter & Müller transport formula the effective Shields value with $D_{ref} = D_m$ (uniform sediment) falls just below the threshold of motion, so that no transport takes place. If, however, a graded sediment approach is used for the same sediment mixture the smaller fractions will still be in motion. In the following example the median diameter is chosen as reference diameter for the transport formula, $D_{ref} = D_{50}$. This results in an effective Shields value of 0.10, so that transport can take place for both uniform and graded approaches.

parameter	value
u (m/s)	1.2
h (m)	6.8
k_s (m)	0.2
C	47.0
D_m (m)	0.006
D_{90} (m)	0.0097
μ (-)	0.66
θ (-)	0.066
θ' (-)	0.043

Table 6.1 Estimated transport parameter values at the upstream boundary of the Waal domain.

If a maximum deviation of 5% is desired for the transport rate in graded versus uniform sediment, the effective Shields value has to be bigger than 0.08 in the case of $\sigma_D/D_m = 1.08$ (Figure 6.7). This is an average value for the upstream part of the Waal as indicated above. This is lower than the actual effective Shields value in this part of the model in the case that instead of D_m D_{50} is used as reference diameter in the transport formula. So the use of a uniform sediment approach would lead to deviations in transport rate of less than 5% compared to a graded sediment approach.

However, the composition of the transported material would deviate more. The average effective Shields value in the Waal of 0.1 results in a $D_{T,N}/D_m = 0.74$ for $\sigma_D/D_m = 1.08$ (Figure 6.8), i.e. the deviation is 16%.

The results of the theoretical analysis indicate that a pragmatic harmonization of graded sediment and uniform sediment can be reached by applying uniform sediment formulations with a slightly higher calibration factor to compensate the differences in transport capacity. Another possibility is to modify grain sizes in the uniform sediment model. The fact that the choice of the reference diameter in the transport formula and the hiding and exposure formulation has a significant impact on the analysis (Section 6.2.2) indicates that this might be an effective method. Of course this variation is only allowed within acceptable limits, governed by the scatter in the data. The advantage of using grain sizes is the possibility to introduce spatial variations, for instance to match transverse sorting effects on domain boundaries.

6.3 Model tests

6.3.1 New Delft3D functionality

The combination of graded sediment formulation in the upstream part of a model with uniform sediment formulation in the downstream part follows a simple approach. At the domain boundary, the sum of the fluxes [kg/(m·s)] of all sediment fractions arriving from the upstream domain is imposed on the downstream domain as upstream boundary condition. In this way the transported sediment mass is conserved.

The approaches used with respect to the transport formula may differ in the upstream and downstream domain. So far, the new functionality has been implemented for bed load transport only.

6.3.2 Description of the model tests

Several tests are carried out using graded sediment formulations only for the Bovenrijn and uniform sediment formulations for the rest of the model. Since simulations with graded sediment processes are computational intensive, the DVR model is reduced in size. The test model contains the domains of the Bovenrijn and the Pannerdensch Kanaal, as well as the upstream part of the Waal up to Nijmegen (see Figure 6.10). All tests are carried out at a discharge of $Q = 2500\ m^3/s$ in the Bovenrijn. In the test simulations graded sediment formulations (8 fractions) are used for the Bovenrijn, whereas the downstream branches are modelled with uniform sediment. The bed level development at the domain boundaries is analysed.

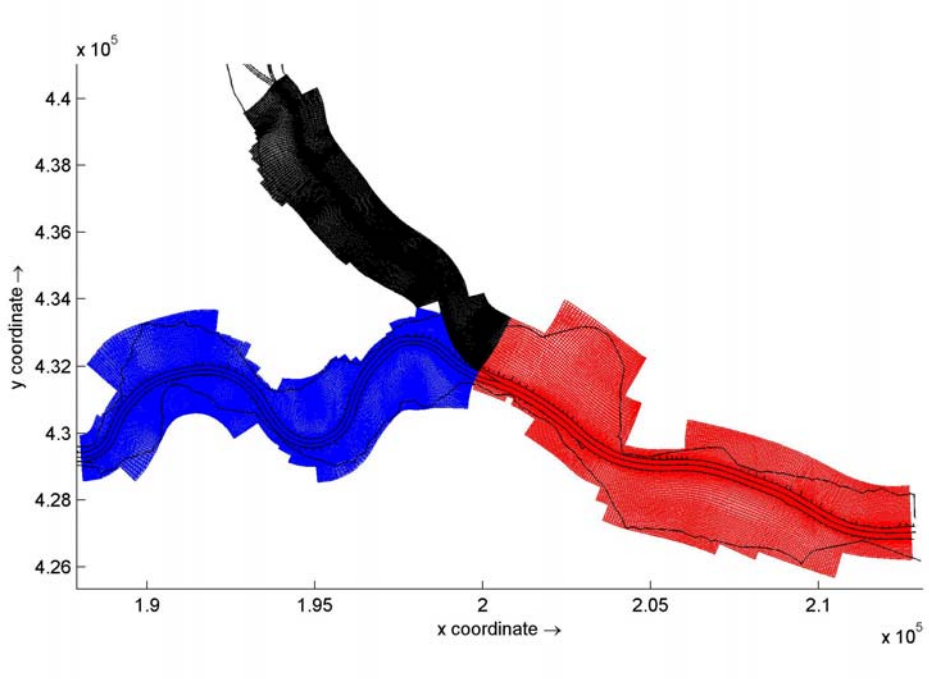

Figure 6.10 Reduced model used for the tests with graded and uniform sediment.

The analysis in Section 6.2 shows that a gradient in transport rates will occur at the domain boundaries. This will lead to a morphological response at these boundaries. Since transport rates in the downstream uniform branches are smaller than in the inflow from the Bovenrijn, sedimentation will occur in these branches. In the model tests the grain diameters in the upstream part of the Waal domain are varied to see in how far this can be prevented.

For the first model test the mean diameter is chosen as reference diameter for the transport formula of Meyer-Peter & Müller. In this case, the Shields values in the two downstream branches with uniform sediment are even smaller than the critical Shields value (compare Section 6.3.3), whereas part of the graded sediment in the upstream branch is still in motion. Three more tests are carried out, in which the reference diameters at the upstream end of the Waal are decreased to enable sediment transport downstream of the domain boundary, too. Table 6.2 shows the size of the reference diameters at the upstream end of the Waal. The diameters range from the mean diameter (case 1) to the median diameter (case 4).

case	diameter at the upstream boundary of the Waal (mm)
1	6.0 (= D_m)
2	4.0
3	3.0
4	2.5 (= D_{50})

Table 6.2 Size of the reference diameters at the upstream boundary of the Waal domain for the four test cases.

The analysis of the results of this test shows to what extent the choice of the reference diameter influences the outcomes of the model for bed evolution. It also shows the spatial variations (2D) in these effects.

In the following Section the results for all test cases are presented. In Section 6.4 the results are discussed and recommendations are made regarding the future use of the new functionality.

6.3.3 Results

Figure 6.11 shows the change in bed level after half a year for the Bovenrijn and the Waal in all four test cases. As anticipated no transport takes place in the uniform sediment domain (Waal) if $D_{ref} = D_m$ (case 1), while part of the graded sediment in the Bovenrijn is still in motion. This leads to sedimentation just downstream of the domain boundary. In case 4 ($D_{ref} = D_{50}$) the downstream reference diameter is decreased to an extent that leads to a deep erosion pit just downstream of the domain boundary. So the diameter for which neither erosion nor sedimentation takes place here lies in between D_m and D_{50}. The bed level changes in cases 2 and 3 show that an appropriate reference diameter has to be even closer to the mean diameter of the sediment mixture. This holds for the effective Shields values that correspond to a total discharge in the Bovenrijn of Q = 2500 m^3/s. At higher discharges the Shields values are also higher and get into the range of values for which the transport

rates calculated with uniform and graded sediment formulations do not differ significantly any more (compare Section 6.2).
In that case the use of the mean diameter in the transport formula would not lead to serious sedimentation or erosion problems at the domain boundary any more.

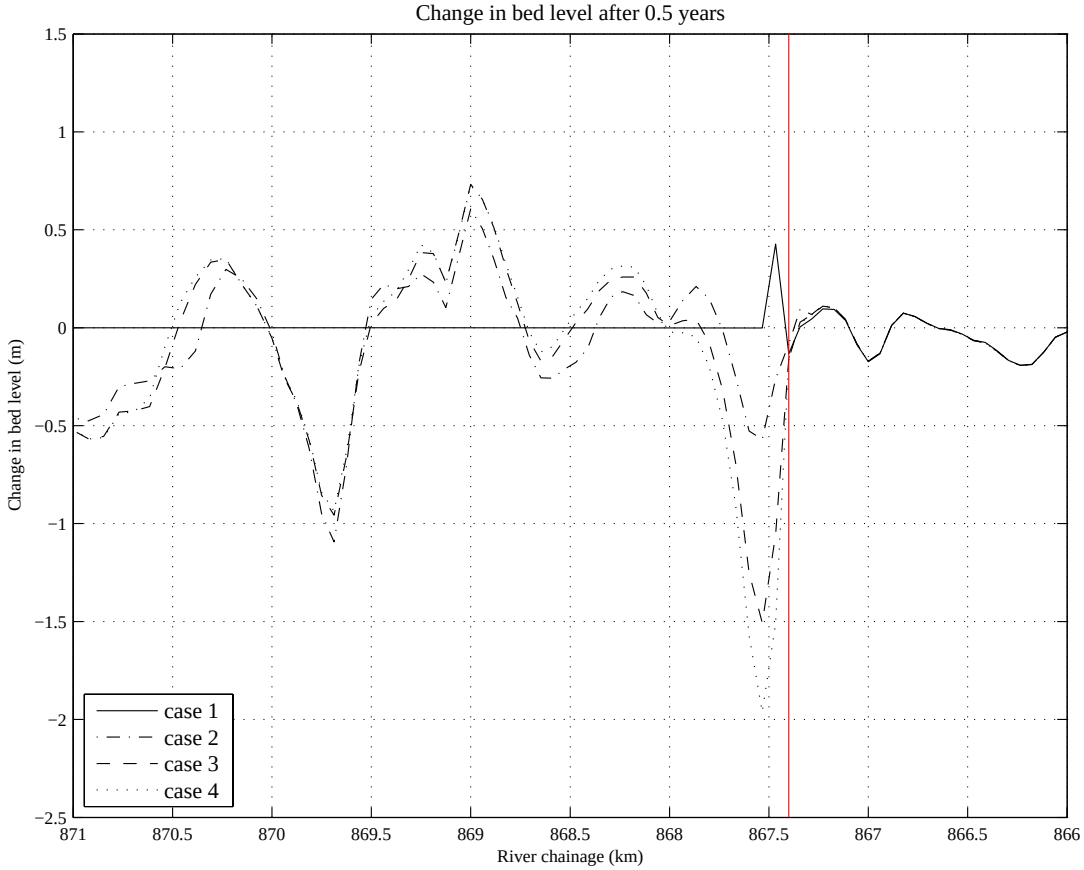

Figure 6.11 Change in bed level after half a year for the Bovenrijn (gridline m=40) and the Waal (river axis m=72) with graded sediment in the Bovenrijn and uniform sediment in the other branches at a total discharge of Q = 2500 m^3/s (red line = domain boundary).

Figure 6.12 and Figure 6.13 show the initial bed level and the bed level after 0.5 years at the domain boundary between Bovenrijn, Waal and Pannerdensch Kanaal for case 4. Figure 6.14 presents a transverse cut of the change in bed level after 0.5 years at the upstream boundary of the Waal (n-gridline = 2) for case 1. It becomes evident that the erosion (cases 2 to 4) respectively sedimentation (case 1) process at the domain boundary is not constant over the width but shows a variation in transverse direction. For instance in case 4 in the Waal the erosion is higher on the right half of the river channel. For fine-tuning a variation of diameter adjustment in transverse direction could be considered.

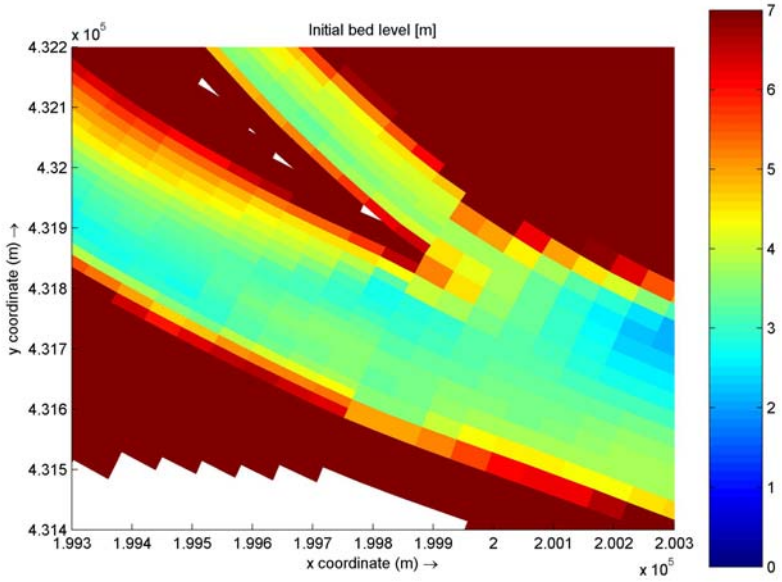

Figure 6.12 Initial bed level at the domain boundary between Bovenrijn, Pannerdensch Kanaal and Waal.

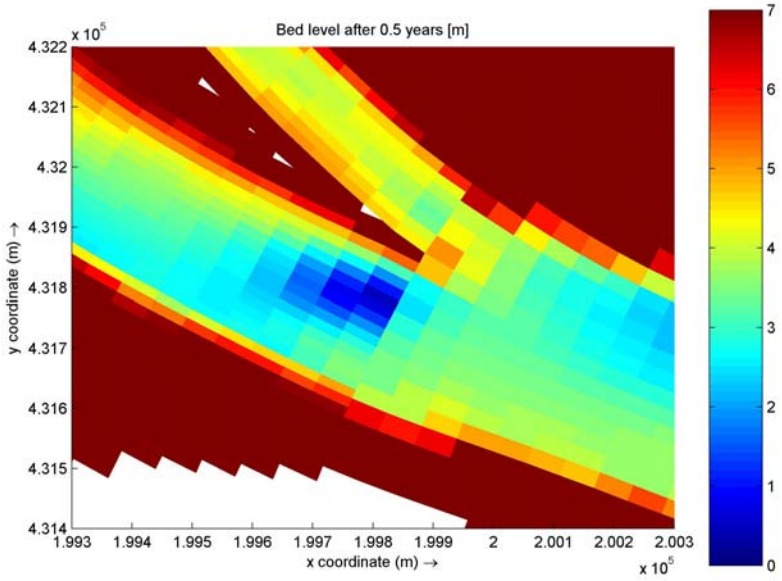

Figure 6.13 Bed level at the domain boundary between Bovenrijn, Pannerdensch Kanaal and Waal after half a year with graded sediment in the Bovenrijn and uniform sediment in the other branches at a total discharge of Q = 2500 m^3/s (case 4).

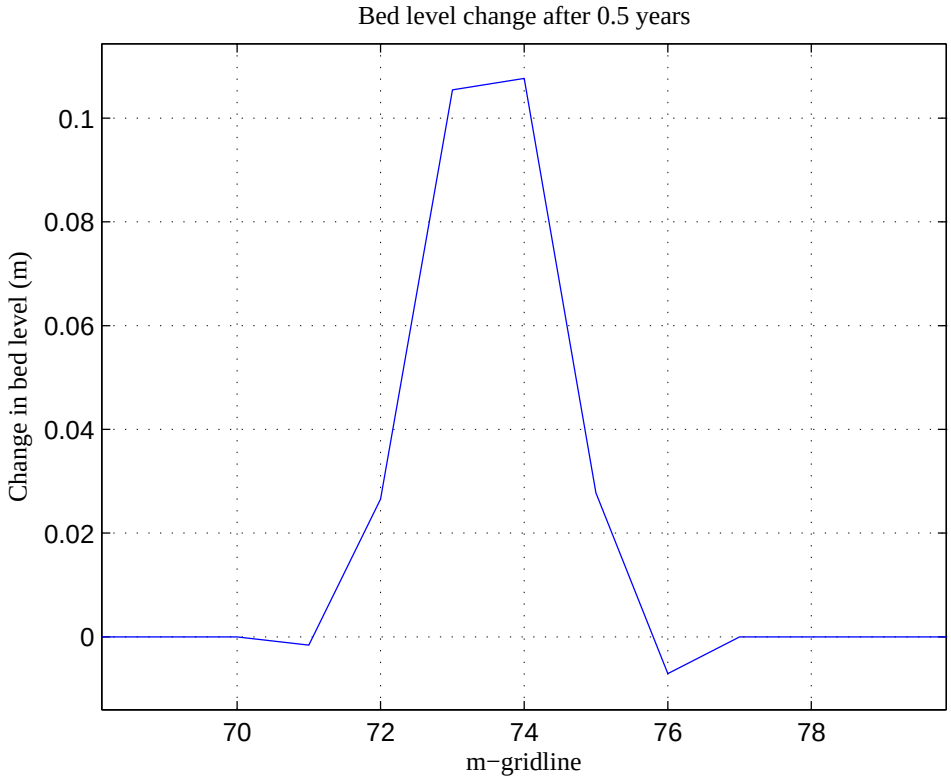

Figure 6.14 Transverse cut of the bed level change after 0.5 years at the upstream boundary of the Waal domain (n-gridline = 2, case 1).

6.4 Conclusion

The results of the theoretical analysis in Section 6.2 show that for one specific sediment mixture the total transport rate calculated for graded sediment is bigger than the one for uniform sediment when using Meyer-Peter & Müller. Thus, if graded sediment formulations are used in one domain of a model and uniform sediment formulations are employed downstream of this domain, the material flux arriving at the boundary from upstream is bigger than the flux away from the boundary at the downstream side. That means that sedimentation occurs at the domain boundary even if the sediment diameters at both sides of the boundary are the same. This effect can be quantified by means of the theoretical analysis shown in Section 6.2.

In a simulation with only uniform sediment the sediment diameters at both sides of a domain boundary would be set to equal and constant values, so that no big jumps in transport rates occur throughout the whole simulation. If one domain uses a graded sediment approach, however, the sediment composition is variable in time. So the sediment composition at both sides of the boundary differs, and strong erosion or sedimentation can occur. This second effect cannot be quantified easily.

The model tests described in Section 6.3 show that decreasing the reference diameter downstream of the domain boundary is a possibility to overcome sedimentation problems.

The results of the theoretical analysis in Section 6.2.2 reveal, however, that the optimum extent of this decrease differs for each discharge level respectively for each effective Shields value. For a simulation using a discharge hydrograph instead of a constant discharge an optimum value has to be found for which, on average, neither big erosion pits nor extreme sedimentations occur at the boundary between domains with uniform and domains with graded sediment formulations. In that case, however, one will still face periods with erosion and periods with sedimentation at the domain boundary. These will influence morphology, because they will trigger erosion and sedimentation waves that will migrate through the whole model.

Only using graded sediment formulations when necessary will yield a considerable reduction of computation time. The computation time of a simulation with a graded sediment model for the Bovenrijn (8 fractions and two under-layers) and a uniform sediment model for the other Rhine branches is about a factor 1.67 larger than the computation time involved with a simulation with a completely uniform sediment model. The Bovenrijn is the smallest domain of the DVR model. In case graded sediment formulations are used for all domains in the DVR model the computation time will substantially increase. From that point of view reducing the number of physical processes in the sub-domains is promising with respect to computation time reduction.

For the DVR-model discharge hydrographs are used, i.e. the bed shear stress and Shields values are varying in time. At the lower discharges the state of the river bed is close to the threshold of motion. In this case erosion or sedimentation problems downstream of the domain boundary at the Pannerdensche Kop can only be overcome in average over a longer period of time. Temporarily erosion or sedimentation waves will develop. These could only be prevented by using discharge dependent reference diameters, but this is not a sensible option.

Considering this, the option of reducing the number of physical processes in the sub-domains is only promising, if the boundary between the uniform and graded domains is placed in a river reach with nearly uniform sediment. It is recommended to place the boundary between graded and uniform domains further downstream in the Waal.

7 Conclusions & Recommendations

7.1 Introduction

WL | Delft Hydraulics worked on the development of an advanced 2-D morphodynamic model that covers, nearly, the entire Rhine system in the Netherlands (see Van Vuren et al. (2006), Yossef et al. (2006) and Mosselman et al. (2007)). The model contains all kind of innovative, recently developed aspects, amongst which domain decomposition, and a functionality for sediment management to assess dredging and dumping strategies.

The DVR model is a promising tool for assessing the river's navigability, for locating nautical bottlenecks and for evaluating river intervention measures in order to improve the navigability. Unfortunately, numerical simulations with the DVR model are rather time consuming. This makes the model less suitable for engineering practice at the moment. The objective of the research presented in this report is to reduce the computation time of a numerical simulation with the DVR model, by the various activities:

1. Optimisation of the grid size;
2. Optimisation of the computation time step and the morphological acceleration factor;
3. Application of parallel computation;
4. Application of a more efficient description of flow through the floodplain;
5. Reduction of the physical processes in sub-domains.

We have investigated the effectiveness of the above-mentioned activities with respect to computation time reduction, considering the model domain of the river Waal branch only. Table 7.1 gives the acceleration of the computation achieved by each of the activities. Conclusions for each of the attemps to reduce the computation time are summarised below.

Table 7.1 Acceleration of the computation achieved by various options for computation time reduction.

Activity	Description	Acceleration of the computation	Computation time reduction
1	Optimisation of the grid size	2.4	8 %
2a	Optimisation of the computation time step	3.4	71 %
2b	Optimisation of the morphological acceleration factor	1.6	37 %
3	Application of parallel computation	2.5	60 %
4a	Application of a more efficient description of flow through the floodplain: Two grid approach	1.22	18 %
4b	Application of a more efficient description of flow through the floodplain: Lateral in- & outflow	to be done	50 %
5	Reduction of the physical processes in sub-domains	1.67 *	

* For purpose of illustration, the computation time of a simulation with a graded sediment model for the Bovenrijn and a uniform sediment model for the other Rhine branches is about a factor 1.67 larger than the computation time involved with a simulation with a completely uniform sediment model containing all Rhine branches.

7.2 Optimisation of the grid size

For the optimising the grid size, it is important to distinguish between the criteria for grid dimensions and the calibration-targets. Regarding the former:

- One should acknowledge the importance of gradually coarsening, when coarsening the grid of the floodplain in cross-flow direction. The transition zone between the main channel and the floodplain, including the groyne section, should be modelled with quite some detail to make sure that the lateral flow exchange between main channel and floodplain is preserved. In particular the schematisation of groynes and summer levees turns out to be important. The averaging-out of geometric information induced by grid coarsening will be reduced when gradually coarsening the grid. Bearing this in mind coarsening the grid up to a factor 4 is allowed.

- When coarsening the main channel grid in transverse direction, it is important to keep at least 8 grid cells in this section, in order to preserve a good representation of the cross-section. When coarsening the grid in transverse direction, the resolution of the grid should be such that it still captures the location of the weirs. The grid cell length should not exceed 100 m.

The aim with respect to the calibration-targets is very much on the possibility of the preservation of the lateral flow exchanges. This target is very important for the grid-choice eventually. The choice for a certain grid should be based on the performance of a hydraulic calibration tool that enables to remove discharge deviation introduced by grid coarsening. This tool should indicate to what extent grid coarsening is possible, in other words the tool should give insight to what extent deviations can be eliminated and reduced by calibration. The decision should be based on the combination of the hydrodynamic performance after calibration and the computation time reduction. Since the calibration tool is not available yet (a first attempt of such a tool is presented in Section 5.3), the choice for the ‘best’ grid is difficult to make at the moment.

The main channel discharge starts to deviate from the reference model along the entire Waal branch for the grid with the maximum allowed dimensions (given by the functional criteria). Deviations become more structural instead of isolated single river locations. Whether these deviations are too large to be removed by a hydraulic calibration depends on the quality of the calibration tool. We have the impression that the deviations induced by the grid are difficult to be removed entirely with a calibration tool. Therefore, it is not recommended to proceed with this grid for the moment. Although this decision could actually not be made in this stage of the project, it is recommended to proceed with the so-called Grid 5 for the rest of the project. This choice should be reviewed after the development of a calibration tool.

Grid 5 contains a gradually coarsened floodplain grid up to a factor 4 in transverse direction. For the coarsening in longitudinal direction of the entire grid and the coarsening in transverse direction of the grid in the main channel and groyne section, a factor 1.33 is used.

A final choice can be made in future, after the development of a calibration tool. Therefore, it is recommended to revise the choice in a later stage of the DVR project after the completion of the calibration tool.

The ratio between computation time required with the reference model and the model of Grid 5 is 2.4. In other words, Grid 5 yields a computation time reduction of 58%.

7.3 Optimisation of the computation time step and the morphological acceleration factor

The time step analysis showed that stable simulations yielding smoothly developing results are achieved with time steps of up to 1.5 minutes. Since the deviations of the model results for this time step from the reference time step of 0.4 min are acceptable, a time step of 1.5 minutes is used for future calculations. This results in an acceleration of the simulations by a factor of 3.4.

The analysis of the morphological acceleration factors showed that the factors used so far can be increased significantly without considerable loss in accuracy of the model results. The following morphological acceleration factor can be used: a factor of 600 for a discharge of 1187 m^3/s, a factor of 480 for a discharge of 2000 m^3/s, a factor of 200 for a discharge of 3080 m^3/s, a factor of 120 for a discharge of 4422 m^3/s. This speeds up further the simulations by a factor of 1.6.

7.4 Application of parallel computation

Domain decomposition in combination with parallel computation turns out to be a useful technique to reduce the computation time. It appears to be important to use a computer with a number of processors sharing the same memory, such as the Mordax machine. Splitting the Waal domain in four sub-domains and run them in parallel on the Mordax machine results in a computation time reduction of 60%.

It is recommended to:

- use a shared memory machine, such as the Mordax machine for future projects;
- optimise the sub-domains of the complete Rhine branches model in such a way that the load is more or less evenly balanced over the number processors;
- to choose the domain boundaries at the river sections with the minimum number of grid cells in transverse direction. In this way the across communication can be minimised;
- to place the domain boundary is a more or less uniform straight river reach with a minimum number of structures at the domain boundary.

7.5 Application of a more efficient description of flow through the floodplain

7.5.1 Two grid approach

The two grid approach is a useful technique to reduce the computation time. When using the two grid approach, the 'SMALL' model should only be used for discharge levels below the bankfull of approximately 1560 m^3/s. Application of the two grid approach to a model of the Boven Waal yields a computation time reduction of 18%. This may is less than expected, when considering the number of days the discharge level stays below bankfull (viz. the discharge of 1187 m^3/s occurs for 219 days a years) in combination with the percentage of grid cells that is not considered in the 'SMALL' model simulation (71%). Apparently the computation time involved with communication and morphological spin up is significant (about 15%).

The test simulations showed that the 'SMALL' grid should be slightly wider than the section covering the main channel and the groyne fields. It appears important to include the flow pattern near the groyne fields to avoid large deviations in flow patterns with respect to the reference model covering the entire model grid.

7.5.2 Lateral inflow and outflow approach

The objective of the lateral in- & outflow approach is to reduce the computation time by using a grid that covers only the main channel and groyne section. For discharges above bankfull, the flow and discharge momentum entering the main channel from the floodplain area is schematised by imposing lateral in- and outflows from the floodplain.

It turned out that to guarantee that the resulting flow field at these exchange locations yields an equivalent flow magnitude and flow direction, the lateral discharges have to be imposed with type "momentum".
This implies that the inflowing discharges are introduced having a prescribed momentum, i.e. discharge rate, flow velocity and angle with respect to North. Furthermore it is relevant to preserve the total mass balance of the model.

The computation time for the reduced grid (with or without lateral inflows) is *half* of that of the full grid for this part of the Waal. An increase of computation speed with roughly a factor 2 is expected if this approach is applied to the DVR model in general.

7.6 Reduction of the physical processes in sub-domains

Not all physical processes are of importance for all Rhine branches. The possibility of reducing the number of physical processes in the sub-domains is a serious option for computation time reduction. For instance, graded sediment processes are important in the Bovenrijn, the Pannerdensch Kanaal and the areas close to the bifurcations, whereas they are of less importance in the other Rhine branches.

This study analyses the possibility to use graded sediment formulations only in the upstream part of the model, the Bovenrijn and use uniform sediment for the other branches in the DVR model. Using only graded sediment formulations when necessary, will yield a considerable reduction of computation time. For purpose of illustration, computation time of a simulation with a graded sediment model for the Bovenrijn and a uniform sediment model for the other Rhine branches is about a factor 1.67 larger than the computation time involved with a simulation with a completely uniform sediment model.

However, it inevitably leads to gradients in sediment transport rates at the domain boundary connecting the two domains. As a consequence, erosion and sedimentation patterns are formed at the transition zones from graded to uniform sediment formulations. These problems are partly inherent in the transport formulae and partly due to the differences in sediment diameters that can develop between either sides of the domain boundary. Namely, in the uniform model the grain size of the bed material is imposed and remains constant throughout the model simulation, whereas the percentages of each grain size fraction of the bed material in the graded sediment model undergo spatial and temporal variations. Model tests show that these problems can only be overcome by adjusting the grain size of the bed material in the domains with the uniform sediment models for situations with constant discharge. In case of discharge hydrographs, however, erosion and sedimentation waves will develop and migrate through the model. Considering this, the option of reducing the number of physical processes in the sub-domains is only promising, if the boundary between the uniform and graded domains is placed in a river reach with nearly uniform sediment. It is recommended to place the boundary between graded and uniform domains further downstream in the Waal.

7.7 Recommendations

In this research project, options for computation time reduction have been investigated for the model domain of the river Waal branch only. By doing so, generic knowledge on how to reduce the computation effort has been produced that also holds for the model domains of the other Rhine branches. Application of the new insights to reduce the computation time to the other model domains of the DVR model is recommended.

The development of a hydraulic calibration tool for Delkft3D similar to that available for WAQUA is recommended. Using such a tool would be of great help on having a definitive decision on the acceptability of a grid.

At the moment it cannot be concluded that the ultimate computational time reduction has been reached because a) it is not clear what the computation time reduction for the entire DVR model (including all domains) would be, when combining all measures to reduce the computation time, b) it is not exactly known what the actual wish is of the client is (how fast should a simulation run), c) maybe there are still other options to further reduce computation time, for instance some specialised consultancies on speeding up computation time with numerical models could be contacted in future, d) in addition to the H-3 cluster and the Mordax machine there exist other machines. It is therefore recommended to determine the computation time reduction if all attempts to reduce the computation time are combined in the entire DVR model. This should make clear whether the ultimate state of the

computation time reduction has been achieved or whether other attempts to further reduce the computation times are required. Of course the wishes of the client concerning the computation time should be clarified.

The investigation of the morfac setting for both contant discharge levels and for discharge time series for the DVR model of the Waal domain is rather complete. This does however not imply that the ultimate state with repsect to the morfac setting has been reached. For instance, the morfac setting should be revised when running the entire Rhine branches model with the 5 domains. Besides, the morfac setting is not investigated in the light of detailed flood waves. Nor is the setting addressed in relation to graded sediment processes. From experiences in Mosselman et al. (2007) concerning the graded sediment model used for the case study of sediment nourishments in de Bovenrijn, it is known that the morfac had to scroll down to 10 in order to achieve stable simulations. This implies that the setting derived for the uniform sediment model is most probably not optimal for a model with graded sediment processes.

As emphasised in Chapter 2, the extent of the grid coarsening stands or falls with the success of the hydraulic calibration tool. Chapter 5 indicated that lateral in- and outflow approach is a promising tool for calibration purposes. This tool can be used to eliminate or reduce the discharge deviations that are introduced by grid coarsening. The performance of the hydraulic calibration tool determines to what extent grid coarsening is possible, in other words the tool should give insight to what extent deviations can be eliminated and reduced by calibration. This study consists only of a first attempt for the lateral in- and outflow approach. To make it widely applicable for calibration purposes the following steps are still to be made,

a) a transfer tool from the required discharge distribution from the WAQUA grid to the Delft3D grid,
b) a convert tool from WAQUA output-files to Delft3D output-files,
c) a online reading tool to read all required hydraulic information on discharge and flow derived with the DVR model,
d) a tool to define the differences in required and estimated discharge distribution, and
e) a tool to impose online lateral in- and outflow (both discharge and flow information).

The hydraulic calibration tool as described above is also required to make the model applicable for impact assessments of measures proposed in the Room for the River project. The DVR model could be a promising tool for morphological impact assessments. A two-step approach is then recommended. First the hydrodynamic response to intervention measures should be investigated with the WAQUA model. Via the lateral in- and outflow approach the impact of the hydrodynamic response on the morphodynamic impact could be investigated. It should be investigated how often an update of the morphodynamic response on the hydrodynamics is required.

8 References

Ashida, K. & M. Michiue (1972), Study on hydraulic resistance and bedload transport rate in alluvial streams. Transactions Japanese Society of Civil Engineers, 206, pp. 59-69.

Egiazaroff, Par.I. (1957), L'équation générale du transport des alluvions non-cohésives par un courant fluide, Proc. IAHR, Pris.

Egiazaroff, Par.I. (1965), Calculation of non-uniform sediment concentrations, ASCE, JHD, HY4, July.

Mosselman, E. (1991), Modelling of river morphology with non-orthogonal horizontal curvilinear coordinates. Communications on Hydr. and Geotech. Engrg., No.91-1, Delft Univ. of Technol., ISSN 0169-6548.

Mosselman, E., C.J. Sloff & H.R.A. Jagers (2005), Voorspelinstrument duurzame vaarweg; Voorbereiding. Rapport Q3963.00, WL | Delft Hydraulics.

Mosselman, E., S. van Vuren, M. Yossef, W. Ottevanger & K. Sloff (2007), Case studies Duurzame Vaardiepte Rijndelta. Rapport Q4245.00, WL | Delft Hydraulics.

Ribberink, J.S. (1987), Mathematical modelling of one-dimensional morphological changes in rivers with non-uniform sediment. PhD thesis, Delft University of Technology, Communications on Hydr. and Geotech. Engrg., No.87-2, Delft Univ. of Technol., ISSN 0169-6548.

Ribberink, J.S. (1987), Mathematical modelling of one-dimensional morphological changes in rivers with non-uniform sediment. PhD thesis, Delft University of Technology, Communications on Hydr. and Geotech. Engrg., No.87-2, Delft Univ. of Technol., ISSN 0169-6548.

Struiksma, N., K.W. Olesen, C. Flokstra & H.J. de Vriend (1985), Bed deformation in curved alluvial channels. Journal of Hydraulic Research, Vol.23, No.1, pp.57-79.

Thompson, J.F., Z.U.A. Warsi & C.W. Mastin (1985), Numerical grid generation. North Holland, Elsevier Science Publishing Co., New York.

Vuren, S. van, E. Mosselman, K. Sloff & B. Vermeulen (2006), Voorspelinstrument duurzame vaarweg; Initiële modelbouw en demonstratieberekeningen. Rapport Q4082.00, WL | Delft Hydraulics.

Vuren, S. van, E. Mosselman, K. Sloff & B. Vermeulen (2006), Voorspelinstrument duurzame vaarweg; Initiële modelbouw en demonstratieberekeningen. Rapport Q4082.00, WL | Delft Hydraulics.

Wijbenga, J.H.A. (1985), Schatting van restfouten in de termen van de bewegingsvergelijkingen in WAQUA kromlijnig. Waterloopkundig Laboratorium Delft.

Yossef, M., E. Mosselman, B. Jagers, K. Sloff, S. van Vuren & B. Vermeulen (2006), Voorspelinstrument duurzame vaarweg; Innovatieve aspecten. Rapport Q4082.00, WL | Delft Hydraulics.